The influence of the tide, wind and waves on the large-scale sediment transport patterns in the Dutch Wadden Sea

S. V. Bult

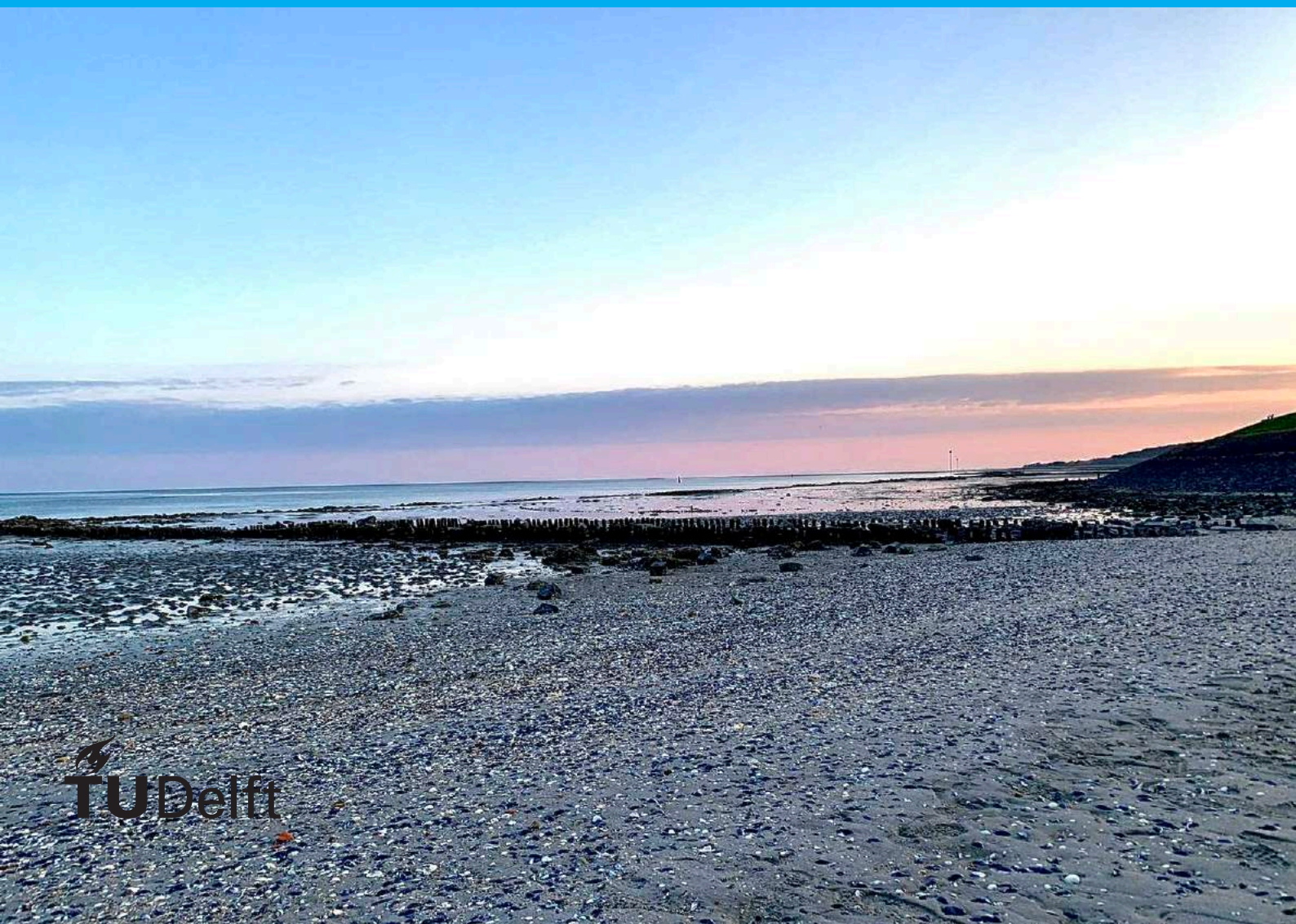

The influence of the tide, wind and waves on the large-scale sediment transport patterns in the Dutch Wadden Sea

by

S. V. Bult

to obtain the degree of Master of Science
at the Delft University of Technology,
to be defended publicly on Tuesday July 13, 2021 at 15:15.

Student number:	4545486	
Project duration:	November 16, 2020 – July 13, 2021	
Thesis committee:	Prof. dr. ir. Z. B. Wang,	TU Delft/Deltares, chair
	Dr. ir. E. P. L. Elias,	Deltares
	MSc. S. R. P. M. Pluis,	Rijkswaterstaat
	Dr. ir. B. C. van Prooijen,	TU Delft
	Dr. ir. J. A. A. Antolínez,	TU Delft

This thesis is confidential and cannot be made public until December 31, 2021.

TU Delft

Deltares
Enabling Delta Life

Rijkswaterstaat
Ministerie van Infrastructuur en Waterstaat

Preface

This master thesis concludes my studies in Hydraulic Engineering at the Faculty of Civil Engineering and Geosciences at the Delft University of Technology. Over the past eight months I have worked on my thesis from home in the online environment from Deltares, in close collaboration with my supervisors from the Delft University of Technology, Deltares and Rijkswaterstaat. I am grateful for the opportunity to work on this project and for my supervisors enabling me to graduate under these special circumstances. I have enjoyed the process and have learned very much from the experience.

I would like to thank Professor Wang for chairing the thesis committee and for arranging the graduate intern position at Deltares. This project would not have been possible without your help. Thank you to Edwin for guiding me through every step of this process. Your explanations, critique and help with the modelling have pushed me to deliver my best work possible. I am grateful for all the time and effort you have dedicated to me, as well as for the encouragements. Thank you to Stefan for your interest in my project, guiding and critiquing the modelling process and for helping me see the context of my research. Presenting my results to your colleagues from Rijkswaterstaat was an amazing opportunity. Thank you to Bram for critiquing my work and ensuring my mental wellbeing. Thank you to José for helping me think out of the box and proposing modelling techniques.

I would also like to thank my temporary colleagues at Deltares and fellow students. Your willingness to help me at all times means a lot. Thank you to Roy, Stuart and Floortje for showing me your work, I would not have been able to work on this project without your models and research. Thank you to Mick for guiding me through the modelling process and for the long hours that were sometimes necessary. I am grateful for all your help with the modelling, visualizing the results and for the fact that you were always available to help me. Thank you to Paula, Hoyte, Denzel, Math and Carlijn for the online chats, these made the continuous working from home way better.

Thank you to all my friends and family for supporting me in the process. A special thank you to Bert and Lennart for proofreading all my versions of the report. Thank you Teun and Lottie for collecting newspaper articles on the Dutch Wadden Sea. Thank you Quintes for the unconditional support and enthusiasm.

Sterre Bult
Delft, July 2021

Abstract

The Wadden Sea is a large system of tidal flats and barrier islands. The transport patterns in the individual inlets of the Dutch Wadden Sea have been of interest in the past, but sufficient knowledge on the sediment transport patterns on the scale of the Wadden Sea is not yet available. The consensus was that the tidal watersheds form more or less closed boundaries that separate the individual inlet systems. Recently, sediment budgets concluded that sediment transport over the tidal watersheds needs to take place, which was confirmed by the exchange of flow over the tidal watersheds. The specific influence of the tide, wind and waves on the large-scale sediment transport patterns has not been determined yet, and is therefore of interest for this thesis. A definition for the sediment sharing system of the Dutch Wadden Sea can be derived from the large-scale sediment transport patterns. Relative sea level rise will increase the sediment demand by the Wadden Sea, therefore maintenance of the system will be necessary. An improved understanding of the large-scale sediment dynamics will benefit the maintenance plans in the future.

The recently developed WadSea FM model is used to model the sediment transport in the Dutch Wadden Sea due to the tide, wind and waves separately. A custom depth-dependent Manning's roughness field was developed to improve the physical reasoning behind the approximation of the tidal propagation. The tide forms the basis, to which the wind and wave forcing are applied. The annual wind and wave conditions are schematized by a representative condition for each forcing mechanism. SedTRAILS, a post-processing tool, is used to visualize the sediment transport pathways due to each forcing mechanism. By comparing the large-scale sediment transport patterns, the effect of each forcing mechanism can be deduced.

The sediment transport pathways show that the tidal forcing initiates an alongshore transport in northeastern direction and dominates the ebb-tidal deltas. The Eierlandse Gat and Vlie Inlet export sediment due to the tide, whereas the Texel Inlet shows a net import. For the Ameland Inlet and Frisian Inlet, a preference can not be observed under tidal forcing alone. The net sediment transport in the back-barrier basins forced by the tide is predominantly directed inward. Applying the representative wind condition to the system results in an enhancement of the alongshore transport. The influence of the wind on the inlet gorges is limited, whereas the wind enhances the net sediment transport in the back-barrier basins. The net sediment transport over the tidal watersheds increases significantly, with the magnitude of net sediment transport depending on the tidal watershed considered. The net sediment transport on the nearshore increases, whereas the inlet gorge dynamics do not change significantly due to waves. The incorporation of waves leads to a net sediment transport over all tidal watersheds. The connectivity within the system is predominantly determined by the tide. The exception is the connection between the Frisian Inlet and the rest of the Dutch Wadden Sea, which is wind- and wave-dominated. The combination of the hydrodynamic forcing mechanisms leads to a system of barrier islands, ebb-tidal deltas, tidal inlets and back-barrier basins that are highly interconnected with one another by the exchange of sediment.

Future research could focus on extending and improving the modelling, for example by further developing the roughness field, improving the connectivity analysis or applying a probabilistic wave analysis. Extending the modelling will lead to less uncertainties or inaccuracies in the results. In addition, quantifying the sediment transport patterns could be another focus of future research. The quantification could be based on available data or data from new techniques, and will improve the reasoning behind future maintenance plans.

Contents

1

Introduction

The objective of this thesis is to get a better insight in the large-scale sediment transport mechanisms in the Dutch Wadden Sea and define it as a sediment sharing system. The introduction will discuss the historical overview and the overall system dynamics of the Wadden Sea. Then, the problem and the subsequent research questions are presented, as well as the research method.

1.1. Historical Overview

The Wadden Sea is a large system of tidal flats and barrier islands, and stretches from the Dutch coast all the way to the northern Danish coast. The focus of this research is the Dutch Wadden Sea, which is shown in Figure 1.1. The formation of the Wadden Sea is thought to have started at the beginning of the Holocene, when there was a rapid rise in the mean sea level (Vos, 2015). During the Holocene, periods of transgression and regression of the coast alternated each other. This was mainly due to the change in rate of relative sea-level rise, the sedimentation rate remained approximately the same (Beets, van der Valk, & Stive, 1992). The difference between the two sectors of the Dutch coast can partly be explained by the smaller sediment exchange between the North Sea and the Wadden Sea throughout the Holocene (de Haas et al., 2018). During the Holocene, the Wadden Sea could keep up with the relative sea-level rise (Elias et al., 2012), but could not fill the basin completely. The formation of the Wadden Sea is mainly due to the relative sea-level rise. For the Holocene, a dynamic equilibrium in the Wadden Sea can be assumed, where due to the dominant tidal and wave propagation to the north and northeast, barrier islands parallel to the coast were formed (Beets & van der Spek, 2000).

Figure 1.1: Aerial photo of the Dutch Wadden Sea (NASA, 2005). The captions indicate the names of the tidal inlets.

Since the Holocene, anthropogenic influences have affected the natural processes that form the Wadden Sea. The most important recent events that have altered the back-barrier basins, are the closure of the Zuiderzee and the closure of the Lauwerszee (van Houweninge & de Graauw, 1982). The closure of the Zuiderzee has largely affected the tidal prisms of the back-barrier basins in the Western Wadden Sea, and thus the size and shape of the adjacent basins. Hence the morphology of the Wadden Sea has changed significantly (Elias et al., 2012). For example, the increase in tidal current velocities has affected the suspended sediment concentrations in the Marsdiep basin, which are much larger now than before the closure (de Jonge, Essink, & Boddeke, 1993). The closure of the Lauwerszee mainly affected the Zoutkamperlaag, which started to import sediment from the outer delta (Wang, Louters, & de Vriend, 1995). These human interventions have thus greatly affected the dynamics of the Dutch Wadden Sea. Other, non-direct affected processes are land subsidence (Hoeksema et al., 2004) and accelerated sea-level rise (Wang et al., 2018). The subsequent relative sea-level rise remains a large threat to the existence of the Dutch coast (Deltacommissie, 2008). The Wadden Sea has not reached a new morphological equilibrium, and as a consequence imports sediment from the adjacent coastlines. Although the quantities of imported sediment are large and these keep influencing the rest of the Dutch Coast, it is expected that this is insufficient for the Marsdiep and Vlie basin to keep up with the accelerated sea-level rise, especially when considering the unfavourable sea level rise predictions (Wang, 2018).

1.2. The Tidal System

The Wadden Sea is a complex system, for which an approximation of the equilibrium of the basins has been determined. A lot of research is currently being done, especially on the mechanisms of residual transport across tidal watersheds and transport through tidal inlets. For the overall sediment transport through the system, alongshore sediment transport and transport through the tidal inlets are of great importance. Additionally, sediment transport due to wind forcing can result in residual transport across the tidal watersheds (Duran-Matute, Gerkema, de Boer, Nauw, & Gräwe, 2014), which causes direct exchange between the different back-barrier basins. The sum of these effects creates sediment transport throughout the system of the Wadden Sea.

The bed material found in the Wadden Sea is a mix of sand and fine-grained muds, where sand makes up the larger share of the material (Compton et al., 2013). Sand has the advantage that it reacts almost immediately to forcing, whereas transport of mud experiences delay, both in pick-up and deposition. When modelling transport of sand, one can therefore assume that when forcing is applied, and it exceeds the critical threshold value (Shields, 1936), the sand particle starts moving. For simplicity, only transport of sand is considered in this research, with a particle diameter of 200 μm. The thesis will focus on the processes within the Wadden Sea itself and its sediment exchange with the coastal zones of the barrier islands. All processes important for the different components of the system, namely the ebb-tidal delta, the tidal inlet, and the back-barrier basin, are included. The components of the system are discussed separately below.

1.2.1. Ebb-tidal Delta

The ebb-tidal deltas are situated at the North Sea side of the region of interest. A general overview of a tidal system is shown in Figure 1.2. Ebb-tidal deltas are large sedimentary accumulations in front of the tidal inlets that influence the sediment transport in the coastal cells (Harrison et al., 2017). Deltas dissipate and redirect wave energy (Fitzgerald, 1984), and form sand storage features that exchange sediment with the tidal inlet and coastal cells (Fitzgerald et al., 1984). The deltas are important when it comes to sediment exchange between the sea and the back-barrier basins (Bosboom & Stive, 2015). The tidal forcing through the tidal inlet forms the ebb-tidal deltas (Van der Vegt et al., 2006). The dominance of the system, either flood- or ebb-dominance, determines whether the ebb-tidal delta accretes or erodes. Additionally, the tidal propagation and waves from the North Sea determine the size of the ebb-tidal delta and residual transport along the barrier islands and through the tidal inlets (Sha & van den Berg, 1993; van Leeuwen et al., 2003).

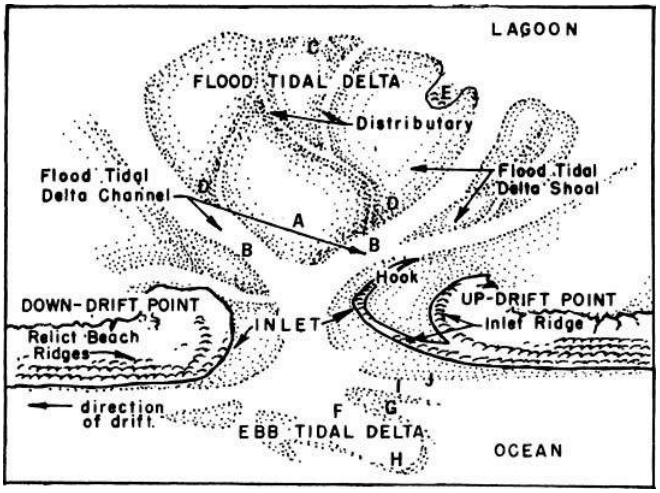

Figure 1.2: Morphological features of a typical tidal system (Fisher & Simpson, 1982). A: flood ramp. B: flood channels. C: ebb shield. D: ebb spit. E: ebb spillover lobes. F: major ebb channel. G: channel-margin bars. H. terminal lobe. I: marginal flood channels. J: swash bars.

1.2.2. Tidal Inlet

Tidal inlets are opening features that govern the exchange of water and sediment between the back-barrier basin and the ocean. It enables the dynamic coupling of the ebb-tidal delta and the back-barrier basin, and when the equilibrium of one of these features is distorted, the inlet is the link that can compensate for the shift in the equilibrium (Elias & van der Spek, 2006). During the compensation for the shift in equilibrium, which can affect the cross-sectional area of the tidal inlet, the velocities in the inlet are assumed to be constant (Bosboom & Stive, 2015). The water depth largely influences the amount of sediment that is brought in suspension, and thus the sediment transport through the inlet (O'Brien, 1933). The tidal inlets are exposed to large velocities due to the constant in- and outflow caused by the tide. The size and the velocities of the jets that arise in these inlets are dependent on the ratio between wave- and tide-energy (Hayes, 1975; Oertel, 1975). Apart from the daily inequality, the tidal amplitude is approximately equal. The non-tidal residual (NTR), the part of the water level when excluding the tidal component, determines the ratio between the wave- and tide-energy. In the Dutch Wadden Sea, the NTR is determined by the wind and waves.

1.2.3. Back-barrier Basin

Back-barrier basins consist of tidal channels, tidal flats and salt marches. The back-barrier basin originates from dynamic flow due to the tide. The position of the tidal watersheds influences the size of the back-barrier basins between two watersheds, and depends on the morphological equilibrium in the basin. The tidal watershed moves to the end of the barrier island where the tidal amplitude is largest (Wang et al., 2011). This is confirmed by the knowledge of the position of the tidal watersheds in the Wadden Sea (Elias et al., 2012) and data of the tidal amplitude along the barrier islands (Nieuwhof & Vos, 2018). Only when dealing with a very non-linear situation, the phase difference becomes more important than the tidal amplitude for the position of the tidal watershed. This is not the case for the Wadden Sea, where the amplitude of the tide dominates the position of the tidal watersheds. The change in tidal amplitude and the phase difference are due to the propagation of the tide in the North Sea around two amphidromic points (Bosboom & Stive, 2015). This theory thus suggests that after a large-scale change, the position of the tidal watershed is approximately stable and the basin starts shifting towards the new morphological equilibrium. Wind forcing is however also an important factor for transport in the Wadden Sea, and can result in residual transport across a tidal watershed (Duran-Matute et al., 2014). Additionally, wind can cause the migration of an entire tidal watershed (Vinther et al., 2004). The influence of wind can be divided into wind-induced flow and waves due to wind. Especially storm conditions can cause sudden bed level changes which can have serious consequences for the temporary morphological tidal watershed position, but these sudden changes can also persist in the long-term evolution of the tidal basin (Van der Spek, 2018). Sediment transport in the back-barrier basins is thus influenced by multiple processes, that in turn influence each other.

1.3. Research Objective

Although the dominant processes in each part of the tidal system are known, the exact influence of each process on the sediment transport throughout the system remains unclear. The sedimentation and erosion patterns are known based on measurements (Elias, 2019), but these patterns do not indicate the exact sediment transport pathways due to each hydrodynamic forcing mechanism. One should understand each process that has an effect on the sediment transport and estimate the resulting transports. The sediment transport in the Wadden Sea is not only determined by the tide, but also by the wind and waves. To understand the influence of these different processes on the sediment transport, the hydrodynamics should be decomposed until each process can be indicated individually. This can give insight in the importance of each process and condition. An objective of this research is to model the sediment transport for each process throughout the Wadden Sea and define the sediment sharing system. Additionally, the exchange of sediment between basins and the processes that govern this, are not yet fully understood (Pearson et al., 2020). Sediment transport pathways indicate the direction of net sediment transport, which can indicate the influence of each process. The transport paths can also give insight in the connectivity between the basins. Another objective of the research is therefore to use the results of the sediment transport pathways to acquire an understanding about the connectivity within the system.

The objectives mentioned above result in the following overarching research objective: improve the understanding of the sediment transports on the scale of the Dutch Wadden Sea and the underlying governing processes. The result of the modelling should be an in-depth definition for the sediment sharing system. The objective results in the following research question, which is divided into multiple sub-questions. The sub-questions reflect the objectives of understanding the influence of the tide, wind and waves on the large-scale sediment transport patterns, the large-scale movement of the individual particles and the connectivity within the system.

How can the Dutch Wadden Sea be defined as a sediment sharing system?

1. What is the effect of the tide on the sediment transport in the Wadden Sea, at the coastline of the barrier islands and in the tidal inlets?
2. What is the effect of the wind on the sediment transport in the Wadden Sea, at the coastline of the barrier islands and in the tidal inlets?
3. What is the effect of waves on the sediment transport in the Wadden Sea, at the coastline of the barrier islands and in the tidal inlets?
4. How do the different processes affect the large-scale movement of individual particles within the system?
5. How can the connectivity within the system be distinguished?

1.4. Research Method

The research requires a process-based model that can simulate the hydrodynamic and morphodynamic processes that occur due to the tide, wind and waves in the Dutch Wadden Sea. The recently developed Delft3D-FM Flow model of the Wadden Sea, better known as the WadSea FM model, is suitable to simulate these processes. The existing roughness field of the WadSea FM model is good in modelling the tidal propagation in the Wadden Sea, but it is definitely not physically substantiated. The first step is thus to perform a calibration and validation process on the roughness field. A roughness field with a depth-dependent Manning's value is developed, which shall be used in the rest of the research. After that, the map that will be used as the basis for this research is determined, i.e. the map that shows the specific locations of the tidal watersheds and the dividing lines between the different basins on the North Sea side of the barrier islands. The dividing lines in the North Sea are just a matter of choice, as no formal definition for this is known up until now. Each dividing line will be positioned in the middle of a barrier island, as done before (Elias et al., 2012; Elias, 2019). The position of the tidal watersheds is first based on the definition of a morphological watershed, namely the position where the bed elevation is highest and the bed slope is minimum. The locations of the tidal watersheds in the Western Dutch

Wadden Sea have been determined very accurately before, but the positions have not yet been determined consistently for the entire Wadden Sea. In addition, the position of the watersheds in the Eastern Dutch Wadden Sea have been approximated by a straight line. For the purpose of this research, it is therefore of importance to create a new map with the position of each divide and the resulting polygons.

The next step is to model the sediment transport pathways for each hydrodynamic forcing, where the focus lays on the tide and the processes due to the wind, which are divided into wind-driven flow and waves. Based on this, the effect of each process on the sediment transport within the system can be determined. The modelling will be done with the WadSea FM model. As the objective of this research is to know how each process changes the sediment transport patterns, the processes are included one by one, beginning with the tide. Modelling of the different hydrodynamic processes will be performed as follows:

- **Tide:** the main tidal constituent in the Wadden Sea is the semi-diurnal M_2 tide (Gräwe et al., 2016). The mean tidal amplitudes and velocities do not change over a longer period of time, even though there is some variation due to spring-neap tides and daily variations. Additionally, the assumed dynamic morphological equilibrium is based on the tidal propagation. As the Wadden Sea was mainly formed by the tide, tidal motion is expected to be the largest contributor to the sediment transport within the system. The first step is therefore to determine the specific influence of the tide and the resulting sediment transport patterns due to the tide. The tidal motion can be retrieved from the data within the model.

To understand the influence of the wind and waves on the sediment transport within the region, wind forcing will firstly be added to the system. This will result in the sediment transport patterns due to the tide and wind, from which the influence of the wind can be deduced. The waves will still be neglected in this case, so the last step is to couple the WadSea FM model to a D-Wave model to include the wave processes. The specifics of the wind and wave processes are discussed below.

- **Wind:** wind acts as a stressor on the water surface, which results in wind-driven flows. These flows induces sediment transport. Wind conditions will be generated for different combinations of direction and wind velocity. The representative wind condition encompasses the mean wind conditions, and includes a wind condition from the south-southwest with a mild wind speed. The storm condition includes maximum wind speeds from the west-northwest. The conditions result in sediment transport patterns from which the influence of the wind can be deduced.
- **Waves:** wind also generates waves, and dependent on the wind speeds and conditions at sea, these waves can reach significant heights. In shallow water, the horizontal velocity of the water particles is much larger than the vertical velocity, but the motion is still assumed to be harmonic. This means that sediment is not necessarily transported by the waves themselves (Bagnold, 1946). The breaking or non-breaking waves induce turbulence in the water column (Babanin & Haus, 2009), which generates suspended sediment in the column, especially near the bottom (Díaz-Carrasco et al., 2019). After the sediment is suspended in the water column, it can be transported by the tide- and wind-driven flow. The implementation of waves means that the conditions can be assumed to approach realistic conditions. The influence of waves is very different in the coastal zones compared to back-barrier basins. On the outer shore the waves coming from the open sea will be dominant, whereas in the back-barrier basins waves are generated locally by wind on the free surface. Therefore, two cases in the same model are distinguished:
  - Waves in **back-barrier basins:** the basins are prone to small waves generated in the basin itself. Waves originating offshore can be neglected, as the tidal motion is dominant in the tidal inlets. At most, the flow due to the tide is enhanced or counteracted. Even though the waves are relatively small, they can become significant in the shallow basins. With data from the wind conditions in the region, a wave field is generated by the D-Wave model. This wave field will be coupled to the Delft3D-FM model, which will result in sediment transport throughout the system. This should give insight in the transport due to waves generated in a back-barrier basin.
  - Waves on **outer shore:** obtaining an understanding about the sediment transport due to breaking waves is not the objective of this research. The resulting turbulence that causes

the presence of larger quantities of suspended sediment and the influence on the large-scale sediment transport patterns, however, is. For simplicity, measurements from buoys at the boundaries are used to determine the representative wave heights and periods. These waves can break in the surf zone, and will likely induce additional sediment transport on the nearshore.

After modelling the sediment transport through the system due to the different hydrodynamic processes, another model for the post-processing of the results is used. This model is the Matlab application SedTRAILS. The model is able to track the pathway of sediment particles over a longer period of time in an efficient way (Elias & Pearson, 2020). To understand the movement of the individual particles through the system, a representative flow condition is determined for each process. With that, the pathways for the multiple forcing conditions can be determined and the influence of each process can be deduced.

The last part of the research is to determine the connectivity patterns within the Wadden Sea system. Polygons are connected if they exchange sediment particles in the modelling period. The objective here is to determine whether or not the connectivity patterns change by adding the hydrodynamic processes to the system. The SedTRAILS data forms the basis for this connectivity analysis. Having obtained the network diagrams with the indicated connectivity between the polygons, some conclusions can be made regarding the sediment sharing system.

1.5. Thesis Outline

The layout of the thesis is as follows. Chapter 2 discusses the theory on the influence of tide, wind and waves on sediment transport. Chapter 3 discusses the possibilities for a roughness field configuration and the final chosen roughness field. In addition, this chapter also describes the methodology for determining the position of the morphodynamic tidal watersheds. Chapter 4 describes the determination of the morphodynamic and hydraulic tide, as well as the choice for one of the two to generate results in SedTRAILS. The chosen representative wind and waves are also discussed in Chapter 4. The results of SedTRAILS are thoroughly discussed in Chapter 5. The connectivity within the system is determined in Chapter 6, where the relative changes in connectivity due to different forcing conditions are discussed. In Chapter 7, the results are discussed, as well as their limitations and possible application. Chapter 8 ends with the conclusion and recommendations for future research.

2

Processes

Tides, wind and waves are important for sediment transport in the Wadden Sea. The underlying principles and the effect of each process on the tidal system differ greatly from one another. Therefore, the theory on each process is discussed separately. The theory on the tide, wind and waves is discussed in Sections 2.1, 2.2 and 2.3, respectively.

2.1. Tide

The equilibrium tidal theory describes the gravitational potential of the surface of the earth's oceans when considering an earth that is entirely covered by water. The tides then are the result of the change in the equipotential due to the variation of the attraction by the Sun and Moon (Agnew & Farrell, 1978). Namely, the variations in the water surface generate flows that occur with a standard period. One speaks of a semi-diurnal tidal response if the tide is mainly affected by the solar and lunar tide, which has a tidal period of approximately 12 hours. When the daily inequality, due to the declination of the earth, is so large that it becomes dominant, one speaks of a diurnal tidal response with an approximate period of 24 hours (Bosboom & Stive, 2015). In the region of the North Sea and Wadden Sea, the tide is mainly semi-diurnal.

Even though the equilibrium tidal theory can describe the general generation of the tide, the real propagation of the tidal wave is more complex than the theory accounts for. The dynamic theory of tides also accounts for the presence of continents and the often limiting water depths, and should thus be considered (Kvale, 2006). The deflection by the Coriolis force and the blocking by land masses creates rotations, such a system is called an amphidromic system. The tide thus propagates with the dominant period around an amphidromic point. The amphidromic system of the North Sea is shown in Figure 2.1. Based on the dynamic theory, the tidal level can be predicted by means of a harmonic analysis:

$$\eta(t) = a_0 + \sum_{n=1}^{N} a_n \cos\left(\omega_n t - \alpha_n\right) \tag{2.1}$$

Where a_0 [m] is the mean level, a_n [m] is the amplitude of tidal component number n, ω_n [1/hr] the angular velocity of tidal component number n, and α_n [-] the phase angle of tidal component number n. The harmonic analysis is later on used to determine the water level boundary conditions solely due to the tide, which are the input for the sediment transport computations.

Tidal asymmetry, a difference in velocities during flood and ebb, is already present on the North Sea, as the tidal wave is affected by the shallow North Sea (Dronkers, 1986). When the tidal wave enters the tidal system, the wave is affected by the basin geometry. The effect of the geometry can lead to an increase in tidal asymmetry. The consequence is often an increase in unequal duration and/or magnitude (Speer & Aubrey, 1985). Whether one is dealing with flood-dominance or ebb-dominance depends on the relative phasing of the overtides that increase in magnitude in the tidal system. The type of distortion determines the overall transport direction. The tidal asymmetry can be enhanced or weakened

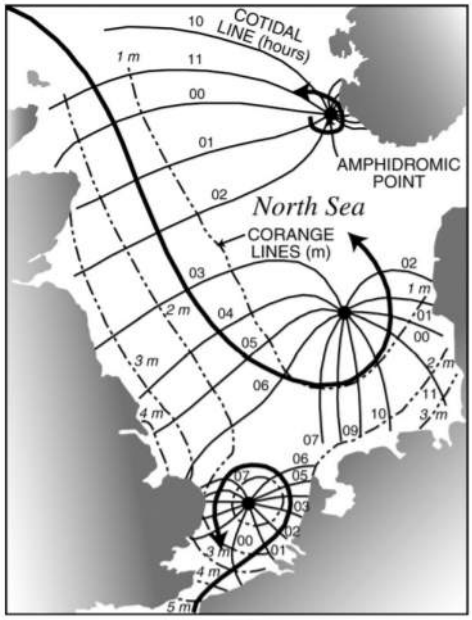

Figure 2.1: Amphidromic system of the North Sea for the M_2 tide (Kvale, 2006). The figure shows the amphidromic points, and the propagation of the tidal wave around these points. The arrows indicate the direction of the propagation, and the solitary numbers the number of hours it takes for the wave to reach this position.

by convergence of the basin, typically the tidal amplitude experiences a decreasing amplification if the convergence increases, while the tidal wave speed increases throughout the basin (Lanzoni & Seminara, 1998). Many formulations exist to describe the tidal propagation in tidal systems, for example the equations by (Savenije et al., 2008).

2.2. Wind

Most studies on wind-driven ocean circulation are based on Ekman's theory on the direct effect of wind stress on currents (Ekman, 1905). However, as this theory is only valid in deep water, i.e. where the depth of the Ekman layer is negligible compared to the water depth (Goldstein & Gedney, 1973), Ekman's theory cannot be used for the case of the Wadden Sea. The Wadden Sea is a system of shallow channels and flats, to which the following depth-averaged momentum balance equation applies (Colosimo et al., 2020):

$$\rho_w h \frac{\delta u_x}{\delta t} - \rho_a c_D u_{10} |u_{10}| + \rho_w c_{f_{wc}} u_x |u_x| + \rho_w g h \frac{\delta \eta}{\delta x} + \rho_w u_x h \frac{\delta u_x}{\delta x} = 0 \tag{2.2}$$

Where ρ_w is the density of seawater, h the water depth, u_x the flow velocity, t the time, ρ_a the density of air, c_D the wind drag coefficient, u_{10} the wind speed at 10m above the water surface, c_{f_c} the bed friction coefficient related to currents, g the gravitational acceleration and η the water level. The first term in Equation 2.2 represents inertia, the second term represents stress induced by the wind, the third term represents the current induced bed-shear stress, the fourth term represents the pressure gradient and the last term represents advection (Colosimo et al., 2020). Assuming the same conditions as for the reference study, the stress induced by the wind, the bed-shear stress and the pressure gradient are dominant. At the tidal flats, inertia and advection are small compared to the other terms. This means that the wind-induced stress, bed-shear stress and pressure gradient dominate the wind-induced flow and sediment transport in the system, at least in the shallow areas of the Wadden Sea. The part of the water column that is influenced by the wind is largely dependent on the total water depth and whether or not opposite flows are present (Bilge et al., 2016). The sum of flows determines the depth-averaged velocity. Opposite flows could result in an underestimation of the flow velocity and sediment transport. Wind set-up is the result from the shear stress of the wind on the water surface, and is characterized by a slope in the water surface. An example of an expression of the set-up S over a fetch F reads

(Mostertman, 1963):

$$\frac{S}{F} = 0.4 \cdot 10^{-6} \frac{U^2}{h} \tag{2.3}$$

Where S is the set-up over the fetch F, U is the wind speed and h is the water depth. From Equation 2.3, it follows that the set-up is mainly dependent on the wind speed. The wind set-up may result in compensatory flows, which directions depend on the geometry of the system. Closed basins experience return flows, but in systems like the Wadden Sea, mostly flows in downwind direction will be observed.

2.3. Waves

Waves that reach the coastal regions have been generated at sea. The waves form groups through frequency dispersion and propagate in shore direction. In deep water, the waves do not experience any influence from the bottom and are free to propagate. These deep water waves can be described by the linear wave theory. However, when these waves reach intermediate and shallow waters, the linear wave theory does no longer suffice (Munk, 1949). The waves start shoaling and wave asymmetry appears. This continues until the water depth becomes too small and the waves become too steep, upon which breaking of the waves occur. The area between position at which the waves break and the water line is called the surf zone. The surf zone is a high energy area of the cross-shore profile, in which the breaking waves create a lot of additional turbulence. Due to this turbulence, a lot of sediment is suspended in the surf zone (Lin & Liu, 1998). Near the water surface the transport is mainly onshore directed due to, among others, the onshore short wave propagation and Stokes drift (van den Bremer & Breivik, 2018). Near the bottom however, an undertow is driven by the imbalance between the wave momentum flux and the uniform pressure gradient (Stive, 1986). The undertow is responsible for offshore directed transport, were it bedload transport or transport of suspended sediment. The main power that drives sediment transport in the surf zone, however, are the incident breaking waves (Battjes, 1988). These waves are refracted once they are located in intermediate water depths, but still enter the surf zone under an angle with respect to the shoreline. This phenomenon creates the so-called longshore currents that transport sediment particles along the coast (Longuet-Higgins, 1970). Depending on the wave climate, the sediment transport in the coastal regions due to waves can be very diverse. Additional sediment can be brought in suspension to be subsequently transported by the tide, or the wave can enhance or counteract the transport by the wind and tide. In Chapter 5, the effect of multiple wave directions on the sediment transport along the islands and through the inlets is assessed.

The waves that are important for sediment transport in the coastal regions, will likely break on the ebb-tidal deltas and therefore not reach the back-barrier basins. The waves that do occur in the basins are locally generated by the wind over the available fetch in the basin (Green & Coco, 2014). The available reach in the Wadden Sea for certain wind directions is extensive, but the waves will not reach the heights that are observed in the coastal zones. Especially the shallow areas are influenced by waves, as even small waves can bring sediment particles into suspension. The suspended load can then be further transported by currents due to the wind and waves, or by the tide. The magnitude of the effect of the waves is determined by the stance of the tide (Li et al., 2019), especially in estuaries with a large tidal range like the Wadden Sea (Hofstede et al., 2018). Storm activities mainly drive sediment transport far from the inlets (Fagherazzi et al., 2007), so close to the tidal watersheds and at the land boundaries. Smaller waves will break in the back-barrier basins due to the smaller water depths, and as opposed to the coastal regions, no distinct surf zone may develop. The main role of waves in the basins is to bring the sediment in suspension. The sediment particle pathways are then determined by the other hydrodynamic forcings.

3

Model Characteristics

The WadSea FM model (Laan, 2019) was developed for a case study of the ebb-tidal delta near Schiermonnikoog, and therefore originally had a refined grid definition near the Schiermonnikoog barrier island. The model was also developed with an overall coarse grid, which is used in this research to schematize the entire Dutch Wadden Sea. As part of this research, the coarse grid is refined. The performance of the overall refined grid is discussed in Section 3.1.3. The bottom roughness coefficient is another model characteristic that is reviewed. The WadSea FM model uses a roughness field that can accurately describe the tidal water level in the domain of the Dutch Wadden Sea. However, this roughness field schematisation was determined empirically by implementing polygons with roughness values different from the overall value. This research still uses an empirical calibration process, but the physical reasoning behind the applied roughness values is improved. The bottom roughness schematisation is discussed in Section 3.1. The last model characteristic that is discussed is the position of the tidal watersheds. The morphodynamic tidal watersheds are determined, as this research focuses on the morphodynamics in the Dutch Wadden Sea. The method for determining the watersheds and the comparison of different measurement cycles are discussed in section 3.2.

3.1. Bottom Roughness

For every body of the free flowing water, part of the friction is determined by interaction with the bed. The Manning's roughness coefficient is a widely used coefficient in numerical models to compute flow, but the exact value of the coefficient is often unknown because of varying conditions (Limerinos, 1970). The Manning's roughness coefficient is largely depth-dependent, especially in tidal systems like the Wadden Sea (Cheng et al., 1993; Gross et al., 2009). This also follows from the general Manning equation for open channel flow (Jarrett & Petsch Jr., 1985):

$$V = \frac{1.486}{n} \cdot R^{2/3} \cdot S_f^{1/2} \tag{3.1}$$

Where V is the average cross-section velocity, n is the Manning's roughness coefficient, R is the hydraulic radius, and S_f is the friction slope. When assuming that the hydraulic radius is equal to the water depth Equation 3.1 can be rewritten to the following expression for the Manning's roughness coefficient:

$$n = \frac{1.486}{V} \cdot d^{2/3} \cdot S_f^{1/2} \tag{3.2}$$

Equations 3.1 and 3.2 were derived for general open channel flows. The flow in tidal systems like the Wadden Sea is very different from general open channel flow, but the equations indicate the importance of the depth. Also, the equations do not take into account grain size distribution. The Western Wadden Sea has a different grain size distribution than for example the Ems-Dollard estuary. Theories that include the grain size, like the Darcy-Weisbach theory (Chanson, 2004), are preferred, but these methods are more complex and thus require more computational effort. Assessing more complex roughness field relations transcends the scope of the present research. The application of the

extensively used Manning's relation is however further examined, as the relation is very effective in improving the accuracy of the water level estimation (Kreitmair et al., 2020; Khanarmuei et al., 2020). The Manning's coefficient is both directly and indirectly influenced by the depth. When assessing the relation in Equations 3.1 and 3.2, it follows that in deep regions of the basins, the value for the Manning's coefficient should be large. In shallow parts of the basins, the opposite is true.

The Manning's formulation was already applied to the WadSea FM model. The chosen schematisation is shown in Figure 3.1. This schematisation was determined by a calibration and validation process. The distribution of the Manning's values had to be determined by comparing the tidal amplitude at multiple measurement stations with the modelled tidal amplitude. First, a uniform Manning's roughness was applied to the domain. Multiple values in this uniform schematisation were assessed on their ability to approach the measured tidal amplitudes as best as possible. The uniform schematisation with a Manning's value of 0.022 proved to approach the tidal amplitudes in the Eastern Wadden Sea and the Ems-Dollard estuary well, but the amplitudes in the Western Wadden Sea were not damped enough. Therefore, in addition to the Manning's value of 0.022 in the domain, a polygon covering the Marsdiep basin and the Eierlandse Gat with a Manning's value of 0.028 was applied to the model. Manning's values of 0.022 and 0.028 are typical values in channels with a sandy bed material (Arcement & Schneider, 1989). Increasing the roughness by implementing a polygon with a higher Manning's value, resulted in an improved approximation of the tidal propagation in the Western Wadden Sea. The overall accuracy of this roughness field schematisation could be quantified by a percentual deviation in tidal amplitude, which was 3.38%. Deviations beneath 10% are assumed good, thus the roughness field schematisation used by the WadSea FM model can approach the tidal amplitudes accurately.

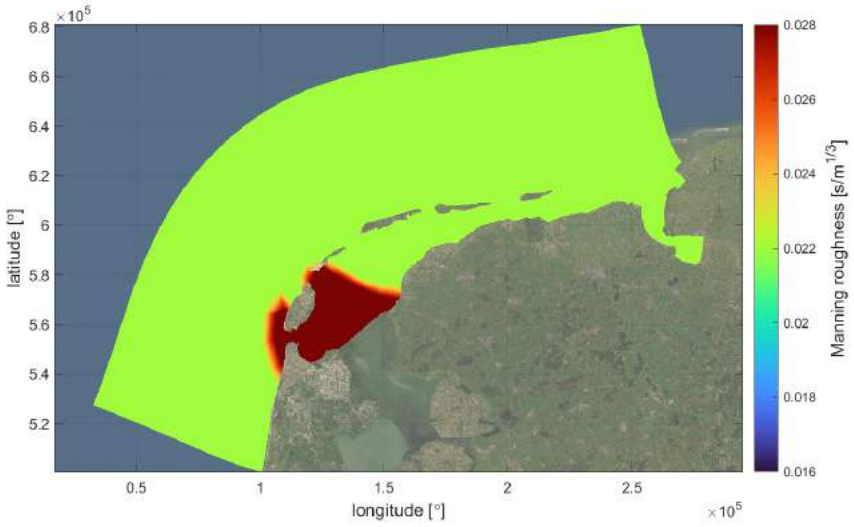

Figure 3.1: Bottom roughness configuration for the WadSea FM model (Laan, 2019). The Marsdiep basin and the Eierlandse Gat have a Manning's value of 0.028, whereas the rest of the model has a value of 0.022, which is also indicated by the colour bar at the right of the figure. The x- and y-axes indicate the position in longitude and latitude.

The roughness field schematisation from Figure 3.1 can approach the tidal propagation in the Dutch Wadden Sea accurately, but the schematisation is only based on the calibration and validation process. The polygon with a higher Manning's value has no physical substantiation, and the used roughness field schematisation is therefore highly empirical. Equations 3.1 and 3.2 already indicated the influence of the water depth on the Manning's value. To improve the physical reasoning behind the applied Manning's roughness field, this research assesses the application of a depth-dependent Manning's roughness field. The method to determine the preferred roughness field and the possible roughness field schematisations are discussed below.

3.1.1. Model Implementation

The performance of each depth-dependent roughness field assessed in this section is determined based on the modelled M_2 tidal amplitude compared to the measured M_2 tidal amplitude, as was done for the uniform Manning's roughness fields. Only the M_2 tidal amplitude and not the amplitude of the entire tidal signal is assessed, as the tide in the Netherlands is mainly semi-diurnal. An example of the results that are used in this analysis is shown in Figure 3.2. The figure not only indicates both the modelled and measured tidal amplitude, but also the tidal phase. The tidal phase also depends on the applied roughness value, but the results showed a much smaller influence of the change in roughness field on the tidal phase than on the tidal amplitude. In this research, the approximation of the tidal amplitude is assumed to be normative. The tidal amplitude is both modelled and measured at eighteen measurement stations in the domain, as can be seen in Figure 3.2. Not all measurement stations are equally important. The stations in the Ems-Dollard estuary are of less importance than the stations in the Western Wadden Sea, as the Ems-Dollard contributes less to the large-scale sediment transport patterns. In addition, some stations are known to be located at non-normative locations, like in small tidal channels behind tidal flats. An example is the measurement station at Den Oever. The tidal propagation between Den Helder and Harlingen is known to be normative for the tidal propagation in the Wadden Sea. The tidal propagation between these two stations is therefore one of the main indicators of the performance of the roughness field. Another important indicator is the approximation of the tidal amplitude at both measurement stations Vlieland and West-Terschelling, as these are situated in a main tidal channel.

The choice for a roughness field based on the tidal amplitude is still an empirical method. One by one, the roughness fields are assessed based on their performance regarding the M_2 tidal amplitude. If the result is unsatisfactory, a new roughness field schematisation is drafted and assessed subsequently. This is an extensive calibration process. Even though the goal is to improve the physical reasoning behind the chosen roughness field schematisation, it is still not possible to choose a value that applies to the specific conditions. Only indications on suitable values are available (Arcement & Schneider, 1989). One could choose to pass on the calibration process and pick an indicated value. This could be justified if the influence of the tide would not be of importance and one would want to assess the influence of wind and waves. Namely, the errors in the tidal propagation are then of less importance. For this particular research however, the influence of the tide on the large-scale sediment transport

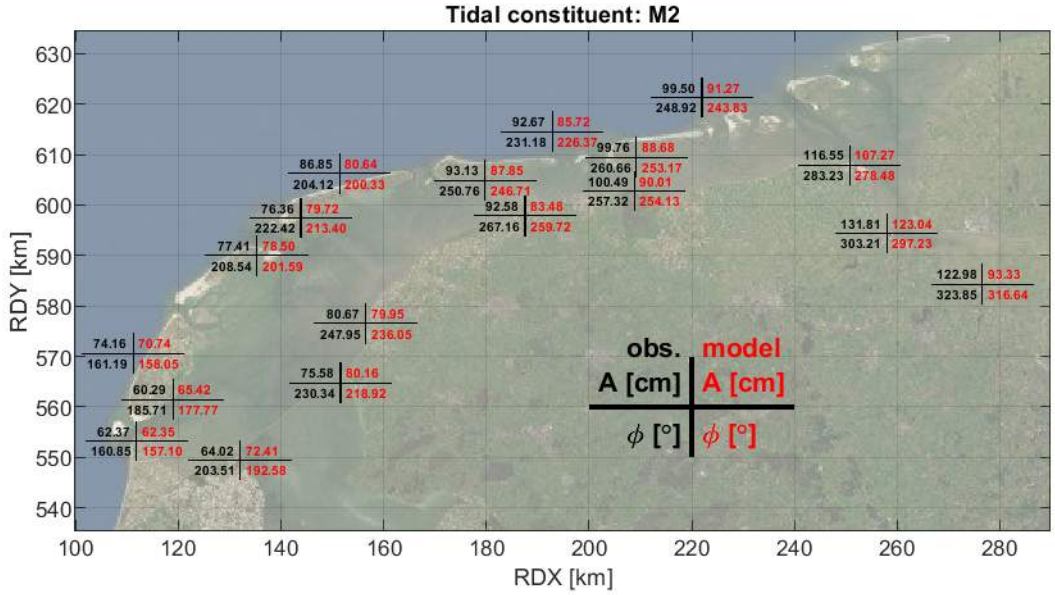

Figure 3.2: Map of the Dutch Wadden Sea with both observed and modelled results for the M_2 tidal amplitude and phase. The table on the bottom right of the figure indicates the meaning of the values at each measurement station. The applied roughness field has a Manning's value of 0.021 in the channel, a value of 0.020 in the sub-littoral zone and a value of 0.010 in the littoral zone.

patterns is one of the main points of interest. The errors in the tidal propagation therefore need to be as small as possible, which requires an extensive calibration process. The calibration process and the choice of roughness field are further discussed in Section 3.1.2.

To assess the applicability of a depth-dependent Manning's roughness field, multiple methods were used. The first, and most extensively researched method, is a method where the Wadden Sea is divided into three regions based on depth, and subsequently three Manning values are assigned. After that continuously varying Manning values were applied to the model, which varied linearly with depth. For the last method, again three regions were recognized, but now also the distinction was made between the Eastern and the Western Wadden Sea. This distinction was primarily made to assess the influence of the mud content on the depth-varying Manning coefficient.

Depth Regions. The first method divides the Dutch Wadden Sea into three depth regions: the channels, the sub-littoral zone and the littoral zone. The depths that were used to distinguish these zones were based on known definitions (Nederhoff, Smits, & Wang, 2017). All bed levels beneath -5m NAP were indicated as 'channel', points between -5m and -1m NAP were distinguished as the sub-littoral zone, and every point above -1m NAP was assigned to the littoral zone. Larger values for the Manning's coefficient were applied in the channels, and the smallest values were applied to the tidal flats. This results in the general roughness field shown in Figure 3.3a.

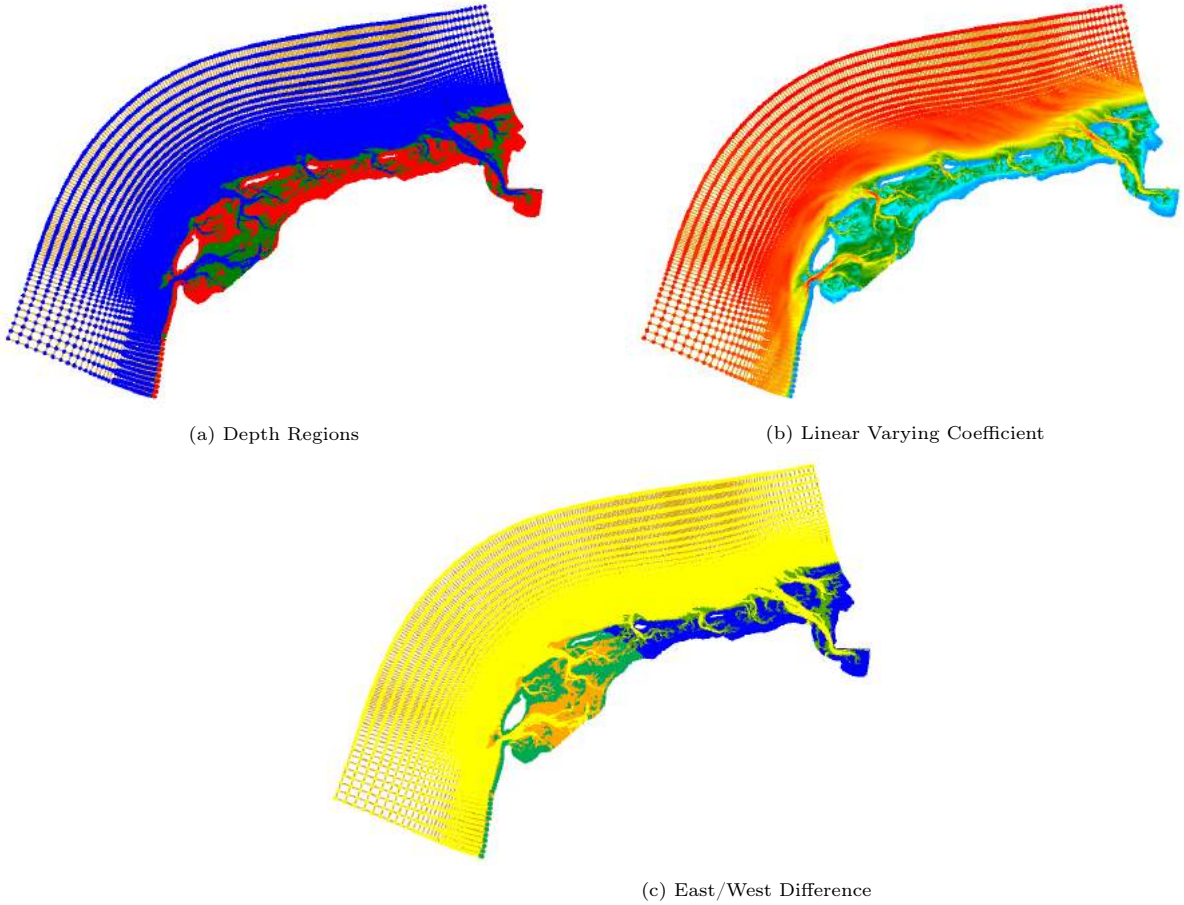

(a) Depth Regions

(b) Linear Varying Coefficient

(c) East/West Difference

Figure 3.3: The three schematisations for the depth-dependent roughness field. The sub-captions indicate the method used to draft the roughness field schematisation. Note that the colour distribution has no specific meaning here, it only shows the difference in value for the Manning's coefficient.

Linearly Varying Coefficient. Instead of assigning three Manning's values to specific depth regions, one can also choose to assign an individual Manning's value to each individual depth value. In this case, this was done by assigning a linearly varying Manning's coefficient to the distribution of the depth. Actually, the distribution of the depth in the Dutch Wadden Sea cannot be described by a linear function.

Namely, most regions in the Wadden Sea have approximately the same depth, with exceptions of the deep tidal channels and the shallow tidal flats. Higher degree equations would be a better approximation of real life. However, a linear function is a good start to assess the success of a continuously varying Manning's coefficient. Once again, the largest Manning's value was assigned to the largest depth, and decreased linearly. The general roughness field for this method is shown in Figure 3.3b.

East/West Difference. Lastly, the method of assigning depth regions can be expanded. In the Western Wadden Sea, the grain sizes tend to be larger than the grain sizes in the Eastern Wadden Sea, where the mud content is larger. The consequence is that the Manning's coefficient is expected to be overall smaller in the Eastern Wadden Sea compared to the Western Wadden Sea (Bathurst, 1978). Therefore, a division line was created between the Vlie basin and the Amelandse basin, and the Manning's coefficient in the Eastern Wadden Sea was set at a slightly lower value at each depth region. The only exceptions were the North Sea and the channels, these regions are generally influenced by the same high wave conditions and are therefore assumed to have the same grain size distribution. The other Manning's values were 0.005 smaller for each region in the Eastern Wadden Sea. The schematisation is shown in Figure 3.3c.

3.1.2. Choice of Roughness Field

The three methods for determining a depth-dependent Manning's roughness field all have their pros and cons. The most important results as discussed in this section are shown in Appendix A. The 'East/West Difference' method gave the most accurate results overall, but with this method it is hard to come up with a depth-dependent Manning's value for the entire Wadden Sea. Additionally, the results with this method were better, but they were not significantly better than for the other methods. It is not justified to choose this method based on the increased accuracy alone, as this method will give confusing results for the depth-dependency of the Manning's value. The 'Linearly Varying Coefficient' method is theoretically a better choice than assigning only a few values to depth regions, as each individual depth has an individual Manning's value based on Equations3.1 and 3.2. However, the 'Linearly Varying Coefficient' method had no higher accuracy than the other two methods, and is therefore not the preferred method to apply to the model. The 'Depth Regions' method is a relatively simple method that can give a clear depth-dependency relation for the Manning's value. The method did not perform best on accuracy, but the simplicity and applicability of the method make it the preferred method. Therefore, the calibration process mostly focused on this method.

Appendix A describes the calibration process that led to the best performing Manning's roughness field. The roughness field for which the model approximated the tidal propagation best, was the schematisation where a Manning's value of 0.021 was applied to the channels, a value of 0.020 to the sub-littoral zone, and a value of 0.010 to the littoral zone. The results from the run with this specific roughness field are shown in Figure 3.2, where the modelled M_2 tidal amplitude is compared to the measured values. In this figure, it can be seen that the modelled amplitude differed only 0.02cm from the measured value at Den Helder, and 0.72cm at Harlingen. This is comparable to the results from (Laan, 2019), and the results at Den Helder are better. The modelled amplitudes at Vlieland and Terschelling also fall within a 3.5cm deviation range. The overall results from this model show a 6.64% deviation from the measured values, which is beneath the 10% that is needed for the results to be considered as good. The chosen roughness field schematisation is shown in Figure 3.4. The resulting depth-dependency relation for the Manning's coefficient is described in Table 3.1.

Table 3.1: Chosen depth-dependency relation for the Manning's coefficient in the Dutch Wadden Sea. The relation divides the Wadden Sea into three depth regions and assigns a value to each region, the regions are indicated in the left column.

	Depth (w.r.t. NAP)	Manning's n Value
Channels	$D < -5$	0.021
Sub-littoral	$-5 \leq D \leq -1$	0.020
Littoral	$D > -1$	0.010

The new bottom roughness field for the WadSea FM model is an important step in the application of depth-dependent roughness fields. Until now, the application of such roughness fields is more of an exception and most models still apply highly empirical roughness fields. Note that the depth-dependent

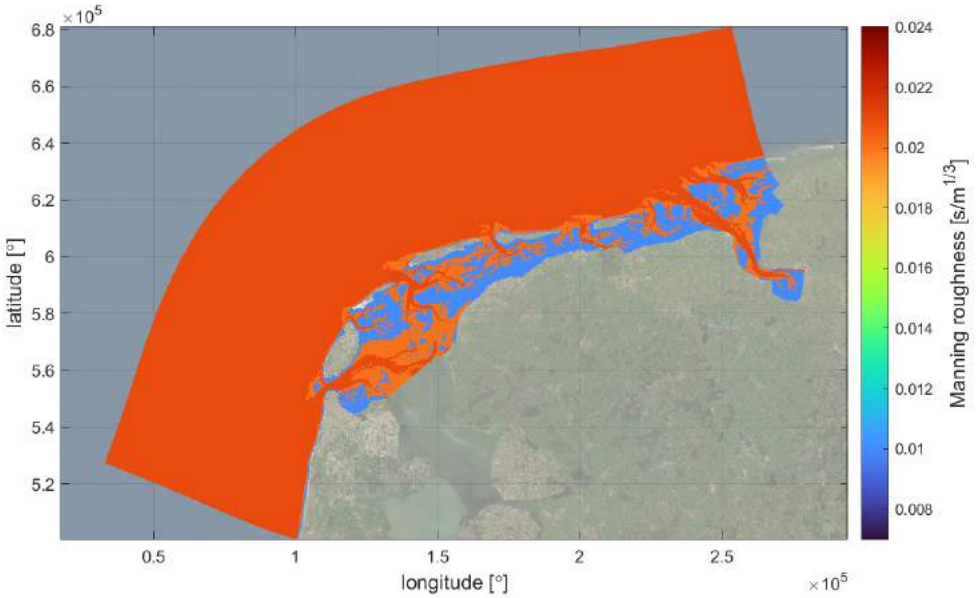

Figure 3.4: Chosen bottom roughness configuration. The North Sea and the channels have a Manning's coefficient of 0.021, whereas the sub-littoral zone has a value of 0.020 and the littoral zone a value of 0.010. Notice the predominantly larger coefficient values in the Western Wadden Sea compared to the Eastern Wadden Sea.

roughness field is still empirically determined and can only be applied to the specific case of the Dutch Wadden Sea, but it has an improved physical reasoning behind it. In addition, this research proves that a depth-dependent roughness field can match the performance of other roughness fields. A next step could be to discover the possibility of the application of the Darcy-Weisbach relation (Chanson, 2004), which incorporates the grain size distribution in the Wadden Sea. Instead of assessing the tidal propagation on the basis of the tidal amplitude at the individual stations, the gradients in the tidal amplitude between measurement stations could also be assessed. This may result in a better approximation of the tidal propagation in and around the Dutch Wadden Sea.

3.1.3. Grid Refinement

Until now, the assessed runs have a relatively coarse grid. This can have the consequence that the results are influenced by the chosen resolution of the model. Therefore, one also wants to assess the results of a grid with a higher spatial resolution. The grid refinement was done by one cycle of triangulation, and some updating of the model to reach a desired value for the orthogonality of the

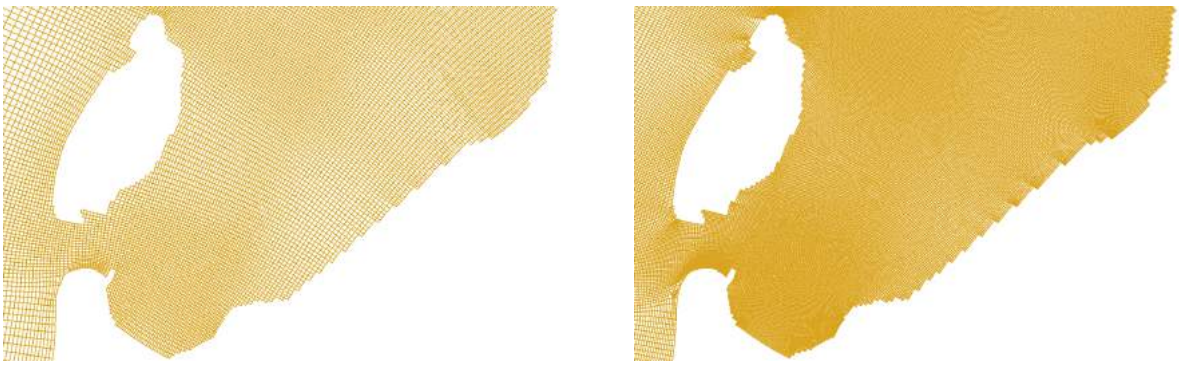

(a) Coarse Grid

(b) Refined Grid

Figure 3.5: The coarse grid configuration and refined grid configuration. Both figures show the grid for the Marsdiep basin. The white blocks in the figures indicate the Noord-Holland coast and Texel.

network. The overall orthogonality of the model was very good, only at the tip of Texel and at Den Helder the orthogonality was such that some diffusion in this region is inescapable. The overall maximum accepted value was 0.10, to prevent too much numerical diffusion in the rest of the model. The new bathymetry was determined by interpolation on the refined grid. The result of the grid refinement is shown in Figure 3.5b. Here, only the Marsdiep is shown to clearly identify the difference in the spatial resolution. To assess accurately the difference in results when choosing a finer grid, both the runs were equipped with the chosen roughness field shown in Figure 3.4. The overall results for the finer grid were somewhat better, but the coarser grid performed better for the tidal propagation between Den Helder and Harlingen. An additional probability analysis on the comparison of the coarse and refined grid is discussed in Appendix B. As the overall results are only slightly better, the tidal propagation in the Western Wadden Sea is worse, and the computation takes over six times longer than the computation for the coarse grid, applying the coarse grid to the next steps in the research is more beneficial.

3.2. Morphodynamic Tidal Watersheds

This section deals with the definition of a morphodynamic tidal watershed and the method used to determine the position of these features. The final position of the watersheds for the sixth measurement cycle of Rijkswaterstaat will be compared to the other measurement cycles, and this final position will be used in the definition of each back-barrier basin.

3.2.1. Method

In this section, the latest position of the morphodynamic tidal watersheds in the Dutch Wadden Sea will be determined. A morphodynamic tidal watershed can be defined as a division line between two back-barrier basins that is formed by the bathymetry, i. e. where the bed elevation is maximum and the slope of the bed is minimum. This is not the same definition as was given by (Vroom, 2011), who defined the morphodynamic tidal watershed as the centre line of the spine-like shape that appears in between the basins of the Wadden Sea. This centre line does not necessarily correspond to the maximum bed elevation and the position of minimum flow velocities. The latter is the definition for a hydrodynamic tidal watershed. However, this research does not follow these definitions and bases its determination of the position of the watersheds mainly on the slope of the bed. Namely, the definition by Vroom neglects recent influences, as the changes in bed level and slope are not taken into account. Especially the slope is a good indicator of flow direction, and not considering this may result in an outdated conclusion on

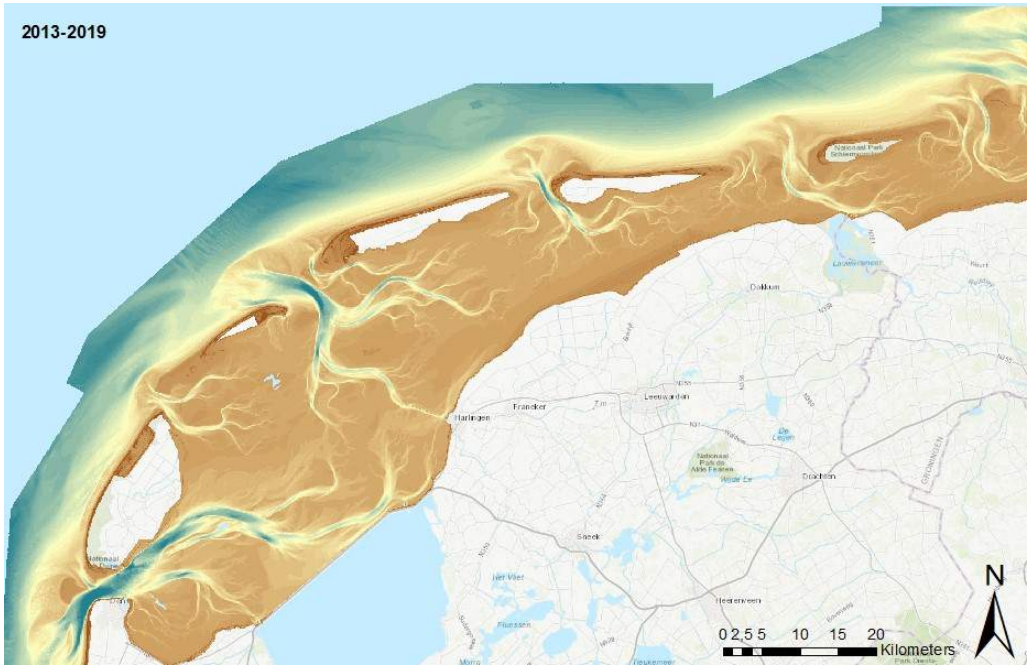

Figure 3.6: Bathymetry of the Dutch Wadden Sea for the years 2013-2019.

the position of the tidal watersheds. The definition of the hydrodynamic tidal watersheds is already better, but this is not applicable to the morphodynamic tidal watersheds. Basing the position of the morphodynamic tidal watersheds on the bed features is a more accurate representation definition wise. Even though the definition and exact method as described below are somewhat different to the other definitions and methods, it will not result in significantly more accurate positions of the morphodynamic tidal watersheds. The decisive benefit of basing the definition on the bed slope is that the positions of all watersheds can be determined consistently over the entire Dutch Wadden Sea. The method that enables this is described below.

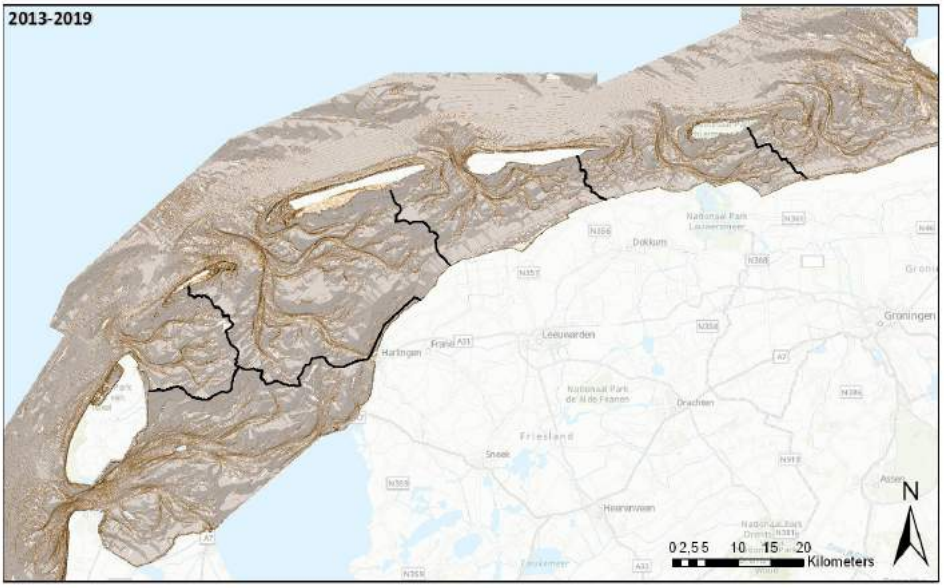

Figure 3.7: Map of the Dutch Wadden Sea and its morphodynamic tidal watersheds with bathymetry data for the years 2013-2019. The first layer shows the slope of the bed level in brown. The flow direction is indicated with the relief layer. The tidal watersheds are indicated with the black lines.

The maximum bed elevation and the minimum slope can be retrieved from bathymetry data (Deltares, 2021). Bathymetry data for the years 2013-2019 was used, as these maps together form the sixth measurement cycle in the Wadden Sea. The bathymetry of the Dutch Wadden Sea for the years 2013-2019 is shown in Figure 3.6. The map with which the position of the tidal watersheds will be determined consists of two layers: a map with the bed level slope at each point in the Wadden Sea, and a map with the flow direction in the basins. Only a map with the slope does not suffice, as the metadata does not reflect the bathymetry accurately enough to show the slopes in enough detail (Park, 2009). This was also shown by the results obtained with ArcGIS. The layer with the bed level slope was computed rather straightforward, as the program only determined the difference in the bed level height. This layer proved however insufficient on its own. The second layer, the one with the flow direction in the basins, needed more steps to obtain the map and required more computational effort. Namely three geoprocessing tools in ArcGIS were needed to derive the flow direction layer (ESRI, 2020). First, the flow accumulation was computed, where the tool calculated ”accumulated flow as the accumulated weight of all cells flowing into each downslope cell in the output raster” (ESRI, 2020). Pour points were then appointed to the cells with the highest accumulation. Finally, the flow direction was computed based on the accumulation in each cell. This resulted in the layer with the flow direction in the basins. The resulting map with both layers is shown in Figure 3.7. The watersheds were eventually drawn by hand. As the flow direction was determined on the basis of the slope, it can be assumed that the watersheds are indeed morphodynamic tidal watersheds.

3.2.2. Measurement Cycles

The method described above is a semi-automatic method. The maps are all derived from standard calculations in ArcGIS. Only the drawing of the watersheds is subjective to interpretation. This makes the method suitable for determining the position of the watersheds for previous measurement cycles,

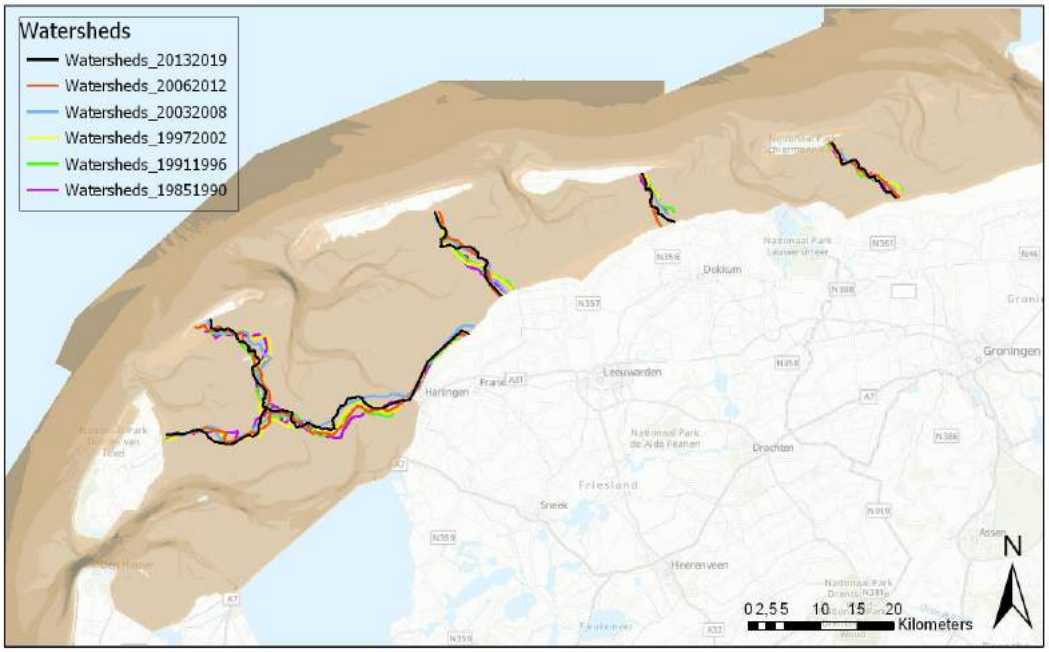

Figure 3.8: Map of the Dutch Wadden Sea and its morphological tidal watersheds determined for all 'vaklodingen' measurement cycles. Each colored line indicates the position of the tidal watershed for each measurement cycle.

as the method is relatively fast. If done for all the measurement cycles performed by Rijkswaterstaat (1985-1990, 1991-1996, 1997-2002, 2003-2008, 2006-2012 and 2013-2019), the result is Figure 3.8. The positions of the tidal watersheds in the Western Wadden Sea change more in the time period of the measurement cycles than the position of the tidal watersheds in the Eastern Wadden Sea. The tidal watershed between the Vlie and Marsdiep basins is migrating northward, whereas the watershed between the Marsdiep basin and the Eierlandse Gat migrates southward in the time frame of the six measurement cycles. This is in accordance with earlier research (Van Geer, 2007). The watershed between the Eierlandse Gat and the Vlie basin moves mainly in westward direction, which is in opposite direction of results from earlier research (Van Geer, 2007). In the Eastern Wadden Sea, the trend in earlier years was an eastward migration of the tidal watersheds (Elias et al., 2019). In Figure 3.8, the migration in the Eastern Wadden Sea is in the opposite direction, namely in westward direction. The time frame is too short to conclude whether or not this is a trend on its own.

3.2.3. Model Polygons

For determining the sediment sharing system of the Wadden Sea, one needs to have a division of the region into polygons. These polygons determine the division lines that will be used to assess the sediment transport between regions. As the interest lays particularly on the sediment transport over the watersheds, along the barrier islands, and through the inlets, only the basin and outer region polygons have to be determined. For the position of the tidal watersheds, the most recent position (measurement cycle 2013-2019) is chosen. As there exists no specific definition for the dividing lines along the coast, the position defined by (Elias, 2019) will be used. The resulting polygons are shown in Figure 3.9. The overall polygon formation follows from the method described above. The only difference is the cut-off of the Marsdiep basin at Harlingen instead of following the coastline for a while. This tidal watershed that follows the coastline is due to the presence of the Boontjes channel. As this only adds a small area to the Marsdiep when considering normal position of the watershed, and the coastline region here is not important for the sediment transport, it is added to the Vlie basin to form polygons with distinct cut-offs. The shown polygons in Figure 3.9 form the basis for the following research, and are named as follows: Marsdiep basin, Marsdiep coast, Eierlandse Gat basin, Eierlandse Gat coast, Vlie basin, Vlie coast, Ameland Inlet basin, Ameland Inlet coast, Frisian Inlet basin and Frisian Inlet coast.

The determined polygons as shown in Figure 3.9 are suitable to determine the surface area of the

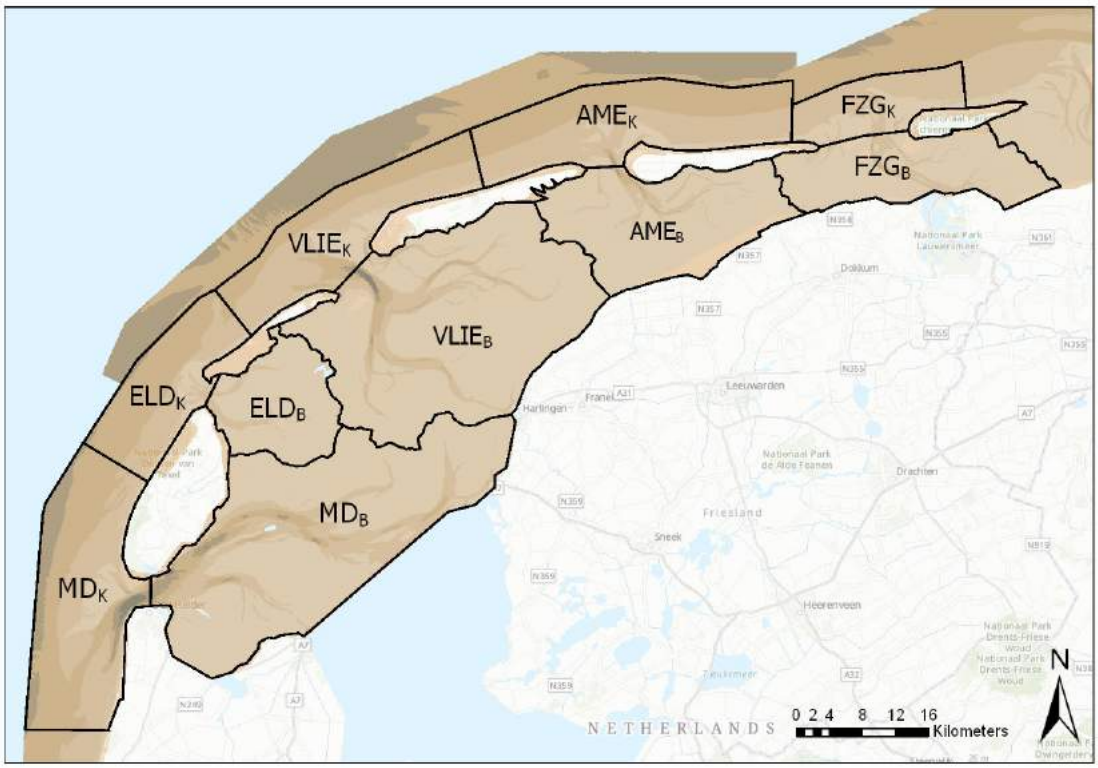

Figure 3.9: Map of the Wadden Sea with the polygons that form the basis for the subsequent research. The texts in the map are abbreviations for the known basins: MD = Marsdiep, ELD = Eierlandse Gat, VLIE = Vlie, AME = Amelandse Zeegat, FZG = Frisian Inlet. The lower score B indicates the back-barrier basins, and the lower score K indicates the coastal regions.

back-barrier basins. The determination of the surface areas was last done over 25 years ago (Louters & Gerritsen, 1994). A small shift in the position of the watersheds will likely also lead to a change in the distribution of surface areas. The polygons from Figure 3.9 are largely followed. The only difference is the course of the watershed between the Vlie and Marsdiep basin. For this watershed, the course indicated in Figure 3.8 is adopted to indicate the surface area as precise as possible. The new resulting areas, as well as the old ones from earlier research, are indicated in Table 3.2. The percentual change in surface area is also indicated in the table. The Eierlandse Gat basin has increased in surface area, whereas the Vlie and Marsdiep basin decrease in surface area. The decrease in surface area of the Marsdiep is different to the trend observed earlier (Dastgheib et al., 2008). The increase in surface area seems to have shifted to the Eierlandse Gat basin. The Ameland Inlet basin and the Frisian Inlet basin both increase in surface area, as well as the total surface area of the Dutch Wadden Sea. The difference in total surface area is a result of the use of different methods, a difference of 2.8% is sufficient to accept the new surface area values. The increase in surface area of the Ameland Inlet basin and the Frisian Inlet basin could likely also be attributed to this use of a different method.

Table 3.2: Old and new values for the surface area of each basin in the Dutch Wadden Sea, as well as the percentual change in basin surface area. The old values are retrieved from earlier research (Louters & Gerritsen, 1994).

Basin	$A_{b,new}$ (km^2)	$A_{b,old}$ (km^2)	ΔA
Marsdiep	702.1	712	−1.4%
Eierlandse Gat	177.7	153	+16.1%
Vlie	659.9	668	−1.2%
Ameland Inlet	322.3	309	+4.3%
Frisian Inlet	232.8	195	+19.4%
Total	2094.8	2037	+2.8%

4

Boundary Conditions

The modelling of the sediment transport pathways in SedTRAILS requires the selection of representative boundary conditions. The data from the year of 2017 is chosen, as the boundary conditions for this year are readily available in the WadSea FM model. The annual run results in a base case that indicate the residual discharges and sediment transport due to the tide. The base case is discussed in Section 4.1. No base case is available that includes the wave forcing, and developing such a base case is beyond the scope of this research. Two methods were developed to determine the representative tide: one for the morphological tide, and one for the hydraulic tide. The methods and the preferred representative tide are discussed in Section 4.2. The choice on the representative wind and wave conditions is discussed in Sections 4.3 and 4.4, respectively.

4.1. Base Cases

The sediment transport in the WadSea FM model is determined with the formulation of Van Rijn (van Rijn, 1993). To model the discharges and the total sediment transport due to the tidal forcing only, the imposed boundary conditions need to be adjusted. The water levels due to the tidal components can be determined accurately by performing a harmonic analysis. This analysis results in boundary conditions for the water levels that are only influenced by the tide. All effects of the wind are neglected. Neglecting the wind enables the close study of the dominant sediment transport patterns due to the tidal forcing only in the Wadden Sea. Running the model with the annual tidal forcing results in the schematisation of the transport patterns shown in Figure 4.2. The units of the mean residual discharges are converted from m^3/s to m^3 per tidal period to be compared to earlier research. The residual discharges correspond closely to the values found by (Duran-Matute et al., 2014), shown in Figure 4.1. Differences

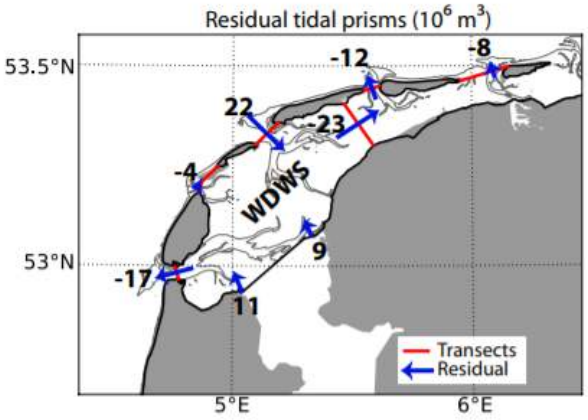

Figure 4.1: Average residual tidal prisms (10^6 m^3) and fresh water input per tidal period (10^6 m^3) through the Den Oever and Kornwederzand sluices (Duran-Matute et al., 2014). The included processes are tide and wind.

in residual discharge values between earlier research and this study are probably the result of annual variations. As the residual discharges are much smaller than the instantaneous discharges through the inlets ($O(10^9)$), the difference in residual discharges between this research and the earlier study is not significant. The discharge values are assumed sufficiently accurate compared to earlier research to continue with modelling the sediment transport patterns. The research on sediment transport values is more limited, especially regarding sediment transport over the tidal watersheds. However, some knowledge on the transport magnitude through the inlets is available. Figure 4.2 indicates a value for the residual sediment transport of 4.1 Mm^3/year in the Texel Inlet. Recent research estimates the import by the Texel Inlet somewhat lower at 1.9 Mm^3/year (Nolte et al., 2020). The value of 4.1 Mm^3/year is probably an overestimation of the residual sediment transport. The overestimation is likely a result of the exclusion of the Helderse Zeewering in the model, which is a common problem in sediment transport modelling in the Texel Inlet (Elias & van der Spek, 2006). Comparing multiple studies on the same inlets results in different values (Nolte et al., 2020; Elias & Bruens, 2012). From this the assumption is deduced that if the sediment transport values approach the values from earlier research at least in order of magnitude, the sediment transport modelling can be continued. As this is the case, the tidal base case is assumed sufficiently accurate.

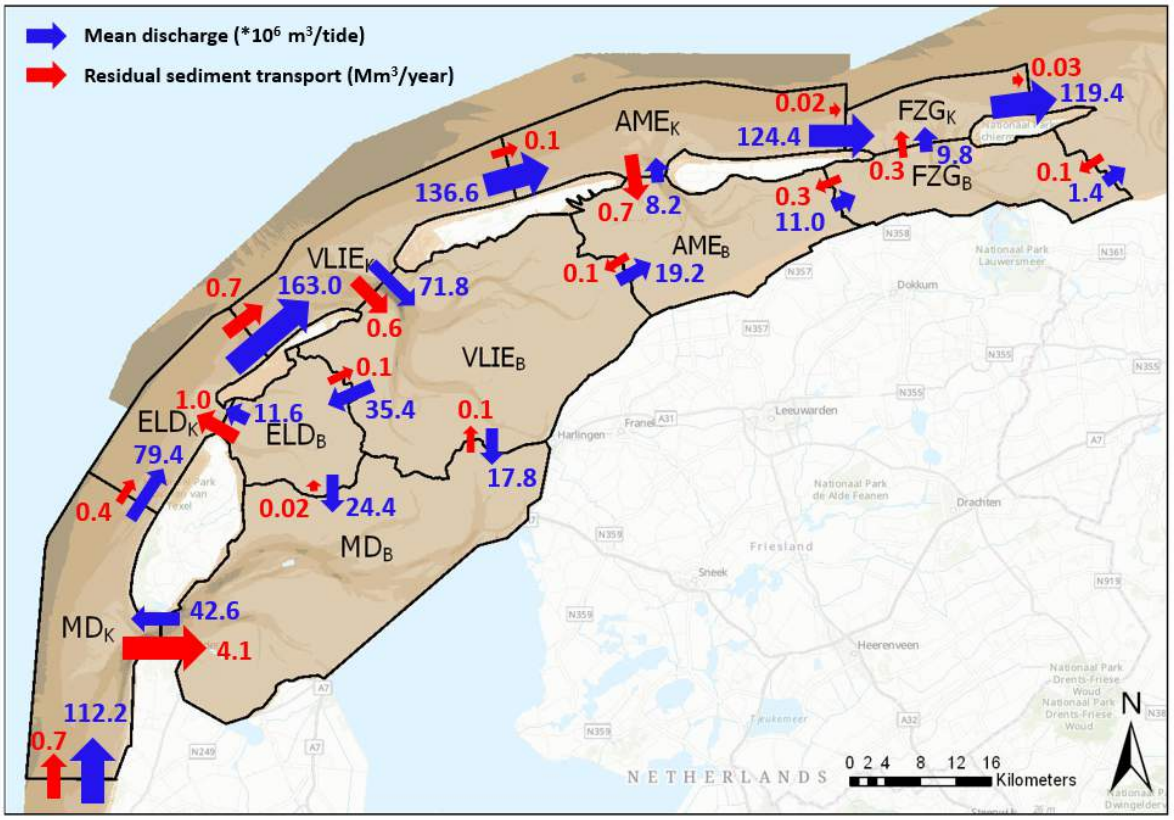

Figure 4.2: The mean residual discharge per tidal period and residual total sediment transport per year over the cross-sections of the defined polygons due to the annual tidal forcing for the year of 2017. The length and width of the arrows indicate the approximate magnitude of the transport volumes, whereas the values indicate the specific magnitude.

4.2. Representative Tide

The representative tidal period forms the basis of the research to which the representative wind and wave conditions are applied. Both the method for determining the morphological tide and the hydraulic tide are discussed in Sections 4.2.1 and 4.2.2, respectively. Even though the hydraulic tide is preferred over the morphological tide in this research, the method for the determining the morphological tide shows potential, and is thus included.

4.2.1. Morphological Tide

The morphological tide is the single tide that best represents the topographic changes, in this case the sediment transport patterns, that occur over a predetermined number of tides (Latteux, 1995). Determining the representative tide is an example of a data reduction scheme, which is necessary when assessing patterns on large-scale domains such as the Wadden Sea (Winter et al., 2006). When determining the morphological tide, one looks at the residual sediment transport due to the total hydrodynamic changes in the basins. Other methods make use of the total fluxes or sedimentation and erosion patterns, but as morphological changes are the result of the total fluxes and do not follow these fluxes at each moment in time, the annual residual sediment transport as an indication is preferred. The goal is to select the best performing tide of 2017, thus the sediment transport patterns due to each tide in that year need to be determined. As the largest transports occur in the tidal channels, these areas are the most interesting part of this analysis. Other parts can also show sediment transport, but these transports are expected to be significantly smaller than the transports in the channels. The mean annual sediment transport in the Texel Inlet is shown in Figure 4.3.

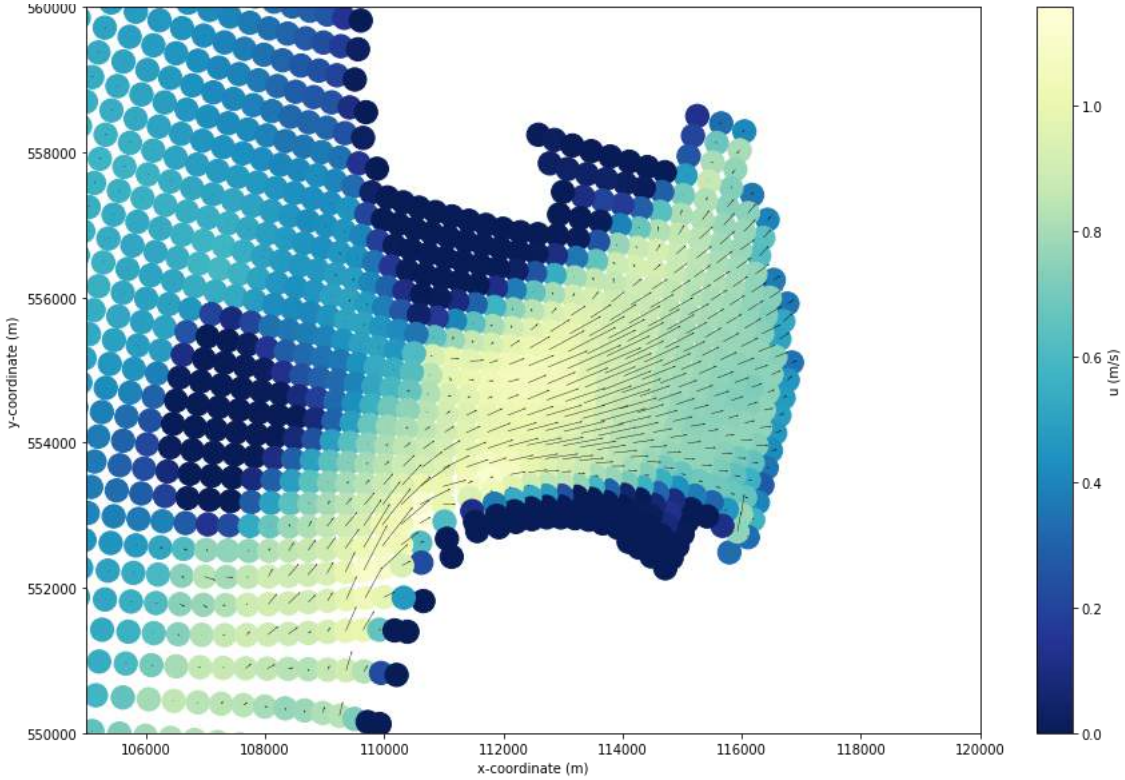

Figure 4.3: Mean annual sediment transport in the Texel Inlet for the year of 2017. The x- and y-axis show the coordinates in meters, and the vectors in the figure show the relative magnitude and direction of the transport at that specific location. The colored dots show the magnitude of the flow velocities, the colorbar at the right of the figure shows which color belongs to which value for the flow velocity.

The current method to determine the morphological tide is limited in the sense that the representative tide is determined for one single inlet instead for all inlets together. The scale of the Dutch Wadden Sea introduces a data set too large for the current scripts to comprehend, thus a choice has to be made on the inlet that is assumed to be normative. As the sediment transport volumes through the Texel Inlet are large compared to the other inlets (Elias, 2019), the Texel Inlet will be the main area for which the morphological tide is determined. The other channels will be checked later on to assess the magnitude and the direction of the transport patterns. The mean annual sediment transport through the Texel Inlet is shown in Figure 4.3. Here it can be seen that the sediment transport is represented by vectors at each predetermined location in the grid. The vectors show the relative magnitude and the direction of the transport. The next step is to determine an assessment of the transport vectors. One can choose to simply determine the difference between the mean annual transport and the transport

due to each tide and select the tide that generates the smallest difference. This will however impart a disproportionate significance on the small annual mean transport vectors and this will not the result in the best description of the mean annual transport through the Texel Inlet. Therefore, before determining the difference between the annual mean and the transport due to each tide, the normalised vector of the mean annual transport is determined. The general definition is given by Equation 4.1 (Jeffreys & Jeffreys, 1988).

$$\hat{u} = \frac{u}{|u|} \tag{4.1}$$

To obtain the normalised vector, the mean annual transport at each grid point is thus divided by the maximum value of the mean annual transport. This normalised vector then determines the weight of each vector to determine the mean difference between the mean annual transport and the transport due to each tide. Actually, the weighted arithmetic mean is thus determined, which general definition is given by Equation 4.2 (Price, 1972).

$$\overline{x} = \frac{\sum_{i=1}^{n} w_i x_i}{\sum_{i=1}^{n} w_i} \tag{4.2}$$

Once the mean difference for each tide is determined, the top five tides that perform the best compared to the annual mean can be selected. The last step is to visually assess these best performing tides on the direction of the vectors. The direction was not yet taken into account, and in addition to the magnitude of the sediment transport, the direction determines if one can simulate the sediment transport patterns that occur due to the annual tidal signal. The chosen morphological tide is shown in Figure 4.4. In this figure, it can be seen that the morphological tide accurately describes the patterns due to the annual tidal signal. Especially the large vectors are approximated well. Also, when assessing the sediment transport patterns in the other inlets for this particular tide, the magnitude and direction of the vectors agree well. A further assessment is described in Appendix C.

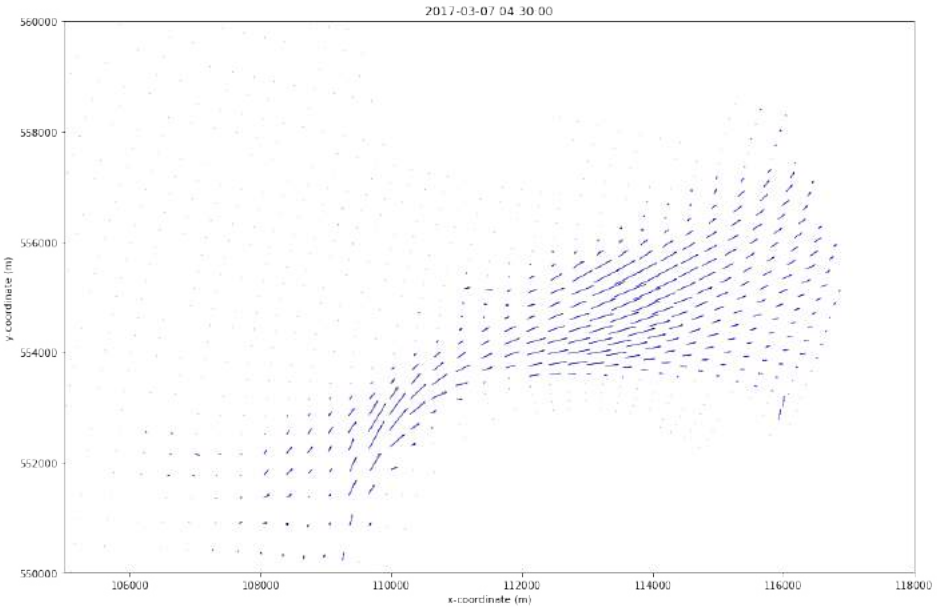

Figure 4.4: Mean annual sediment transport vectors (blue) and vectors of the chosen morphological tide (black). The x- and y-axis show the coordinates in meters. The title of the figure indicates the end date and time of the morphological tide. The figure enables the visual assessment of the performance of the morphological tide.

The method works and can determine the appropriate morphological tide for a given time period and tidal inlet. However, the method needs to be extended when it needs to determine the best morphological tide for a multiple inlet system. Each tidal inlet has its own morphological tide when determining the morphological tide per tidal inlet. Applying multiple morphological tides to the Wadden Sea model is not

possible, and the choice for one will result in unacceptable errors in the sediment transport in the regions of the other inlets. The current shortcomings of the method prevent it from being suitable for use on the scale of the Wadden Sea for now. Therefore, the hydraulic tide is chosen as the representative tide. The method for determining the hydraulic tide is described below.

4.2.2. Hydraulic Tide

The morphological tide determined above represents the condition for which the residual transports resemble the annual residual transports. However, as the residual transport will be especially low at the tidal watersheds, the morphological tide is not the optimum representation for the objective of the research. The total transports are much more interesting when looking at dividing lines, which brings us to the hydrodynamics of the model. The hydraulic tide is the tide that best resembles the discharge fluxes over prescribed transects within a given time period. The mean annual discharges over each dividing line of the predetermined polygons were already determined (Figure 4.2). The tide that best resembles the direction and the magnitude of these discharges, will be appropriate for modelling the total sediment transport. First, the chosen morphological tide was assessed on its performance of resembling the discharge patterns. It almost perfectly simulated the annual mean discharge at the Texel Inlet, which is as expected based on the good resemblance of the residual sediment transport patterns, but it did not perform as well at the other inlets and especially at the watersheds the direction of the flow was opposite of what was needed. Therefore, another tide had to be selected.

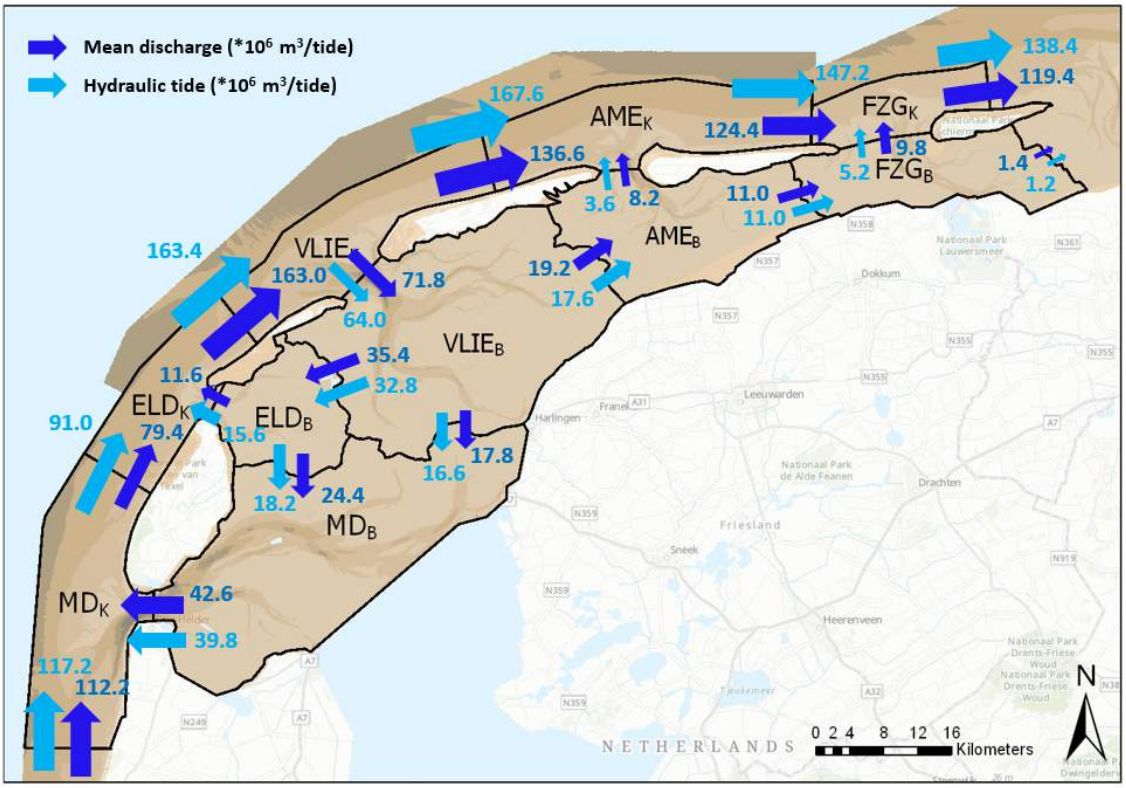

Figure 4.5: The mean annual residual discharge per tidal period and the discharge for the hydraulic tide over the cross-sections of the defined polygons for the year of 2017. The length and width of the arrows indicate the approximate magnitude of the exchange, whereas the values indicate the specific magnitude of each discharge flux.

For the determination of the morphological tide, the annual mean sediment transport vectors were scaled based on their magnitude. This was necessary as the very small vectors would otherwise influence the mean too much. For the discharges however, the difference in order of magnitude has a maximum of one. It therefore is not sensible to apply a normalised vector on the mean tidal discharges. Here, only the absolute difference between the tidal discharges and the annual mean of the discharges is determined. Then, the tide for which the difference was smallest, and the directions of the flow were

correct, was selected to be the hydraulic tide. The normalised deviation percentages were in the order of 5%, which means that it is a good representation of the annual mean. The selected hydraulic tide will be used to generate the results in SedTRAILS.

4.3. Representative Wind Condition

The representative hydraulic tide was determined in Section 4.2.2 by comparing the annual mean discharges through the transects with the discharges for each tide. To determine the representative wind condition however, another method will be applied. As the runs that are used to assess the influence of the wind contain the tide and wind forcing, either direct or indirect, no representative wind condition can be indicated. Therefore, the mean wind direction and the mean wind speed are determined with the Waterdata from the Vlieland measurement station (Rijkswaterstaat, 2017). The Vlieland measurement station is located at the coast of the barrier island, approximately in the middle of the coastline of the Wadden Sea and is not sheltered by the barrier island in the case of the dominant wind direction (southwest) in the Netherlands, which makes it more suitable than the Terschelling measurement station. The result is a mean wind direction of 201°N and a mean wind speed of 7.0 m/s. The mean wind direction is indicated in Figure 4.6, which shows that 2017 is not a representative year with regard to the wind direction. As this wind direction does not result in sheltered conditions by the Holland coast, it is still assumed a suitable representative wind condition. The representative wind condition is applied to the representative hydraulic tide. In reality, the specific representative wind condition and hydraulic tide will most likely not happen at the exact same moment in time. However, as the effect of the hydraulic tide is assessed separately, the effect of the representative wind condition can most likely be distinguished this way. In addition to the representative wind condition, the mean wind speed is also applied to the model with wind directions of 291°N and 21°N to assess the influence of the wind direction on the sediment transport patterns.

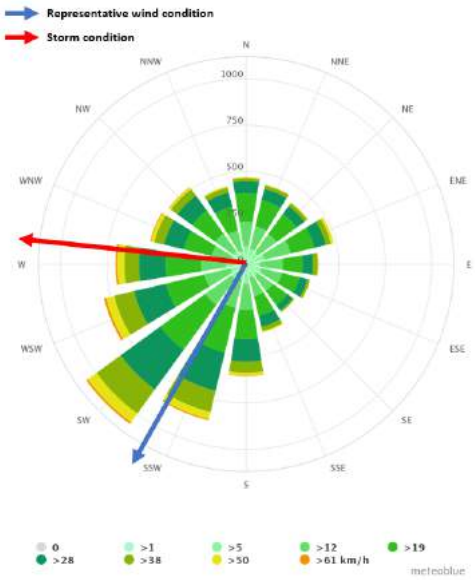

Figure 4.6: Mean wind climate at Vlieland. The figure shows the wind rose, which indicates that the southwest wind direction is dominant under mean conditions. The representative wind condition and the storm condition for 2017 are indicated by the blue and red arrows, respectively.

The entire wind data set from the year of 2017 is available, containing water level and wind condition recordings, which enables the selection of real time storm events. To select a northwestern storm, the maximum wind speeds from the northwestern quadrant were selected. The mean of these maximum wind speeds was determined, as well as the accompanying wind direction, which resulted in a west-northwestern storm with a mean wind speed of 22.0 m/s from 274°N. The wind direction during this storm is indicated in Figure 4.6. Another storm was selected, better known as Storm Sebastian. This storm in particular caused damage in Germany, thus it is interesting to see if this storm had more impact on the sediment transport then the other selected storm. The mean wind speed during this event was

slightly lower, namely 18.0 m/s (KNMI, 2017). Comparing the storm events to the representative wind condition will likely show the influence of wind intensity on the sediment transport patterns in the system.

4.4. Representative Wave Condition

The implementations of waves in the WadSea FM model requires the coupling of the Delft3D-FM Flow model and a new D-Waves model, which is actually a SWAN model. The set-up of the SWAN model is discussed in Section 4.4.1. The representative wave conditions at the boundaries of the SWAN model are discussed in Section 4.4.2.

4.4.1. Model Setup

The SWAN model consists of two grids overlapping each other, with both their own bathymetry layer. The grid setup of the model is shown in Figure 4.7. The larger grid encompasses a very large area, with its southern boundary extending far into the area of the Dutch coast. The result is that the grid size is quite large. The smaller grid looks more like the grid of the flow model, and has a finer grid size than the larger grid. This should result in more detail at the coast of the barrier islands and in the back-barrier basins. The grid is still too coarse to resolve waves on an individual level, but this setup should be a good starting point to indicate the influence of waves on the large-scale sediment transport patterns. The bathymetry follows the grid points of both grids. The grid is fine enough to distinguish the main tidal channels in the bathymetry plot, but some transitions are hardly visible. Especially in the back-barrier basins this could lead to over-/underestimation of the influence of the waves on the sediment transport. The model deals only with stationary waves and the default settings of the SWAN model were chosen. The default settings will likely give reasonable results of the sediment transport patterns. Investigating the influence of turning on or off specific settings is beyond the scope of this research.

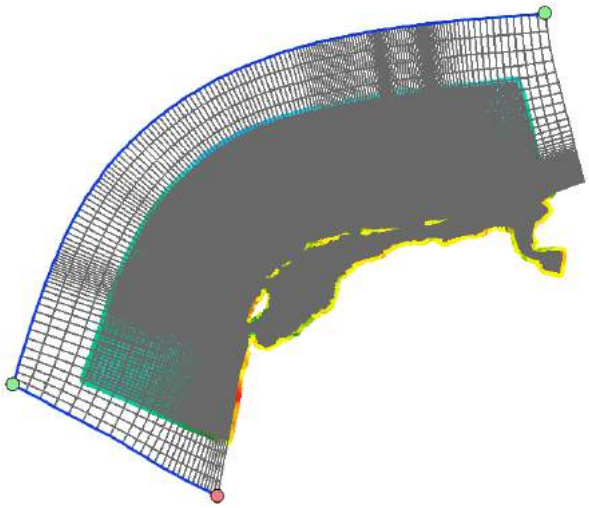

Figure 4.7: Grid setup of the D-Waves model. The larger grid, indicated by the grey grid, encompasses a larger area with fewer grid cells, and extends further into the North Sea. The smaller grid, indicated by the colored grid, has a finer grid size and brings therewith more detail to the Wadden Sea and its coastal regions. The model has two boundaries: the largest one on the northwest side and one on the southwest side.

4.4.2. Representative Boundary Conditions

To determine the representative wave conditions, measurements on wave heights at local measurement buoys were used (Rijkswaterstaat, 2017). The Eierlandse Gat buoy was chosen, as this buoy has the preferred orientation with respect to the dominant wave direction. Assumed here is that the waves come from the same direction as the wind. The Eierlandse Gat buoy is situated outside of the ebb-tidal delta, but is still in shallow water compared to the water depths in the North Sea at the position of the outer boundary of the larger grid. The chosen buoy could result in some overestimation of the height of the waves that reach the coast, as the waves will increase in height due to shoaling. The represen-

tative wave height was chosen to be the mean of the wave data set at the Eierlandse Gat buoy, even though the mean wave direction is dominantly southwest instead of south-southwest (Rijkswaterstaat, 2017). This results in a representative wave height H_{m0} of 1.15 m with a representative wave period T_{m02} of 4.50 s and wave direction of 201°N. Preferred was to implement the peak period T_p instead of the mean period T_{m02}, but the peak period data was not available for the Eierlandse Gat buoy. The relation between T_p and T_{m02} is estimated at $T_p = 1.30*T_{m02}$ (van der Meer et al., 2000), but here they are assumed to be equal. For the storm condition, the maximum wave heights were selected in the northwestern quadrant, and from this the mean was determined. The accompanying wave period T_{m02} determined the period of the storm waves at the boundaries. The storm condition has a wave height Hm_{m0} of 6.63 m, a wave period T_{m02} of 8.24 s and a wave direction of 274°N. These representative and storm conditions were also applied to the other runs, no new wave conditions were determined. The only adjustment was the wave direction.

5

Results

The results for the sediment transport pathways are determined with SedTRAILS. The model is a post-processing tool that visualizes the sediment pathways based on the sediment transports generated through van Rijn (van Rijn, 1993). The length of the pathways depends on the modelling period and acceleration factor. The SedTRAILS results are assessed on the Wadden Sea scale and the individual inlet scale. On the Wadden Sea scale, mainly the alongshore sediment transport patterns and the sediment transport over the tidal watersheds are discussed. On the individual inlet scale, the exchange between ebb-tidal delta and back-barrier basin, and the transport patterns in the ebb-tidal delta, inlet and back-barrier basin are assessed for each inlet. Transport patterns on the Wadden Sea scale are discussed in Section 5.1, and transport patterns on the inlet scale are distinguished in Section 5.2. A summary of all results is given by Section 5.3, as well as a conceptual model of the transport patterns.

5.1. Wadden Sea Scale

Sediment transport patterns on the scale of the Dutch Wadden Sea mainly include alongshore transport in the coastal zones and exchange of sediment between the back-barrier basins. The transport patterns in the system of each inlet are discussed in more detail in Section 5.2. The sediment transport patterns for both representative and storm conditions are distinguished, as these are very different from one another. The results for the representative conditions are discussed in Section 5.1.1, and the results for the storm conditions are discussed in Section 5.1.2.

5.1.1. Representative Conditions

The effect of the hydraulic tide on the sediment transport patterns on the scale of the Wadden Sea is assessed first. The large-scale sediment transport patterns are shown in Figure 5.1. The patterns resemble the tidal base case given by Figure 4.2. The Texel Inlet imports sediment, whereas the Eierlandse Gat and Vlie Inlet export sediment. For the Ameland Inlet and Frisian Inlet, the transport direction is not as clear, and is further assessed in Section 5.2. Net alongshore sediment transport near the barrier islands is in northeastern direction, with significant pathway lengths compared to the other pathways in the system. The significant pathways indicate an alongshore transport pattern due to tidal forcing. The net alongshore transport is especially significant in the outer coastal regions. Recent research indicates that the tidal boundary layer velocities can be significant in the outer coastal regions (Amador et al., 2020). Small variations in ebb and flood velocities could therefore lead to a significant net sediment transport. At Ameland, the alongshore transport is insignificant. Near Terschelling, the sediment transport pathways are also shorter than the pathways along Texel and Vlieland. The insignificant sediment transport at Ameland and the significant alongshore sediment transports near the other barrier islands agree with the tidal base case. The phenomenon could be explained by the position of the amphidromic point and the tidal propagation along the coast. The tidal propagation is obstructed by the presence of the ebb-tidal deltas, to a greater extent by the Vlie Inlet and Ameland Inlet ebb-tidal deltas than by the Texel Inlet and Eierlandse Gat ebb-tidal deltas. On the downdrift side of the ebb-tidal deltas, lee zones are created where the tidal flow is smaller. The result could be smaller sediment transport pathways. At the tidal watersheds, the transport pathways are small.

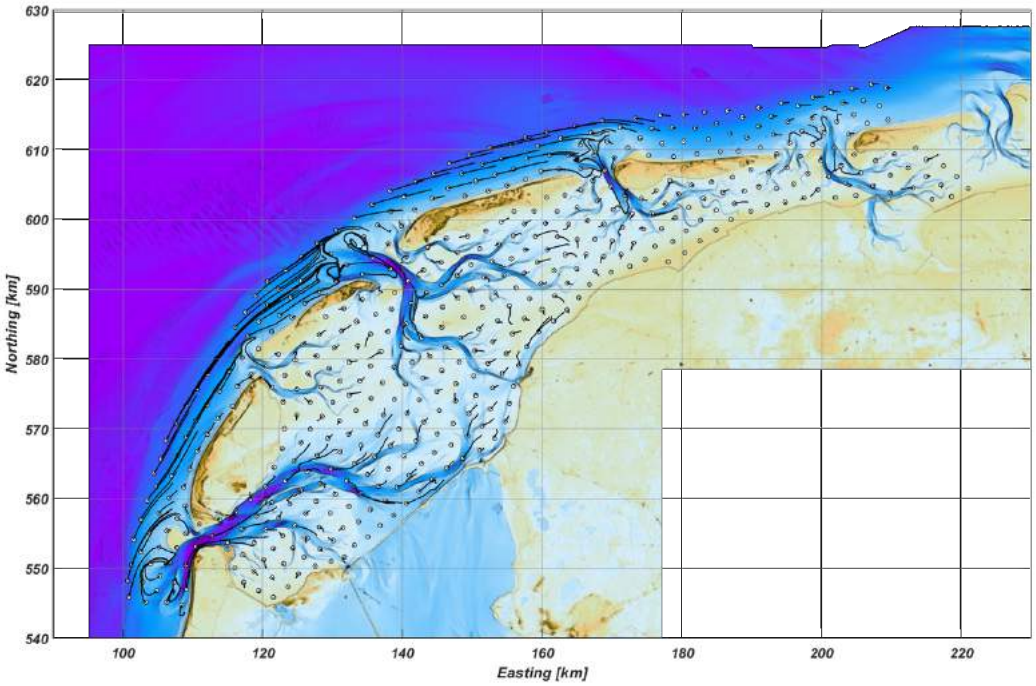

Figure 5.1: Large-scale sediment transport pathways forced by the representative hydraulic tide of 2017. The white circles indicate the starting position of the individual particles after placement in the system. The black lines indicate the pathways of the sediment particles. To obtain these particular pathways, an acceleration factor of 100 and a modelling period of 600 days were used.

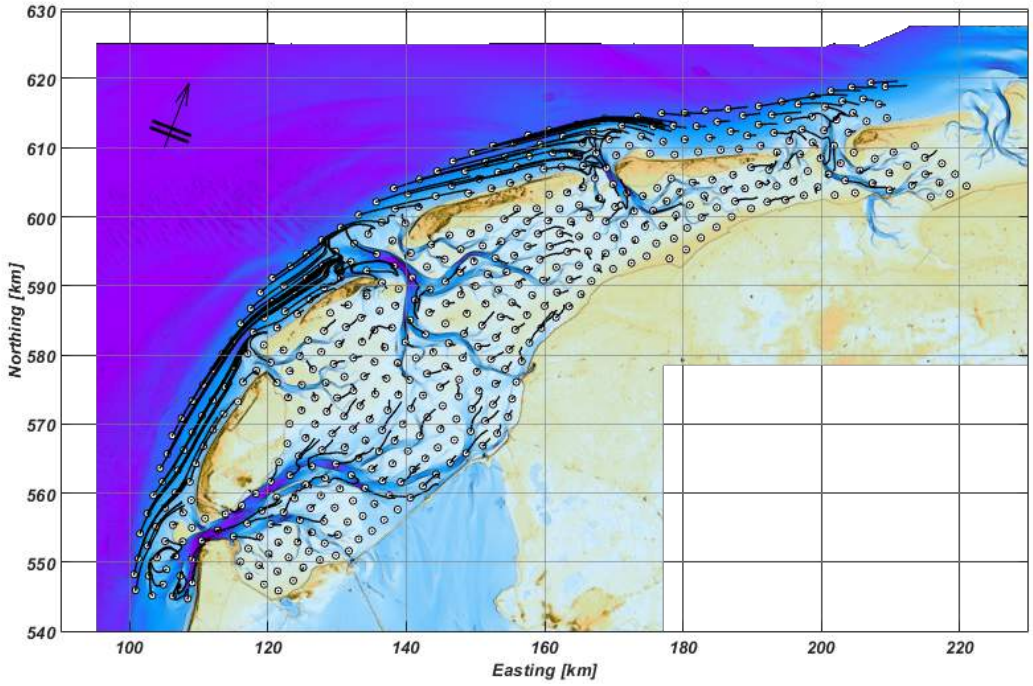

Figure 5.2: Large-scale sediment transport pathways forced by the hydraulic tide and the representative wind condition for the year of 2017 (U = 7.0 m/s, Dir = 201°N). The white circles indicate the starting position of the individual particles after placement in the system. The black lines indicate the pathways of the sediment particles. To obtain these particular pathways, an acceleration factor of 100 and a modelling period of 600 days were used.

Adding the representative wind condition to the system results in the sediment transport pathways shown by Figure 5.2. The length of the alongshore particle pathways increases under wind forcing, especially near the barrier islands. Near the islands the water depth is limited, and thus the wind-induced current is strongest here. The increase of the pathways near Texel and Vlieland is strongest, as the other barrier islands shelter their coastal zones from the representative wind condition. The alongshore sediment transport in the outer coastal region of Ameland is enhanced, although these pathways are still small compared to the other net alongshore transports. Generally, sediment particles present in the coastal regions become less trapped in the circulation patterns of the ebb-tidal deltas that are present under tidal forcing alone. Rather, the particles are transported further along the barrier islands. The longer pathways are the result of higher flood velocities when considering the representative wind condition, as shown in Figure 5.3. Applying other wind conditions, with the same intensity but a different wind direction, does change the flood velocities and therefore the net sediment transport in the coastal regions. This is also the case for the transport patterns over the tidal watersheds in the back-barrier basins. Figure 5.2 shows that the transport pathways over the tidal flats become longer under the forcing of the representative wind conditions. As the pathways become longer, the net sediment transport over the tidal watersheds increases. However, wind conditions with wind directions other than the representative wind direction will change the net sediment transport patterns in the back-barrier basins. Especially wind directions in the northeastern quadrant will counteract the transport patterns over the tidal flats. SedTRAILS results from other wind conditions are shown in Appendix D.

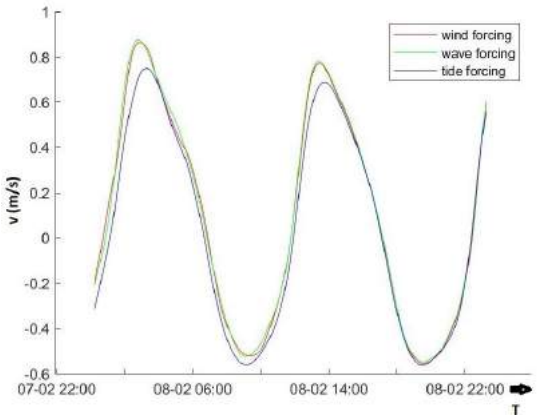

Figure 5.3: Flow velocities at the transect perpendicular to the coast of Vlieland in the year of 2017. The legend assigns each graph to the particular forcing condition.

The effect of waves on the large-scale sediment transport patterns is most apparent in the transport pathways near the coast of the barrier islands. The sediment transport pathways are shown in Figure 5.4. The length of the pathways in the outer regions of the coastal zone does not change, which is as expected based on Figure 5.3, but near the beaches the length of the pathways does increase. The lengthened pathways are probably the result of wave breaking in the surf zone, which enhances the nearshore current. The influence of incorporating wave forcing near the tidal watersheds is small, but not insignificant. The dominant transport direction in all back-barrier basins becomes northeastward, which forces a net sediment transport over all tidal watersheds. The amount of sediment that is brought in suspension can not be deduced from the SedTRAILS results.

5.1.2. Storm Conditions

In addition to representative forcing conditions, also the influence of storm conditions on the large-scale sediment transport patterns can be assessed. Tidal forcing does not change under storm conditions, but wind and wave forcings do. The results from a typical northwestern storm are shown in Figure 5.5. The figure includes tidal, wind and wave forcing. The results from tidal and wind forcing only are presented in Appendix D. The patterns for the storm condition are very different from the patterns under representative conditions. The sediment transport pathways along the barrier islands are significantly longer, especially at Ameland and Schiermonnikoog. Instead of a highly varying sediment transport pattern field, the main transport direction is now eastward. Most pathways in the coastal zone are

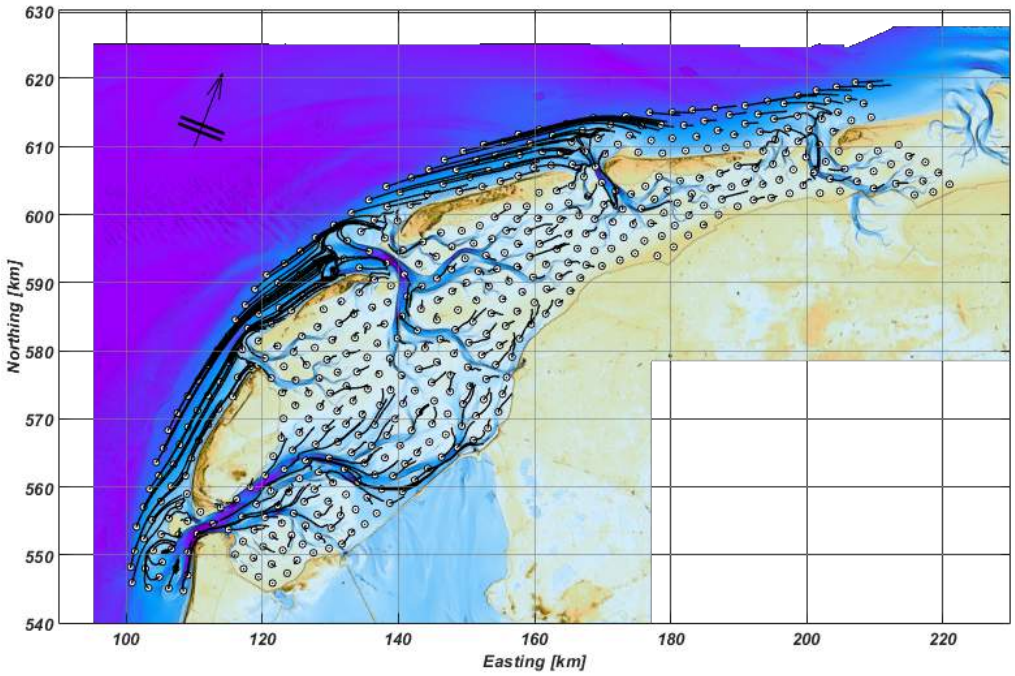

Figure 5.4: Large-scale sediment transport pathways forced by the hydraulic tide, the representative wind condition for the year 2017 (U = 7.0 m/s, Dir = 201°N) and the assumed representative wave condition (H_{m0} = 1.15 m, T = 4.50 s, Dir = 201°N). The white circles indicate the starting position of the individual particles after placement in the system. The black lines indicate the pathways of the sediment particles. To obtain these particular pathways, an acceleration factor of 100 and a modelling period of 600 days were used. The arrow indicates the wind and wave direction.

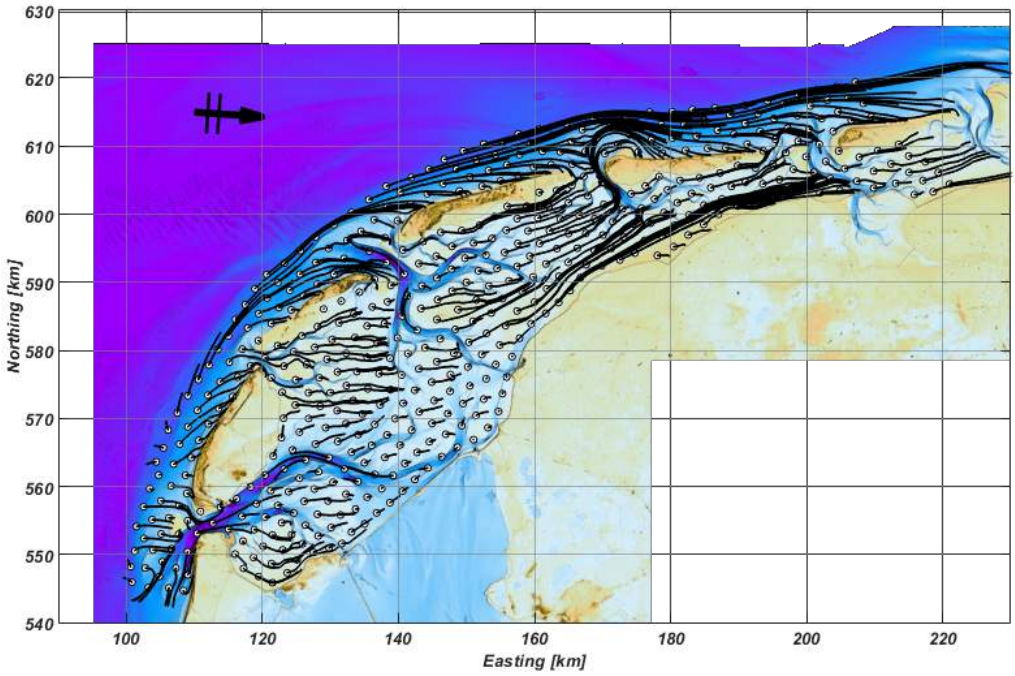

Figure 5.5: Large-scale sediment transport pathways forced by the hydraulic tide, the maximum storm conditions in the year 2017 (U = 22.0 m/s, Dir = 274°N) and the assumed maximum wave conditions (H_{m0} = 6.63 m, T = 8.24 s, Dir = 274°N). The white circles indicate the starting position of the individual particles after placement in the system. The black lines indicate the pathways of the sediment particles. To obtain these particular pathways, an acceleration factor of 10 and a modelling period of 200 days were used. The arrow indicates the wind and wave direction.

deflected to the coast of the barrier islands, which increases the cross-shore transport. The deflection of the pathways is caused by the wave forcing, which indicates the importance of the waves on the redistribution of sediment in cross-shore direction during storm conditions. The net sediment transport over the tidal watersheds increases significantly, especially in the Eastern Wadden Sea. The sediment transport pathways are longest at the tidal flats. The length of the pathways may not be representative for real time conditions, as storm conditions generally last only a few hours up until a day. The pathways indicated in Figure 5.5 represents time scale much longer than that. However, they do indicate the large-scale sediment transport patterns that may occur under storm conditions, which are very different from representative forcing conditions.

5.2. Inlet Scale

Sediment transport patterns on the scale of the individual inlets are discussed in more detail. The dynamics of the ebb-tidal deltas, the transport directions in the inlets and the dynamics in the back-barrier basins are of general interest in this section. As for the transport patterns on the scale of the Wadden Sea, all forcing conditions are considered. The Texel Inlet, Eierlandse Gat, Vlie Inlet, Ameland Inlet and Frisian Inlet are discussed in Sections 5.2.1, 5.2.2, 5.2.3, 5.2.4 and 5.2.5, respectively.

5.2.1. Texel Inlet

The SedTRAILS results for the different forcing conditions in the Texel Inlet are shown in Figure 5.6. When forced by the hydraulic tide only (Figure 5.6a), the Texel Inlet imports sediment, especially near the Den Helder. Near Texel, the transport direction seems to result in export. This observation corresponds to field data (Elias, 2006). In the back-barrier basin, the Marsdiep transports sediment mainly

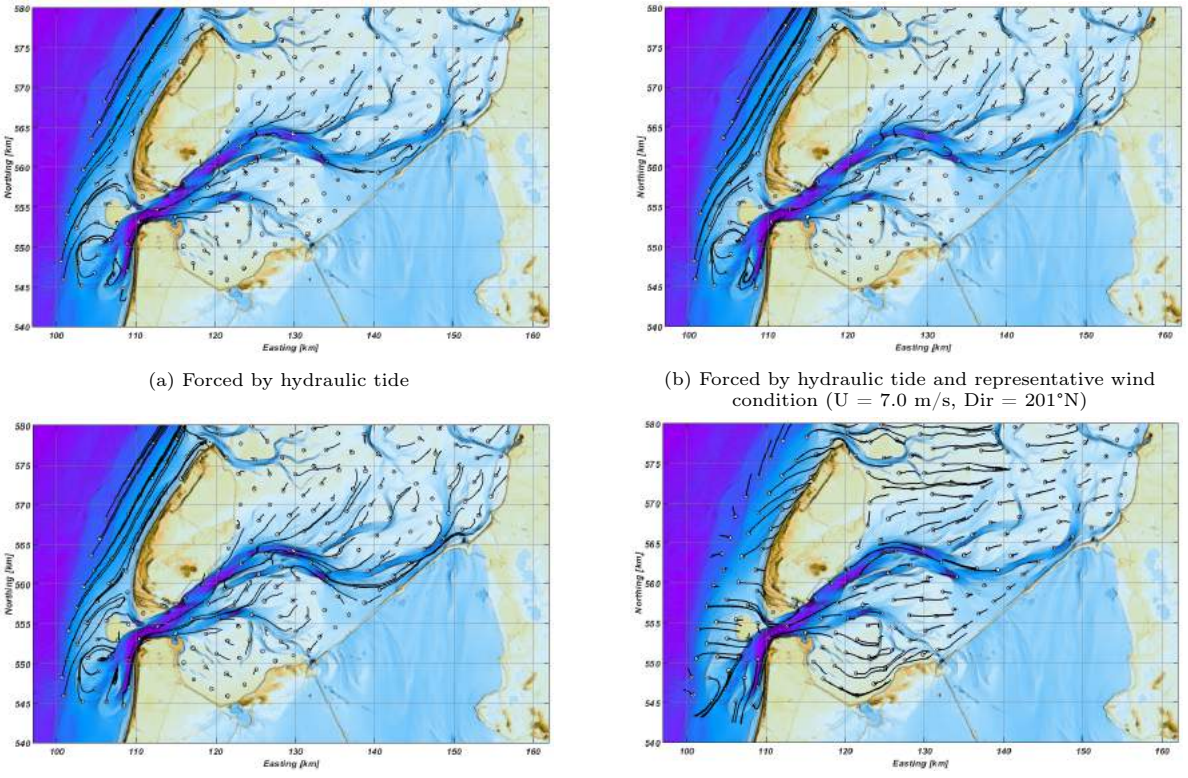

(a) Forced by hydraulic tide

(b) Forced by hydraulic tide and representative wind condition (U = 7.0 m/s, Dir = 201°N)

(c) Forced by hydraulic tide, representative wind condition (U = 7.0 m/s, Dir = 201°N) and representative wave condition (H_{m0} = 1.15 m, T = 4.50 s, Dir = 201°N)

(d) Forced by the hydraulic tide, the maximum storm condition (U = 22.0 m/s, Dir = 274°N) and the maximum wave condition (H_{m0} = 6.63 m, T = 8.24 s, Dir = 274°N)

Figure 5.6: Large-scale sediment transport pathways in the Texel Inlet system. The sub-caption indicates the specific forcing condition. The white circles indicate the starting position of the individual particles after placement in the system. The black lines indicate the pathways of the sediment particles. To obtain these particular pathways, an acceleration factor of 100 and a modelling period of 600 days were used, except for Figure 5.6d, here an acceleration factor of 10 and a modelling period of 200 days were used.

inward. The net sediment transport in the shallower parts of the basin is predominantly in northeastern direction. The exception is the tidal flat near Noord-Holland, where the net sediment transport at the tidal flats is in southern direction. The ebb-tidal delta of the Texel Inlet shows circulation patterns, especially at the southern side of the Noorderhaaks shoal. The sediment particles in the circulation seem to accumulate in front of the Noorderhaaks. At the northern side of the shoal, the pathways are deflected towards the inlet. Applying the representative wind condition to the system results in the sediment transport pathways indicated by Figure 5.6b. The dynamics in the inlet itself do not change; the Den Helder side imports sediment, whereas the Texel side exports sediment. The circulation patterns in front of the Noorderhaaks shoal are still present, but the deflection of the pathways towards the inlet at the northern side of the shoal is no longer present under wind forcing. The most changes due to wind forcing occur in the back-barrier basin. In the shallower parts of the basin and at the tidal flats, the transport direction is roughly the same and the pathways are somewhat longer. In the Marsdiep channel however, the variation in transport direction increases. Along the Lutjeswaard, the transport direction is outward instead of inward. Wave forcing (Figure 5.6c) increases the length of the pathways in the back-barrier basin significantly. All pathways are directed inward under wave forcing, and over time this will result in the import of considerable amounts of sediment. The sediment demand of the Marsdiep basin was already observed in earlier research (Elias et al., 2012). The dynamics in the Texel Inlet remain the same under wave forcing, as do the dynamics in front of the Noorderhaaks shoal. Wave forcing increases the sediment transport at the ebb-tidal delta of the Texel Inlet. The deflection of the pathways towards the inlet reappears under wave forcing. Evidently, the combination of wind and waves is important for the morphology of the ebb-tidal delta of the Texel Inlet. The storm condition changes the sediment transport pathways significantly. The Texel Inlet imports sediment over the entire cross-section. The pathways on the tidal flats increase significantly, whereas in the sub-littoral zone, the increase in pathway length is limited. The Marsdiep channel transports sediment outward, towards the inlet. The outward transport indicates a return flow due to wind set-up. The circulation patterns in the ebb-tidal delta of the Texel Inlet disappear under storm conditions. Pathways on the northern side of the Noorderhaaks shoal are deflected towards the inlet. Pathways on the southern side of the shoal are deflected southward towards the Holland coast.

5.2.2. Eierlandse Gat

The SedTRAILS results for the Eierlandse Gat are shown in Figure 5.7. Tidal forcing alone (Figure 5.7a) results in export by the Eierlandse Gat, both at the Texel and Vlieland side of the channel. The export of sediment by the Eierlandse Gat has been reported earlier (Elias, 2019; Wang, 2018). The sediment transport pathways in the back-barrier basin are generally outward directed, except for the pathways close to the tidal watersheds. The opposite directed transports create a virtual diverging line in the back-barrier basin. The dynamics in the ebb-tidal delta of the Eierlandse Gat are limited, sediment particles exported by the inlet are transported alongshore Vlieland by the current in the coastal region. No circulation patterns are present in the ebb-tidal delta. The pattern that is present in the ebb-tidal delta under tidal forcing alone, remains under wind forcing (Figure 5.7b). The pathways through the inlet are also approximately the same when adding wind forcing to the system. On the Vlieland side of the inlet, the pathways are somewhat longer, but on the Texel side, the pathways remains the same. The particle pathways under wind forcing are longer in the back-barrier basin, especially at the shallow tidal flats. Instead of a diverging line, the patterns under wind forcing are highly variable, with a general northeastern transport direction. Applying wave forcing has no significant effect on the sediment transport patterns in the Eierlandse Gat system (Figure 5.7c). The sediment transport along the barrier islands increases, but this has no effect on the patterns in the ebb-tidal delta and the inlet. Sediment particles are exported by the inlet and are transported alongshore once they reach the ebb-tidal delta. The transport direction of the sediment pathways in the back-barrier remains the same, the only difference is the slight elongation of the pathways at the tidal flats. Storm conditions do have a significant effect on the sediment transport patterns in the Eierlandse Gat (Figure 5.7d). Especially in the ebb-tidal delta and inlet, the patterns are very different from patterns under representative conditions. Instead of transporting sediment particles alongshore Vlieland, particles that reach the ebb-tidal delta are deflected towards the inlet. The inlet imports sediment instead of exporting it, and the pathways follow the coastline of the barrier islands closely in the inlet. The sediment transport pathways also increase significantly in the back-barrier basin. Most pathways are in eastern direction, which is downwind of the dominant wind direction during a typical storm. The Eierlandse Gat system shows more variability

between representative and storm conditions than the Texel Inlet system. The transport direction in the ebb-tidal delta and inlet of the Eierlandse Gat system is counteracted by the storm conditions, which is not the case for the Texel Inlet system.

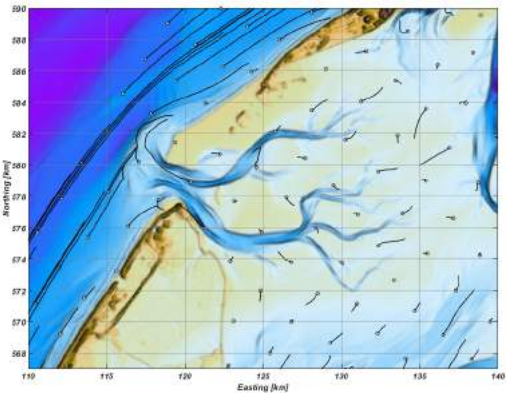

(a) Forced by the hydraulic tide

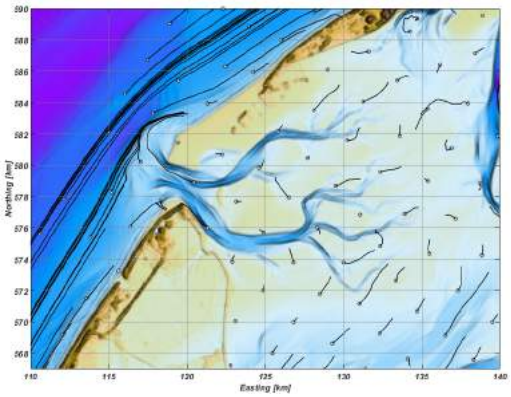

(b) Forced by hydraulic tide and representative wind condition (U = 7.0 m/s, Dir = 201°N)

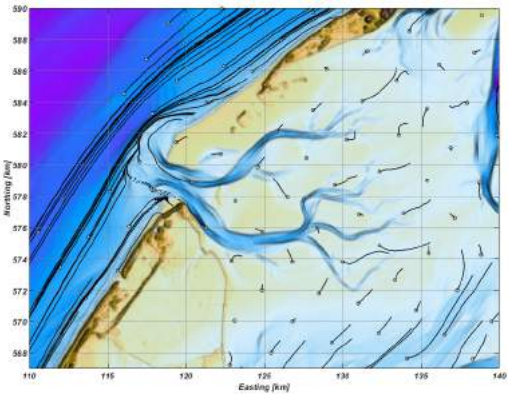

(c) Forced by hydraulic tide, representative wind condition (U = 7.0 m/s, Dir = 201°N) and representative wave condition (H_{m0} = 1.15 m, T = 4.50 s, Dir = 201°N)

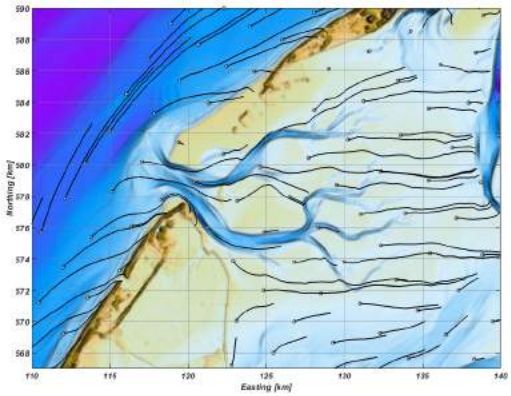

(d) Forced by the hydraulic tide, the maximum storm condition (U = 22.0 m/s, Dir = 274°N) and the maximum wave condition (H_{m0} = 6.63 m, T = 8.24 s, Dir = 274°N)

Figure 5.7: Large-scale sediment transport pathways in the Eierlandse Gat system. The sub-caption indicates the specific forcing condition. The white circles indicate the starting position of the individual particles after placement in the system. The black lines indicate the pathways of the sediment particles. To obtain these particular pathways, an acceleration factor of 100 and a modelling period of 600 days were used, except for Figure 5.7d, here an acceleration factor of 10 and a modelling period of 200 days were used.

5.2.3. Vlie Inlet

The results for the Vlie Inlet are shown in Figure 5.8. The ebb-tidal delta of the Vlie Inlet is highly dynamic under tidal forcing only (Figure 5.8a). The alongshore transport at Terschelling is therefore limited. At the Vlieland side of the inlet, particles are first transported inward. However, in the middle of the channel an outward directed flow exports the sediment particles and transports them towards the ebb-tidal delta. The general transport direction in the inlet is an export of sediment, which is in contradiction with Figure 4.2, the tidal base case. The small import given by the tidal base case is probably due to import movement of the pathways at the Vlieland side of the inlet, as the base case only takes the mean transport direction into account. The limited number of particles in the inlet could also explain the difference. The main tidal channel, when situated in the back-barrier basin, predominantly transports sediment inward. At the shallow parts of the basin, the general transport direction is also inward, but the direction of the pathways is more variable than in the tidal channels. The pathways in the back-barrier basin elongate under wind forcing (Figure 5.8b). Pathways in southwestern direction under tidal forcing alone are counteracted by the representative wind condition. The general transport direction in the main tidal channels is still inward, but some pathways are outward directed under wind forcing. The phenomenon of outward directed transport has no clear explanation. On the

Terschelling side of the inlet, the channel exports sediment. On the Vlieland side of the inlet however, sediment particles are first imported, then exported by the flow in the middle of the channel, and then follow the circulation pattern in the ebb-tidal delta that transports them along the tail of Vlieland into the back-barrier basin. The circulation pattern in the outer regions of the ebb-tidal delta disappears under wind forcing. Particles exported by the inlet are transported along the barrier islands in the outer edge of the coastal zone. The sediment transport patterns in the back-barrier basin remain largely the same when applying wave forcing to the system (Figure 5.8c). The transport pathways are elongated, especially near the smaller tidal channels, but the transport directions are approximately equal compared to the direction under tidal and wind forcing only. The import of sediment by the inlet along the tail of Vlieland disappears under wave forcing, and the inlet dominantly exports sediment when considering representative conditions. In the ebb-tidal delta, the pathways are more deflected towards the coast. The sediment particles are transported along the coast, and other than under wind forcing alone, the pathways are situated more closely to the coast. The storm conditions change especially the transport dynamics in the inlet (Figure 5.8d). Both at the Vlieland and Terschelling side of the inlet, the inlet imports sediment. Sediment is exported in the middle of the channel, but these pathways are deflected in the ebb-tidal delta and deflect towards the inlet on the Terschelling side. Therefore, during storm conditions the Vlie Inlet will predominantly import sediment instead of exporting it. The circulation patterns almost fully disappear and the alongshore transport is maintained under storm conditions. The outward transport by the tidal channels is enhanced, whereas the pathways on the tidal flats are elongated and are directed downwind. The longest transport pathways are present in the shallow areas of the back-barrier basin, where wind and waves have the most influence.

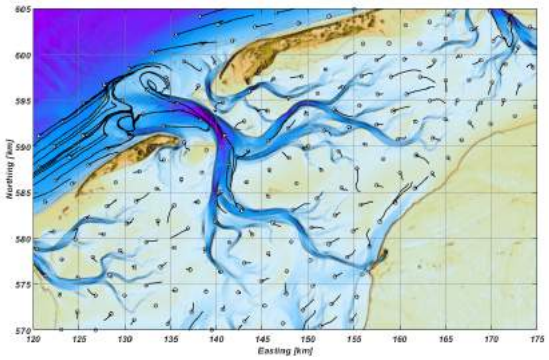

(a) Forced by the hydraulic tide

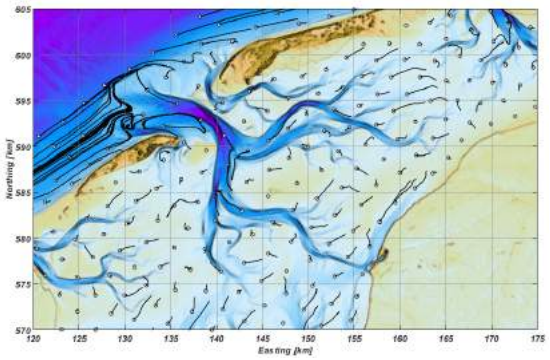

(b) Forced by hydraulic tide and representative wind condition (U = 7.0 m/s, Dir = 201°N)

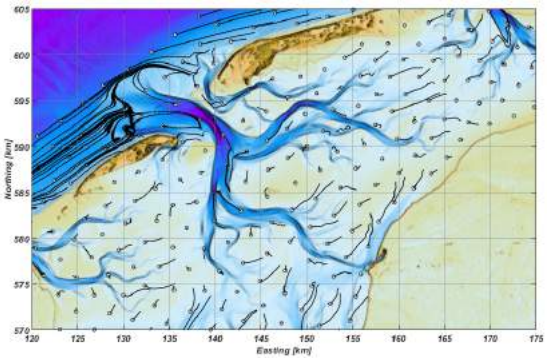

(c) Forced by hydraulic tide, representative wind condition (U = 7.0 m/s, Dir = 201°N) and representative wave condition (H_{m0} = 1.15 m, T = 4.50 s, Dir = 201°N)

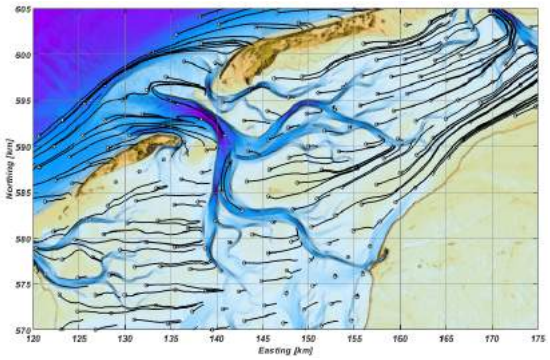

(d) Forced by the hydraulic tide, the maximum storm condition (U = 22.0 m/s, Dir = 274°N) and the maximum wave condition (H_{m0} = 6.63 m, T = 8.24 s, Dir = 274°N)

Figure 5.8: Large-scale sediment transport pathways in the Vlie Inlet system. The sub-caption indicates the specific forcing condition. The white circles indicate the starting position of the individual particles after placement in the system. The black lines indicate the pathways of the sediment particles. To obtain these particular pathways, an acceleration factor of 100 and a modelling period of 600 days were used, except for Figure 5.8d, here an acceleration factor of 10 and a modelling period of 200 days were used.

5.2.4. Ameland Inlet

The SedTRAILS results for the Ameland Inlet system are shown in Figure 5.9. In the Ameland Inlet, a clear diverging line is present under tidal forcing only (Figure 5.9a). Sediment particles that are initially present in the northern part of the inlet are exported, whereas the particles present in the southern part are imported. In the larger tidal channels in the back-barrier basin, the particles are mainly transported inward. The sediment transport pathways on the tidal flats are short, especially near the tidal watersheds that separates the basin with the Frisian Inlet basin. This indicates small net sediment transports. The ebb-tidal delta is highly dynamic, with circulation patterns and converging pathways. Adding the representative wind condition to the forcing of the systems increases the length of the pathways and the presence of the circulation patterns in the ebb-tidal delta (Figure 5.9b). The inlet dynamics move to mainly export of sediment, which becomes apparent from the pathways on the Ameland side of the inlet. The pathways of the sediment particles on the tidal flats in the back-barrier basins are generally deflected under wind forcing, with no clear transport direction. Under wave forcing, the pathways of the particles in the back-barrier basins are as expected (Figure 5.9c). The addition of wave forcing results in a dominant export of sediment. The circulation patterns in the ebb-tidal delta disappear mostly, but the converging lines follow the same pathways as for the tidal and wind forcing conditions. The storm condition (Figure 5.9d) emphasizes the export of sediment. Even sediment particles initially present at the tidal flats can reach the main tidal channel and be exported under such conditions. The dynamics in the ebb-tidal delta remain largely the same, but the transport patterns in the back-barrier basin change significantly. The sediment transport pathways are much longer compared to the path-

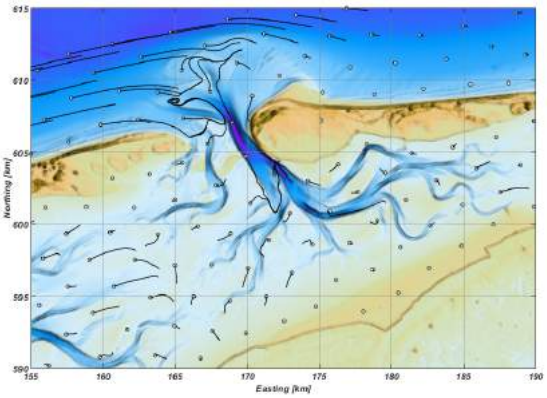

(a) Forced by the hydraulic tide

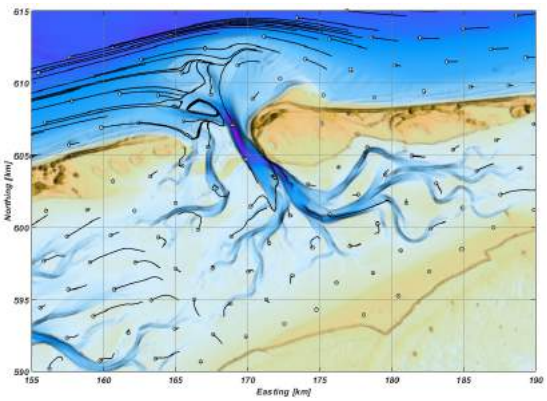

(b) Forced by hydraulic tide and representative wind condition (U = 7.0 m/s, Dir = 201°N)

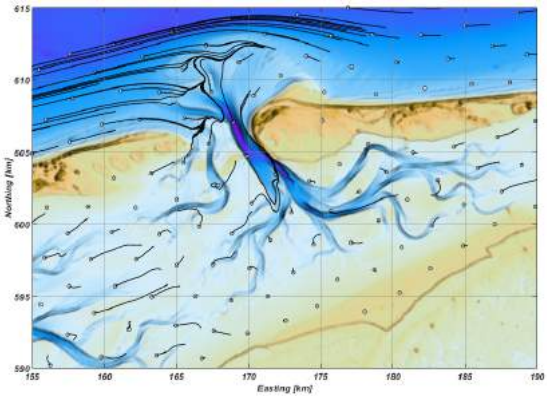

(c) Forced by hydraulic tide, representative wind condition (U = 7.0 m/s, Dir = 201°N) and representative wave condition (H_{m0} = 1.15 m, T = 4.50 s, Dir = 201°N)

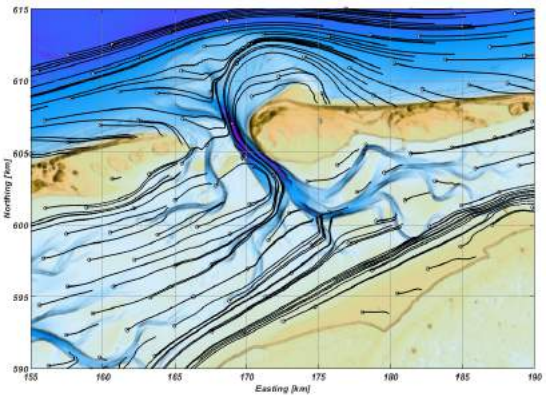

(d) Forced by the hydraulic tide, the maximum storm condition (U = 22.0 m/s, Dir = 274°N) and the maximum wave condition (H_{m0} = 6.63 m, T = 8.24 s, Dir = 274°N)

Figure 5.9: Large-scale sediment transport pathways in the Ameland Inlet system. The sub-caption indicates the specific forcing condition. The white circles indicate the starting position of the individual particles after placement in the system. The black lines indicate the pathways of the sediment particles. To obtain these particular pathways, an acceleration factor of 100 and a modelling period of 600 days were used, except for Figure 5.9d, here an acceleration factor of 10 and a modelling period of 200 days were used.

ways under representative forcing conditions, and especially the sediment transport along the Frisian coast is enhanced. The enhanced net sediment transport in eastern direction will result in an increased exchange between the back-barrier basins.

5.2.5. Frisian Inlet

The results for the Frisian Inlet are shown in Figure 5.10. As for the Ameland Inlet system, the particle pathways are relatively short in the Frisian Inlet system under tidal forcing alone compared to the other inlet systems. The Pinkegat shows almost no net sediment transport under tidal forcing only. The Zoutkamperlaag mainly shows a net export of sediment. The sediment transport pathways in the back-barrier basin are mainly directed inward, but their overall length is limited. The ebb-tidal delta is an extension of the inlet, with outward directed pathways that are deflected and are included in the alongshore flow. The pathways elongate under wind forcing (Figure 5.10b). The transport over the tidal flats is in northeastern direction, which is expected based on the representative wind direction. The Pinkegat exports sediment, whereas the Zoutkamperlaag predominantly imports sediment. The inward directed net transport is extended in the main tidal channel far into the back-barrier basin. In the ebb-tidal delta, the pathways that originate west of the inlet are predominantly deflected towards the inlet. Pathways originating east of the inlet are in eastern direction and result in alongshore transport pathways near Schiermonnikoog. Wave forcing does not change the sediment transport pathways significantly (Figure 5.10c). The Pinkegat export sediment, whereas the Zoutkamperlaag imports sediment. The pathways over the tidal are roughly the same, as are the dynamics in the ebb-tidal delta under wave forcing. The sediment transport patterns change significantly in the system when forced by

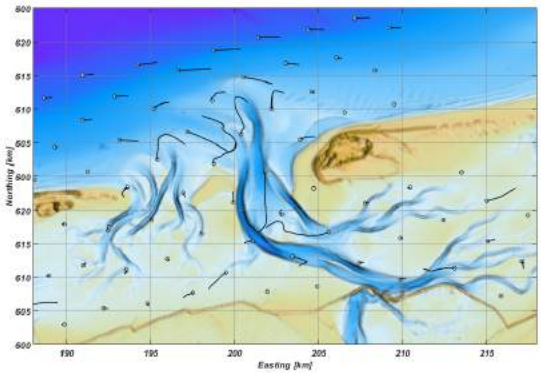

(a) Forced by the hydraulic tide

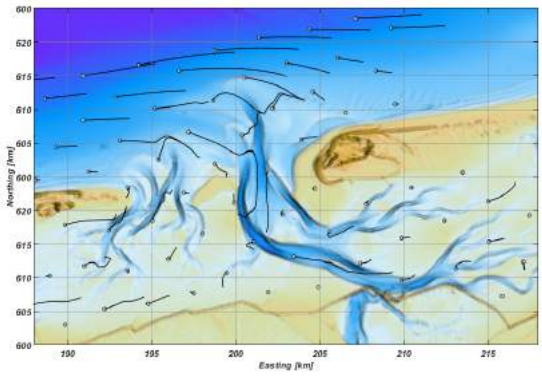

(b) Forced by hydraulic tide and representative wind condition (U = 7.0 m/s, Dir = 201°N)

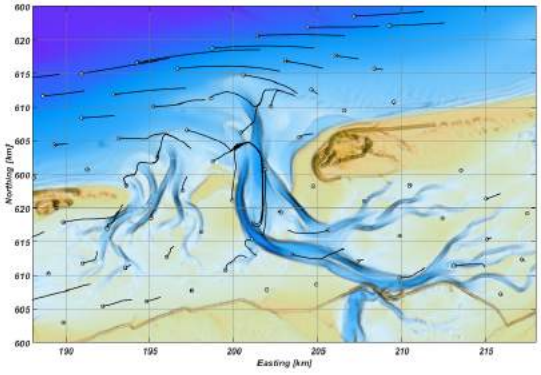

(c) Forced by hydraulic tide, representative wind condition (U = 7.0 m/s, Dir = 201°N) and representative wave condition (H_{m0} = 1.15 m, T = 4.50 s, Dir = 201°N)

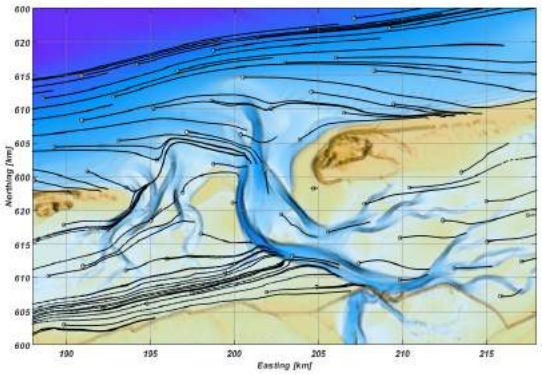

(d) Forced by the hydraulic tide, the maximum storm condition (U = 22.0 m/s, Dir = 274°N) and the maximum wave condition (H_{m0} = 6.63 m, T = 8.24 s, Dir = 274°N)

Figure 5.10: Large-scale sediment transport pathways in the Frisian Inlet system. The sub-caption indicates the specific forcing condition. The white circles indicate the starting position of the individual particles after placement in the system. The black lines indicate the pathways of the sediment particles. To obtain these particular pathways, an acceleration factor of 100 and a modelling period of 600 days were used, except for Figure 5.10d, here an acceleration factor of 10 and a modelling period of 200 days were used.

storm conditions (Figure 5.10d). The Pinkegat still exports sediment, which is once again imported by the Zoutkamperlaag. However, the particle pathways in the back-barrier basin elongate significantly, with especially long pathways along the Frisian coast. This is probably due to the very shallow water depths in these regions, where the influence of the wind is large. These pathways are predominantly directed towards the northeast. The complex dynamics in the ebb-tidal delta smoothen under storm conditions. The pathways predominantly follow the alongshore current, with some deflection of the pathways towards the coast of Schiermonnikoog.

5.3. Concluding Remarks

The results as discussed in the previous sections are summarized below. The dominant sediment transport patterns that follow from the SedTRAILS results are indicated in the conceptual models for the tide, wind, waves and storm condition in Figures 5.11, 5.12, 5.13 and 5.14, respectively.

- The net sediment transport flow in northeastern direction along the coasts of the barrier islands is initiated by tidal forcing and enhanced by wind. The representative wind condition increases the flood velocities along the barrier islands, which leads to an increase in net sediment transport in northeastern direction. The increase in net sediment transport can be observed when comparing Figures 5.11 and 5.12. The transport is not interrupted and the sediment transport pathways are longer. Wave forcing leads to an enhanced net sediment transport near the shore of the barrier islands. Storm conditions lead to a significant increase in net sediment transport along the coast of the barrier islands and more cross-shore sediment transport, which can be observed in Figure 5.14.
- The net sediment transport over the tidal watersheds is limited under tidal forcing only. The net transport over the tidal watersheds increases especially when the system is forced by wind, and to a lesser extent when the system is additionally forced by waves. The increased net sediment transport over the tidal watersheds can be seen subsequently in Figures 5.11, 5.12 and 5.13. Storm conditions significantly increase the sediment transport over the tidal watersheds, which is shown by Figure 5.14.
- The import of sediment by the Texel Inlet is predominantly due to tidal forcing. Outward flow in the inlet near Texel is enhanced by considering wind and wave forcing, but the inlet has a remaining net import of sediment at all times. The sediment transport patterns in the back-barrier basin are initiated by tidal forcing and enhanced by applying wind and wave conditions. The ebb-tidal dynamics are initiated by tidal forcing. The inlet imports sediment over the entire cross-section under storm conditions. The back-barrier basin and ebb-tidal delta are affected most by storm conditions, with a return flow in the main tidal channel as one of the most distinct changes.
- The export of sediment by the Eierlandse Gat is due to tidal forcing and preserved when considering wind and wave forcing, as can be seen by Figures 5.11, 5.12 and 5.13. The dynamics in the ebb-tidal delta are more limited than for the other inlet systems, with dominant deflection of particle pathways towards the alongshore flow. The sediment transport in the back-barrier basin is slightly enhanced by applying wind conditions, but the increase in pathway length is limited. The inlet imports sediment under storm conditions, which is opposite to the net transport direction forced by representative conditions.
- The export of sediment by Vlie Inlet is due to tidal forcing and slightly enhanced when considering wave conditions, wind increases the import of sediment along the tail of Vlieland. Wind forcing alters the ebb-tidal delta dynamics, which are initiated by tidal forcing. The rate of deflection of the pathways towards the coast depends on the angle of inclination of the conditions. The transport patterns in the back-barrier basin are initiated by tidal forcing and enhanced by applying wind conditions. Storm conditions drive import by the Vlie Inlet and increased net sediment transport over the tidal flats.
- The distinct export of sediment by the Ameland Inlet is driven by wind and enhanced when considering wave forcing, and can be observed clearly in Figure 5.13. The ebb-tidal delta shows complex converging pathways that are due to tidal forcing and are enhanced by wind. The sediment transport patterns in the back-barrier basin show more variation than for the other inlet

systems, which is mainly caused by wind forcing. Storm conditions enhance the net export of sediment by the inlet and increase the net sediment transport especially over the tidal flats.

- The net sediment transport patterns due to tidal forcing in the Frisian Inlet are limited. Applying the representative wind condition results in net export by the Pinkegat and net import by the Zoutkamperlaag, which can be observed in Figure 5.12. Wind forcing mainly drives the net sediment transport in the back-barrier basin and enhances the dynamics in the ebb-tidal delta. The import/export patterns by the tidal channels are enhanced under storm conditions. Storm conditions also significantly increase net sediment transport at the tidal flats, and the pathways in the ebb-tidal delta are elongated.

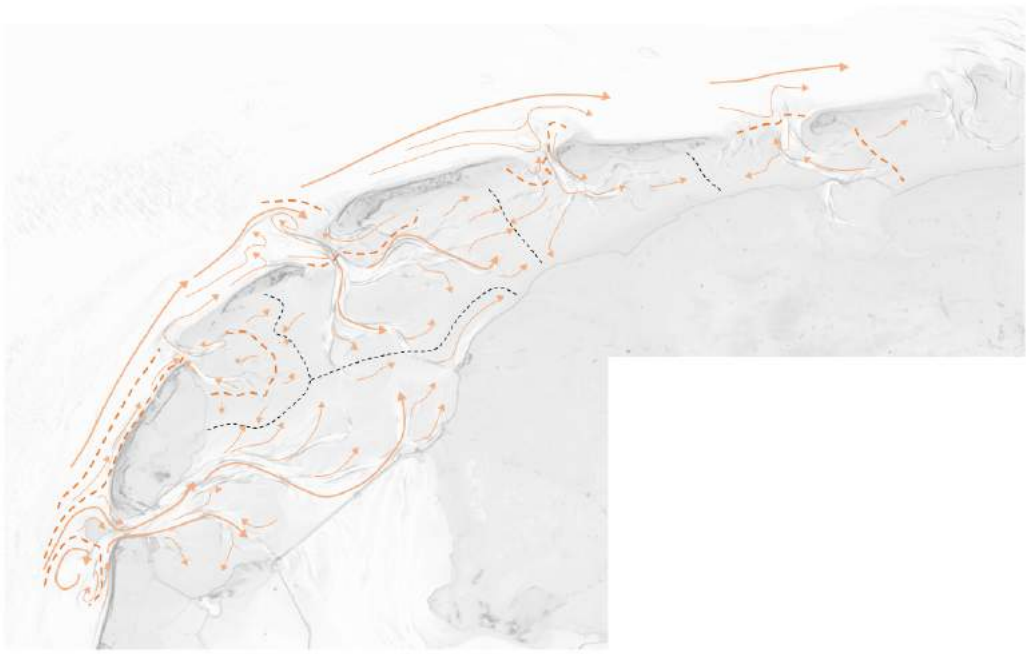

Figure 5.11: Conceptual model of the sediment transport pathways forced by the hydraulic tide. The arrows indicate the dominant transport directions. The coloured, dotted lines indicate the position of diverging net sediment transports. The black, dotted lines indicate the position of the tidal watersheds that do not have net sediment transport over them.

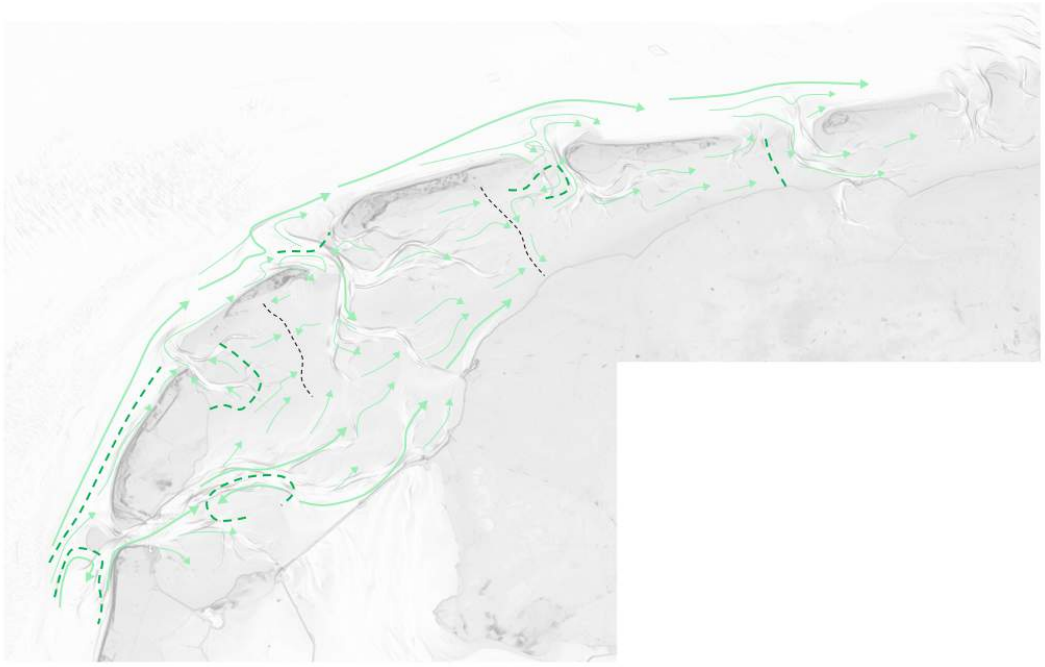

Figure 5.12: Conceptual model of the sediment transport pathways forced by the hydraulic tide and the representative wind condition. The arrows indicate the dominant transport directions. The coloured, dotted lines indicate the position of diverging net sediment transports. The black, dotted lines indicate the position of the tidal watersheds that do not have net sediment transport over them.

Figure 5.13: Conceptual model of the sediment transport pathways forced by the hydraulic tide, representative wind condition and representative wave condition. The arrows indicate the dominant transport directions. The coloured, dotted lines indicate the position of diverging net sediment transports.

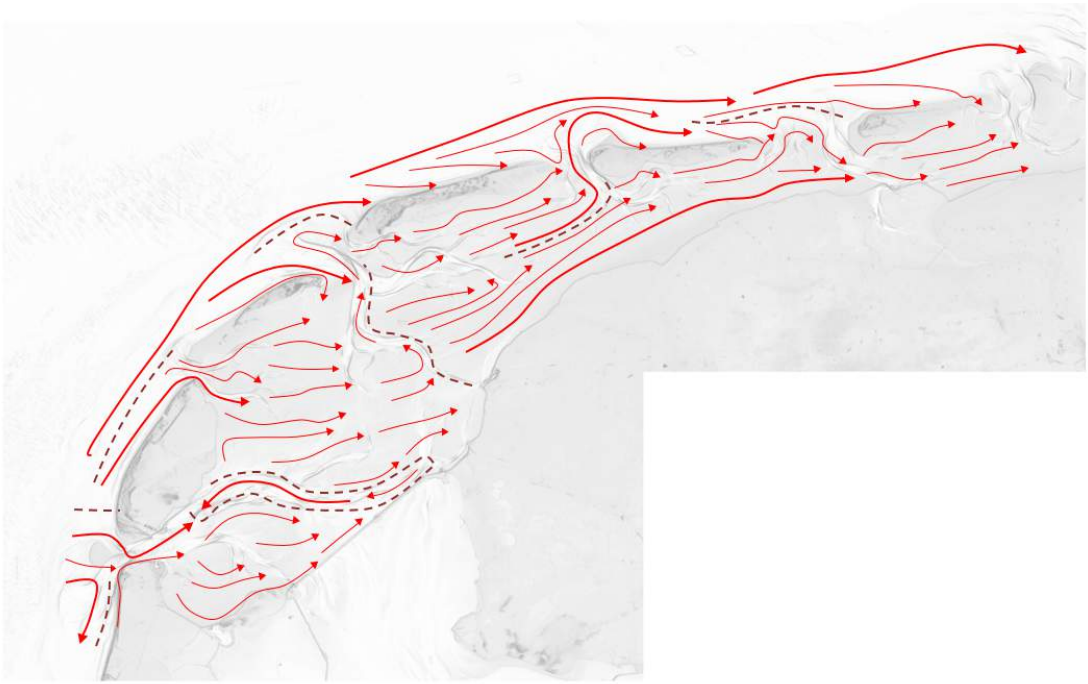

Figure 5.14: Conceptual model of the sediment transport pathways forced by the hydraulic tide and storm condition. The arrows indicate the dominant transport directions. The coloured, dotted lines indicate the position of diverging net sediment transports.

6

Connectivity

The results from SedTRAILS are very useful to model the sediment transport pathways, but the figures can sometimes become very chaotic because of the many long lines that appear. Therefore, a method was developed to present the connectivity between multiple polygons and indicate the dominant transport patterns. This methodology is described in Section 6.1. The resulting connectivity diagrams for the different runs are presented and discussed in Section 6.2. The conclusion on the connectivity of the system is then discussed in Section 6.3.

6.1. Methodology

The method for determining the connectivity in complex systems finds its origin in neurological research (Whitfield-Gabrieli & Nieto-Castanon, 2012; Kruschwitz et al., 2015). The programming language Matlab even has a special toolbox that is designed to analyze the connectivity in brain data sets (Rubinov & Sporns, 2010). Even though this involves an entirely other research field, the tools can also be used to analyze sediment transport patterns. From the results in the previous chapters it namely turns out that the sediment pathways are often complex, which makes it hard to determine the dominant patterns. Therefore, a method to determine the connectivity and the dominant pathways is necessary. Originally, the method used was designed such that the connectivity between each individual deposited particle could be determined (Pearson, 2019; Pearson et al., 2020). This can identify interesting phenomena, but does not connect to the specific goal of this thesis. More important for this research is the connectivity between the polygons. The method was slightly changed to model connectivity between polygons instead of individual particles. The method was still mostly followed, and the main steps of the method are described below.

- The functional connectivity is far more interesting than the structural connectivity, as the interest in complex coastal systems is directed on the sediment fluxes between nodes, not the geographic relation between nodes. The polygons form the receptor cells and the source cells are taken from the SedTRAILS computation.

- The pathways of the individual particles and the total time form the basis for the determination of the connectivity between the polygons. The connectivity between two polygons is computed by dividing the number of time steps that the source spends in another polygon than its origin polygon by the total number of time steps. The sum of all connectivity computations is presented in an adjacency matrix.

- The last step of the method is to present the adjacency matrix in a (structured) network diagram. The diagram shows the main transport direction, and the weight of the connectivity determines the color and thickness of the arrows. Only the top-ten percent of the transport is included in the network diagram to prevent the appearance of chaotic structures. If the physical position of the polygons is omitted, the result is an unstructured network diagram. This is a more abstract way of displaying the connectivity, but can better indicate the most important patterns.

It should be noted that the connectivity matrices largely depend on the modelled period, the acceleration factor applied to the transport pathways and the number of deposited sediment particles. As will be observed in the subsequent section, the transport direction in the inlets and over the tidal watersheds does not resemble the tidal base case (Figure 4.2). The number of deposited sediment particles in these regions is too small to resemble the correct net sediment transport patterns that are present in the base case. The method is therefore not suitable to indicate magnitudes of connections and net transport directions. However, the method can indicate the relative connections when comparing the network diagrams for different forcing conditions. It is no foolproof method and the results should be handled with care, but the method gives a first estimation of the connectivity in the system (Elias & Pearson, 2020; Pearson et al., 2020).

6.2. Connectivity Diagrams

The connectivity diagrams that show the top-ten percent of the total sediment transport between the polygons can better indicate the main transport patterns than the sometimes chaotic results from SedTRAILS. From this, connectivity patterns can be distinguished. The connectivity diagrams for the tidal forcing only, wind forcing and wave forcing are discussed in Sections 6.2.1, 6.2.2 and 6.2.3, respectively. The connectivity diagrams for the storm condition are discussed in Section 6.2.4.

6.2.1. Tidal Connectivity

The structured and the unstructured network diagrams for the tidal forcing only are shown in Figure 6.1 below. The structured network diagram shows that the basins and their coastal zones are strongly interconnected, be it in one way or in two ways with a clear exchange pattern. Also, there is a strong sediment transport patterns along the coasts of the barrier islands, which was already apparent in Figure 5.1. The Frisian Inlet shows no connectivity with the adjacent polygons, which can be explained by the alongshore sediment transport that decreases near Ameland. Therefore, this part is left out in the unstructured network diagram. The transport over the tidal watershed between the Marsdiep basin and the Eierlandse Gat is not shown in the structured network diagram, but it is shown in the unstructured network diagram. This indicates a transport pattern between the back-barrier basins, also in northeastern direction, that starts in the Marsdiep and flows to the Ameland Inlet via the Eierlandse Gat and the Vlie. This was not as clear from Figure 5.1 as the other patterns were.

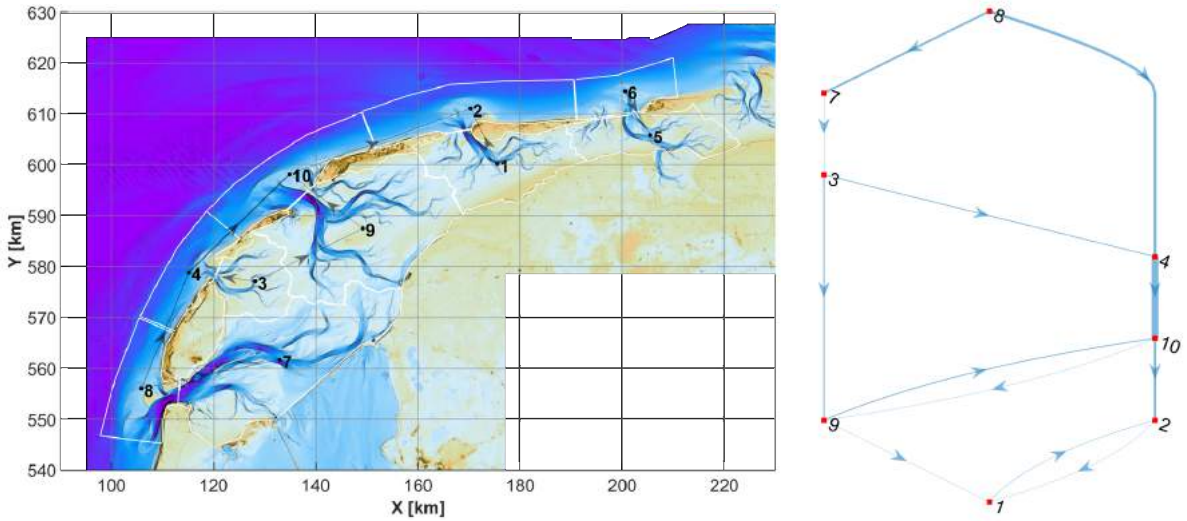

Figure 6.1: Structured (left) and unstructured (right) network diagram based on the results from SedTRAILS forced by the tide only. The arrows indicate transport between basins. Thicker lines in the unstructured network diagram mean more exchange of sediment between adjacent basins.

6.2.2. Connectivity for Wind

The connectivity within the system when the system is forced by the tide and wind is schematized in Figure 6.2. The structured network diagram looks a lot like the structured network diagram for tidal

forcing only. The differences are that the coastal regions of the Marsdiep basin and the Vlie basin are now also connected, and that the Marsdiep and Eierlandse Gat basin are no longer connected in this diagram. The direct connection between the coastal regions can be doubted, as this only occurs on the long-term. The connection between the Marsdiep and Eierlandse Gat basin is still present, as can be seen in the unstructured network diagram, but is smaller compared to the other connections under the wind forcing. The alongshore transport in northeastern direction is still present, with an extension to the coastal region of the Frisian Inlet. This connects the Frisian Inlet to the rest of the Wadden Sea system. The Vlie Inlet and Ameland Inlet still exchange sediment between the back-barrier basins and the coastal regions. The representative wind condition also forces an exchange of sediment between the Vlie basin and the Marsdiep basin over the tidal watershed. This was not as clear from Figure 5.2 as the other patterns observed in the connectivity diagrams. The representative wind condition results in approximately the same connectivity patterns in the system as for the tidal forcing alone, with some extensions. These extensions are mainly the connection of the Frisian Inlet with the other polygons and the increased transport over the watersheds.

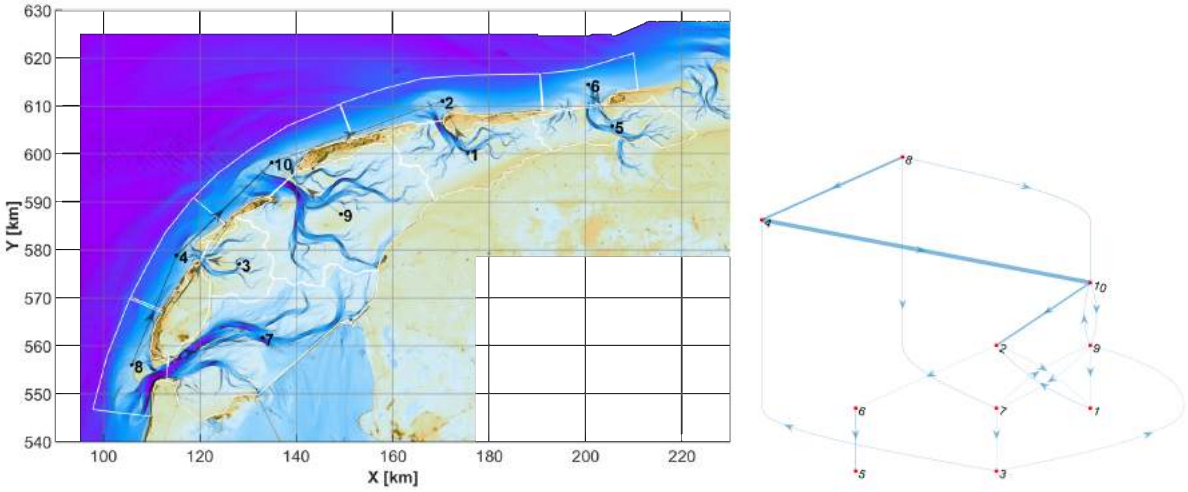

Figure 6.2: Structured (left) and unstructured (right) network diagram based on the results from SedTRAILS forced by the tide and the representative wind condition (U = 7.0 m/s, Dir = 201°N). The arrows indicate transport between basins. Thicker lines in the unstructured network diagram mean more exchange of sediment between adjacent basins.

6.2.3. Connectivity for Waves

Both the structured and unstructured network diagram for the representative wave condition are shown in Figure 6.3. As for the representative wind condition, the network diagrams look a lot like the diagrams for the tidal forcing only. The structured network diagram is a copy of the structured diagram shown in Figure 6.2, except for the connections of the Eierlandse Gat basin. For the representative wind condition, the export of sediment through the inlet was included in the top ten percent connections, but under wave forcing this is replaced by transport over the tidal watershed to the Vlie basin. This does not mean that the export is no longer existent, as is shown by the unstructured network diagram. Many transport patterns remain the same, like the alongshore sediment transport in the coastal regions and the exchange of sediment between the Marsdiep and Vlie basin. Differences are that the Ameland Inlet solely exports sediment and that the Frisian Inlet and Texel Inlet transport sediment both inward and outward. In addition, the Frisian Inlet is also connected to the Ameland basin via sediment transport over the tidal watershed. Adding the wave forcing to the system seems to trigger insignificant changes to the sediment transport patterns and the connectivity in the system at the first sight, but these slight changes can have large consequences for the long-term dynamics of the system. Figure 6.3 presents the most accurate connectivity diagrams of the system of the Dutch Wadden Sea, when assuming that the representative wave condition takes the most important hydrodynamic and morphodynamic processes into account.

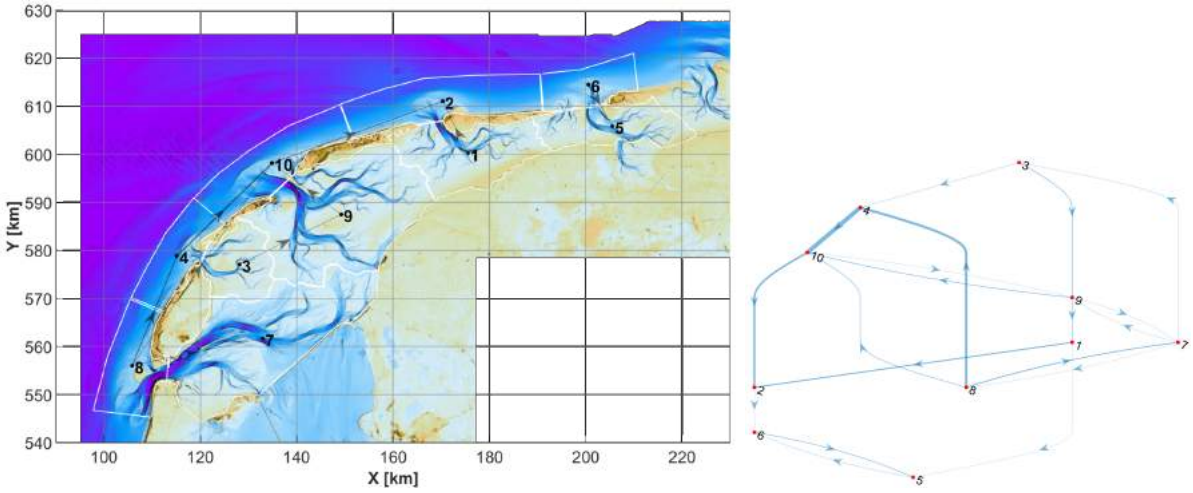

Figure 6.3: Structured (left) and unstructured (right) network diagram based on the results from SedTRAILS forced by the tide, the representative wind condition (U = 7.0 m/s, Dir = 201°N) and the representative wave condition (H_{m0} = 1.15 m, T = 4.50 s, Dir = 201°N). The arrows indicate transport between basins. Thicker lines in the unstructured network diagram mean more exchange of sediment between adjacent basins.

6.2.4. Storm Connectivity

The unstructured network diagram for the storm condition is shown in Figure 6.4. The back-barrier basins are strongly connected, with a sediment transport flow in northeastern direction. This transport flow is also still evident in the coastal regions. The unstructured network diagram shows more clearly the main transport patterns in the system than the structured network diagram. The only inlet that still shows a clear import of sediment is the Texel Inlet. The other inlets show an exchange of sediment, thus the inlets both import and export sediment. The Vlie basin becomes one of the main links in the connectivity of the system under storm conditions. The coastal regions still transport sediment, but the back-barrier basins are now more important for the sediment transport than the coastal regions. Even though other connections become more important during storm conditions, the unstructured network diagram for the storm condition including waves resembles the unstructured network diagram for the representative wave condition well (Figure 6.3). The exchange of sediment between the Marsdiep and its ebb-tidal delta disappears under the storm condition, and the inlet only imports sediment. However, other than the (dis)appearance of exchange patterns, the connections between the polygons are not

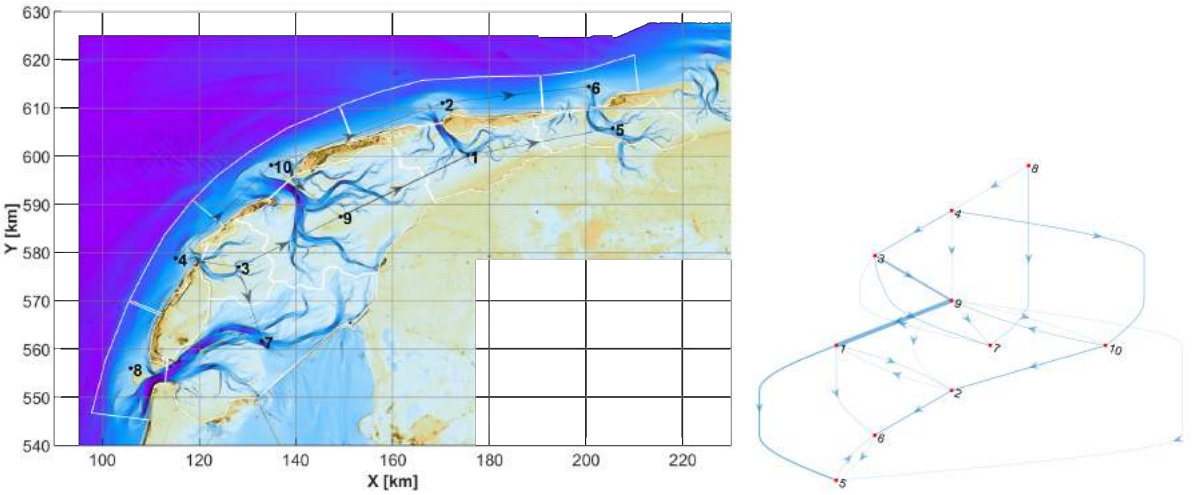

Figure 6.4: Structured (left) and unstructured (right) network diagram based on the results from SedTRAILS forced by the tide and the storm condition including waves (U = 22.0 m/s, H_{m0} = 6.63 m, T = 8.24 s, Dir = 274°N). The arrows indicate transport between basins. Thicker lines in the unstructured network diagram mean more exchange of sediment between adjacent basins.

very different under storm conditions. The main transport patterns are in northeastern direction. In Section 5.3, it was clear that the sediment transport patterns change under the storm condition, but here it can be seen that the other transport patterns do not affect the connectivity of the system significantly. Figure 6.4 does show that the system becomes largely interconnected under storm conditions.

6.3. System Connectivity

In the previous section, the influence of each forcing type, the tide, wind and waves, respectively, on the the connectivity of the Dutch Wadden Sea system was assessed. A conceptual model on the connectivity patterns and their dominant forcing mechanisms is shown in Figure 6.5. The conceptual model does not take into account storm conditions, as these are not normative for the representative conditions. For the storm conditions, the unstructured network diagram from Figure 6.4 is the most important figure to consider. In the case of the representative condition, the alongshore transport in northeastern direction in the coastal regions is responsible for the largest connection in the system. The back-barrier basins in the Western Wadden Sea are largely interconnected via transport over the tidal watersheds, and the transport via the basins in eastern direction in the Eastern Wadden Sea is also not insignificant. The connectivity diagrams show the importance for distinguishing transport patterns in the chaotic results of SedTRAILS. The storm condition does not significantly alter the connectivity patterns in the system. It mostly influences the transport through the inlets, which has some consequences for the connectivity between the back-barrier basins and the coastal regions. In addition, some (long-distance) connections are added to the network diagrams, but these connections can be doubted based on the mean duration of the typical Dutch storms. As storms only occur a small percentage of time on an annual basis, the conceptual model for the connectivity in the Dutch Wadden Sea system is normative. From Figure 6.5, it can be concluded that the tide forces most connections in the Dutch Wadden Sea, with some additional connections forced by applying representative wind- and wave conditions.

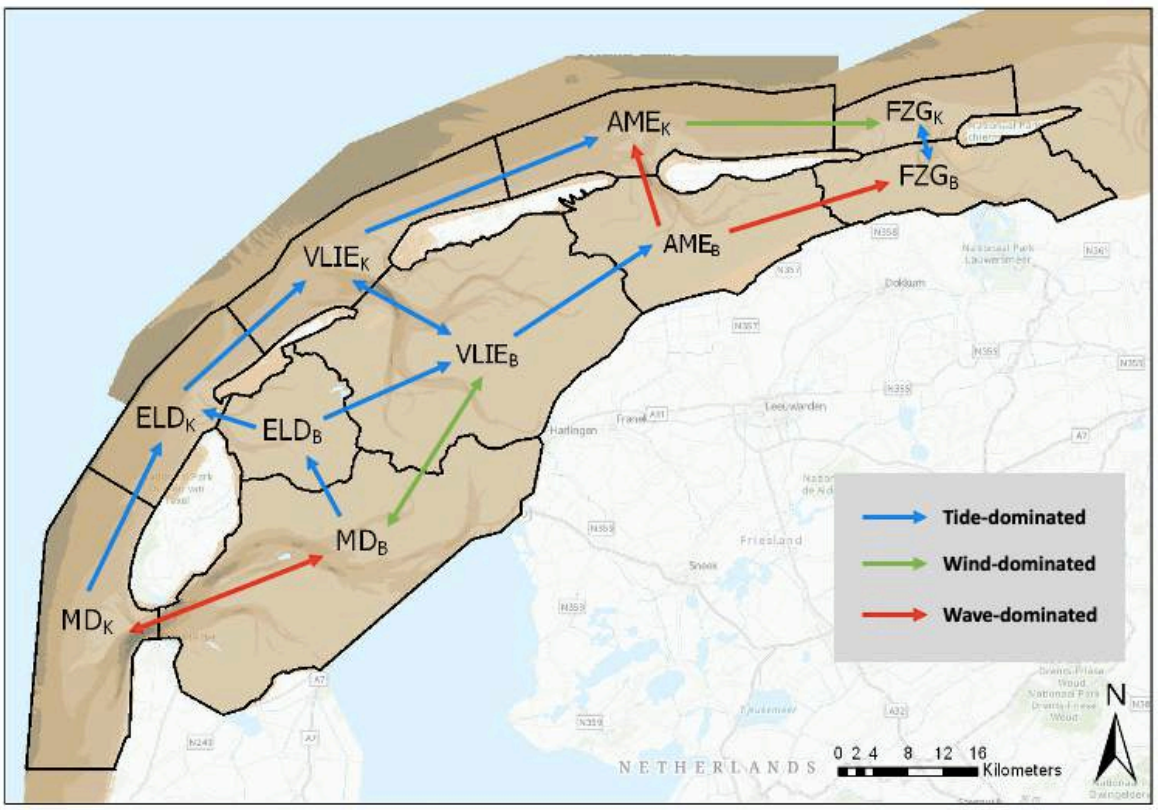

Figure 6.5: Conceptual model of the connectivity within the Dutch Wadden Sea system for the hydrodynamic forcing conditions of the year 2017. The color of the arrows indicates the dominant forcing of the connectivity.

7

Discussion

In the previous chapters, the influence of the tide, wind and waves on the sediment transport patterns has been assessed, as well as the connectivity within the system of the Dutch Wadden Sea. The most important findings of this research are discussed in this section, as well as their implications, limitations, and applications.

Large-scale sediment transport patterns
Research studies in the past have focused on sediment transport patterns in the individual tidal inlets of the Wadden Sea (Elias & van der Spek, 2006; Elias et al., 2020; Rijkswaterstaat, 2021). It was often assumed that the tidal divides form more or less closed boundaries separating these systems (Townend et al., 2016; Vroom, 2011). Only few studies have looked into the large-scale sediment transport patterns of the entire Wadden Sea system. The research focused on the sediment budgets of the Wadden Sea (Elias, 2019), which showed that there needs to be sediment transport over the tidal watersheds for the sediment budget to be balanced. This research has proved that separate basins may exist under tidal forcing, but sediment transport over the tidal watersheds exists under the influence of wind and waves. The contribution of each process depends on the basin considered. In addition, more insight on the influence of the tide, wind and waves individually on the large-scale sediment transport patterns has been acquired.

The expanded knowledge on the large-scale sediment transport patterns could serve as the basis for sand nourishment campaigns. Until now, nourishments have mostly been applied to local beaches and channels, with the exception of works like the Sand Motor (Tonnon & Nederhoff, 2016). The sediment demand of the Wadden Sea will increase due to relative sea level rise, which could make the application of large-scale nourishments attractive. Knowledge on the large-scale sediment transport patterns will then be essential to determine the optimal locations to execute the nourishments. The influence of local nourishments will be harder to predict based on this research, but it could serve as a first estimate to determine possible options. Additionally, the patterns could serve as a base case to compare the nourishment scenarios with to determine the influence of such works.

Individual processes
Tide initiates an alongshore transport in northeastern direction in the coastal regions of the barrier islands. The alongshore sediment transport pathways are longer in the outer coastal regions than in the nearshore regions. Sediment transport patterns in the ebb-tidal deltas are dominated by tidal forcing, the degree of net sediment transport depends on the inlet. The longer sediment transport pathways in the Vlie Inlet and Ameland Inlet compared to the Frisian Inlet indicates that a larger residual transport takes place in these two inlets. The export of sediment by the Eierlandse Gat and Vlie Inlet is due to tidal forcing, as well as the import by the Texel Inlet. The Ameland Inlet and Frisian Inlet show no import or export due to tidal forcing alone. The shallower regions of the back-barrier basins predominantly show inward directed net sediment transport, as well as the main tidal channels. The exception is the Eierlandse Gat, where the pathways are predominantly directed outward. The sediment transport pathways in the Western Wadden Sea are generally longer than the pathways in the Eastern Wadden

Sea. The net sediment transport over the tidal watersheds is limited under tidal forcing alone.

Wind forcing enhances the alongshore transport in northeastern direction in the coastal regions of the barrier islands. The flood velocities increase due to the representative wind condition, thus the sediment transport pathways elongate. The flood velocities are dependent on the wind direction, thus another wind direction may result in decreased flood velocities. Wind has a varying influence on the inlet dynamics. Wind enhances the ebb-tidal delta dynamics of the Frisian Inlet and alters the ebb-tidal delta dynamics of the Vlie Inlet. The outward flow along Texel in the Texel Inlet is enhanced by wind, but wind forcing has almost no effect on the inlet dynamics of the Eierlandse Gat and the Vlie Inlet. Wind drives the distinct export by the Ameland Inlet and the transport dynamics through the Frisian Inlet. The Pinkegat exports sediment whereas the Zoutkamperlaag imports sediment. The net sediment transport in the back-barrier basins of the Texel Inlet, Eierlandse Gat and Vlie Inlet is enhanced by wind. The sediment transport patterns in the basin of the Ameland Inlet show more variations under wind forcing, whereas wind drives the net sediment transport in the back-barrier basin of the Frisian Inlet. The net sediment transport over the tidal watersheds increases significantly due to wind forcing. The net sediment transport over the tidal watersheds between the Vlie Inlet basin and the Eierlandse Gat and Ameland Inlet basin remains limited under representative wind conditions.

The effect of waves on the net sediment transport is hard to deduce from the sediment transport pathways generated with SedTRAILS. Wind forcing is associated with direct sediment transport, but this is not necessarily the case for wave forcing. Waves can induce a current that transports sediment, but waves can also bring the sediment in suspension. The sediment is then transported by the other hydrodynamic forcings. The visualization by SedTRAILS can not make the distinction between the different effects of waves. Therefore, the changes in pathways with respect to the situation with tide and wind forcing alone are discussed. An alongshore transport in northeastern direction in the coastal regions of the barrier islands is preserved under wave forcing. The sediment transport pathways on the nearshore elongate at Texel, Vlieland and Terschelling. The sediment transport pathways increase around the Noorderhaaks shoal, but the change in the other ebb-tidal deltas is not significant. The net export of sediment is enhanced in the Vlie Inlet and Ameland Inlet, but the inlet dynamics do not change significantly due to wave forcing. The length of the pathways in the tidal channels of the Marsdiep basin increases significantly when wave forcing is taken into account. The pathways in the other back-barrier basins do not elongate, but the transport direction is predominantly northeastward. The incorporation of waves leads to a net sediment transport over all tidal watersheds.

Storm conditions as considered in this research include the hydraulic tide, higher wind speeds and larger waves at the offshore boundaries. The observed alongshore transport in northeastern direction in the coastal regions of the barrier islands is enhanced under storm conditions. In addition, the outer shore pathways are deflected towards the coast, which indicates more cross-shore transport. The entire cross-section of the Texel Inlet imports sediment when considering storm conditions. The Eierlandse Gat and Vlie Inlet have a net import of sediment under storm conditions, which is opposite to the representative conditions. The sediment import or export by the Ameland Inlet and Frisian Inlet does not change. In the overall deeper Marsdiep basin and Vlie Inlet basin, a return flow in the main tidal channels is present under storm conditions. The net sediment transport over the tidal flats increases significantly, which leads to an increased net sediment transport over the tidal watersheds.

Tide-driven alongshore transport

The flow along the barrier islands forced by the tide alone has proven to generate significant net sediment transport pathways. The transport pathways were somewhat longer when adding wind and wave forcing to the system, but this elongation is generally small. An earlier study by Van Rijn has found that the tide has a sediment transport capacity (Van Rijn, 1997). This was confirmed by other research, where it was found that the tidal pressure gradient is a key contributor to alongshore flow inside the surfzone (Hansen et al., 2013). The findings from the last study do explain the net sediment transport in the nearshore coastal zones, but not the larger net sediment transport pathways in the outer coastal regions and the increasingly shorter pathways in the seemingly lee zones along Terschelling and Ameland. A recent study could explain the longer pathways in the outer coastal regions: the alongshore velocity can increase with increasing water depths (Amador et al., 2020). A small variation in ebb and

flood velocities may result in larger net velocities in the outer coastal regions than in the nearshore region. The apparent lee zones along Terschelling and Ameland could result from the orientation of the amphidromic point west from the Holland coast in the North Sea. The tidal propagation is especially obstructed by the ebb-tidal deltas of the Vlie Inlet and the Ameland, which could result in shorter sediment transport pathways. No specific research on this phenomenon has been published yet. This is a limitation of the results of this research, as the results can not be compared to earlier research. Provided that the results for the tide-driven sediment transport pathways are correct, this research has resulted in new, preliminary insights in the tide-driven alongshore sediment transport.

Manning's bottom roughness field

A depth-dependent Manning's roughness field was derived to improve the theoretic reasoning behind the roughness field of the WadSea FM model. The requirement for this roughness field was that it could accurately model the tidal propagation, which has been succeeded in this research. Depth-dependent roughness fields have been used earlier in models (Gross et al., 2009), but the application of empirically determined polygon fields is still the norm in many models. This is due to the fact that the Manning's formula is still an empirical formula, and the values for this Manning's coefficient may largely vary under different flow conditions (Arcement & Schneider, 1989). Selecting one value for certain depth regions is not entirely correct, and it is still a limitation of the model, but it is a better approximation of the real conditions than the roughness field that was used before in the model. This research has also proven that the use of depth-dependent roughness fields is possible, and can match the tidal propagation obtained with other empirical roughness fields. Options to further develop a more physically correct roughness field would be to relate the roughness field to field measurements for flow. Theoretically it would be preferred to incorporate the grain size in the roughness field configuration by for example using the Darcy-Weisbach equation (Chanson, 2004), but the application and performance of such roughness fields has not be assessed yet.

Use of SedTRAILS

The sediment transport pathways derived with SedTRAILS show the course of individual sediment particles. The pathways are a visualization based on the sediment transports generated through van Rijn (Van Rijn, 1997). It could also have been possible to show the sediment transport vectors in the Dutch Wadden Sea domain. This would have resulted in a field of varying vectors, which was used to visualize the performance of the morphological tide. The disadvantage of showing the sediment transport vectors is that the vectors do not indicate the course of sediment particles, only the magnitude and direction of net sediment transport. The magnitude and direction of net sediment transport can be useful for other purposes, but are not the preferred way to visualize sediment transport patterns. The approximate pathways are hard to deduce from the sediment transport vectors by hand. SedTRAILS is a useful tool that can efficiently determine the sediment transport pathways based on the sediment transports modelled with Delft3D-FM. SedTRAILS does not track individual particles, thus the quantity and duration of the sediment transport can not be deduced from the sediment transport pathways (Elias & Pearson, 2020).

System connectivity

The system connectivity has been derived from the sediment transport pathways obtained from SedTRAILS. The connections are determined based on the length of the pathways, and the top-ten connections are visible in the network diagrams. This method of visualizing the transport pathways has been widely applied in other research fields, but is relatively new in the coastal engineering field. Only the directions of the connections have been assessed, as the magnitude of each connection is hard to derive from the network diagrams. The tide forces most of the connections within the Wadden Sea system. The sediment transports over the tidal watersheds proved to be small, but these transports are large enough to induce a connection between most back-barrier basins. The wind forcing introduces sediment exchange between the Vlie basin and Marsdiep basin, as well as a connection between the coastal zones of the Ameland Inlet and the Frisian Inlet. The wave forcing induces a connection between the Ameland Inlet basin and the Frisian Inlet basin. The wave forcing also changes the connection within the Ameland Inlet to a predominantly exporting connection, whereas it forces a sediment exchange in the Texel Inlet. This research shows that the method for the network diagrams can be used to display the complex sediment transport pathways.

The main limitation of the connectivity methodology is the large modelling period dependency. Based on the transport directions, the large-scale sediment transport patterns can be derived from the transport pathways, even if the pathways are relatively short. For the connectivity diagrams however, the script is entirely dependent on the length of these pathways, and therewith the modelling period applied. Some connections that will be present in real life may be neglected in the network diagrams, which will increase the virtual importance of other connections. The network diagrams will quickly result in a distorted view of the system connectivity, and must therefore be handled with care. An obvious solution to the limitation of the use of such network diagrams would be to increase the modelling period, which increases the length of the sediment transport pathways. However, this will increase the computational effort significantly. As the script does not run in Delft3D-FM, but in Matlab, the data limit in the program will prevent the use of much longer modelling periods. Optimizing the network diagram determination, as well as the optimization of SedTRAILS, would be an interesting next step.

8

Conclusion

The objective of this thesis is to define the Dutch Wadden Sea as a sediment sharing system by determining the effect of the tide, the wind and the waves on the sediment transport, determining the normative sediment transport patterns in the system and distinguishing the connectivity within the system. The sub-questions and the main research question are answered in Section 8.1. Lastly, recommendations are given in Section 8.2.

8.1. Research Objectives

The first three sub-questions concern with the influence of the tide, wind and wave forcing separately.

- *What is the effect of the tide on the sediment transport in the Wadden Sea, at the coastline of the barrier islands and in the tidal inlets?*
  - Tidal forcing initiates an alongshore transport in northeastern direction in the coastal regions, with larger net sediment transports on the updrift side of the ebb-tidal deltas and smaller net sediment transports on the downdrift side of the ebb-tidal deltas.
  - The main tidal channels are dominated by tidal forcing, the magnitude and direction of net sediment transport depend on the inlet system.
  - The Texel Inlet imports sediment, whereas the Eierlandse Gat and Vlie Inlet show a net export of sediment due to tidal forcing. For the Ameland Inlet and Frisian Inlet, a preference can not be observed.
  - The net sediment transport in the back-barrier basins due to tidal forcing is inward directed, with the exception of the Eierlandse Gat basin.
  - The back-barrier basins are not connected under tidal forcing alone.
- *What is the effect of the wind on the sediment transport in the Wadden Sea, at the coastline of the barrier islands and in the tidal inlets?*
  - The representative wind condition enhances the alongshore transport in northeastern direction in the coastal regions.
  - The influence of the wind on the net sediment import or export depends on the inlet. Wind drives the net export by the Ameland Inlet and the import/export dynamics in the Frisian Inlet. Wind enhances the dynamics in the Texel Inlet and Eierlandse Gat at most, whereas wind forces an import flow in the Vlie Inlet.
  - The net sediment transport in the back-barrier basins is predominantly enhanced due to the wind forcing.
  - The net sediment transport over the tidal watersheds is driven by wind forcing. Most tidal watersheds show a significant net sediment transport. The net sediment transport over the tidal watersheds that connect the Vlie Inlet basin with the Eierlandse Gat basin and Ameland Inlet basin remains limited under wind forcing.

- *What is the effect of waves on the sediment transport in the Wadden Sea, at the coastline of the barrier islands and in the tidal inlets?*
  - The net sediment transport on the nearshore increases when wave forcing is included.
  - The inlet dynamics do not change significantly due to wave forcing.
  - The net sediment transport in the Marsdiep basin increases significantly when wave forcing is included.
  - The incorporation of waves leads to a net sediment transport over all tidal watersheds.

The fourth sub-question concerns with the large-scale movement due to the individual processes.

- *How do the different processes affect the large-scale movement of individual particles within the system?*

The large-scale movement of individual particles in the coastal regions of the system is not significantly affected by applying different processes to the system. The transport pathways are enhanced when applying wind and wave forcing, and the coastal regions of the Vlie Inlet and the Frisian Inlet are more connected to the other coastal regions, but the large-scale movements remain the same. Under tidal forcing, the pathways in the back-barrier basins are directed inward, thus the direction of the pathways depend on the geometry of the back-barrier basin. Under wind forcing, but especially under wave forcing, the pathways are predominantly in northeastern direction. The dominant transport direction under wind and wave forcing induces net sediment transport over the tidal watersheds.

The fifth sub-question concerns with the system connectivity.

- *How can the connectivity within the system be distinguished?*

The connectivity between polygons is dependent on the length of the sediment transport pathways, in other words the time that individual particles spend in specific polygons. The connections between the inlet systems are predominantly initiated by the tide. Only the Frisian Inlet system behaves separately from the other inlet system under tidal forcing alone. The connection between the coastal regions of the Ameland Inlet and Frisian Inlet is forced by the wind. The sediment exchange between the back-barrier basins of the Texel Inlet and Vlie Inlet is also induced by the wind forcing. The waves force the new connection between the back-barrier basins of the Ameland Inlet and Frisian Inlet. The wave forcing is also responsible for the adjustment of the connections through the Texel Inlet and the Ameland Inlet. The tide, wind and waves create a highly interconnected system with few areas that are not connected to the rest of the system.

The research question combines the sub-questions to define the sediment sharing system.

- ***How can the Dutch Wadden Sea be defined as a sediment sharing system?***

The Dutch Wadden Sea is a tidal system with back-barrier basins that are not only connected with their coastal regions through the tidal inlets, but also with each other through sediment transport over the tidal watersheds. The tide initiates the sediment transport within the system, but the exchange of sediment between the back-barrier basins is limited under tidal forcing alone. The wind and wave forcing increase the exchange of sediment within the system. Wind enhances the tide-induced sediment transport patterns. In addition, wind induces net sediment transport over most tidal watersheds. Incorporating wave forcing enhances the nearshore net sediment transport, which leads to the incorporation of the barrier islands in the sediment sharing system. Applying wave forcing to the system also leads to net sediment transport over the remaining tidal watersheds. The combination of the hydrodynamic forcing mechanisms leads to a system of barrier islands, ebb-tidal deltas, tidal inlets and back-barrier basins that are highly interconnected with one another by the exchange of sediment.

8.2. Recommendations

This research estimates the influence of hydrodynamic forcings on the large-scale sediment transport patterns, but it leaves room for future research. Future research objectives are listed below.

- *Grid refinement*: the performed grid refinement was assessed on the tidal propagation within the Wadden Sea system. The refinement did not perform significantly better on the performance requirement, but it was not tested on the modelling of the wind and wave response. Grid refinements could prove to lead to a better approximation of the real time conditions, especially when considering wave resolvement. In addition, the accuracy in sediment transport modelling could improve significantly. Future research should discover the benefits in accuracy and drawbacks in computational effort of grid refinements.

- *Improved wave analysis*: the applied wave conditions were determined independently from the wind conditions. For this research, the representative wave condition was chosen to contain a single mean wave height, but it would be better to implement a more realistic representation of the wave climate in future research. A probability analysis will reduce the uncertainties in the wave modelling, which could lead to smaller errors in the sediment transport patterns. Future research should focus on extending the wave model by applying more and improved wave conditions.

- *Tide-driven alongshore transport*: the tide-driven alongshore transport near the barrier islands of the Wadden Sea is significant. Earlier research substantiates the tide-driven net sediment transport, but it does not explain the reduced sediment transport near Terschelling and Ameland. The reduced net transport could be result of lee zones created by the ebb-tidal deltas, but no research on this phenomenon is available yet. The model approaches the tidal propagation well, but future research needs to show whether or not the observed phenomenon in the coastal regions due to the tidal forcing is correct.

- *Development roughness fields*: the newly developed depth-dependent Manning's roughness field has better physical reasoning behind it than the old roughness field. The old field consisted of two polygons, which is in agreement with most roughness fields applied until now. The new roughness field developed in this research makes use of the depth-dependency of the Manning's coefficient. The applicability of depth-dependent roughness field has been proved by this research, and future research could further investigate and improve the performance of depth-dependent roughness fields. The performance could be improved by for example relating the roughness field to field measurements for flow or by calibrating the roughness field based on gradients in the tidal propagation instead of individual stations. This research has based the performance of the field on the performance of individual stations, but the gradients in tidal amplitude and phase could result in a better approximation of the sediment transport in the system. In addition, one could apply the Darcy-Weisbach equation, and relate the roughness field to the local grain size. Relating the roughness field to grain size is still mainly theoretical, and the performance of such roughness fields has not been assessed yet.

- *Connectivity analysis*: the connectivity network diagrams indicate the top-ten connections in the system, but the presence of connections and the magnitude of them is largely dependent on the modelling period. This makes the network diagrams subject to misinterpretations, and the network diagrams should always be compared to the sediment transport pathways. The method would be more useful if it was less dependent on the modelling period. Future research should focus on increasing the modelling period without too much additional effort, or by interpreting the direction of the pathways during the connectivity analysis.

- *Quantifying sediment transport patterns*: the sediment transport pathways can be compared with directions in the base case, but this does not estimate the accuracy of the chosen representative conditions. A better estimation of the quantities of sediment transport volumes also enables a better coastal protection plan. For accurate sediment transport volumes, field measurements are needed. These measurements can help quantify the pathways modelled with SedTRAILS and estimate the duration associated with pathway lengths.

References

Agnew, D. C., & Farrell, W. E. (1978). Self-consistent equilibrium ocean tides. *Geophysical Journal of the Royal Astronomical Society*, *55*, 171–181.

Amador, A., Arzeno, I. B., Giddings, S. N., Merrifield, M. A., & Pawlak, G. (2020). Cross-shore structure of tidally driven alongshore flow over rough bathymetry. *Journal of Geophysical Research: Oceans*, *125*.

Arcement, G. J. J., & Schneider, V. R. (1989). Guide for selecting manning's roughness coefficients for natural channels and flood plains.

Babanin, A. V., & Haus, B. K. (2009). On the existence of water turbulence induced by nonbreaking surface waves. *Journal of Physical Oceanography*, *39*, 2675–2679.

Bagnold, R. A. (1946). Motion of waves in shallow water - interaction between waves and sand bottom. *Proceedings of the Royal Society London A*, *187*, 1–18.

Bathurst, J. C. (1978). Flow resistance of large-scale roughness. *Journal of the Hydraulics Division*, *104*, 1587–1603.

Battjes, J. A. (1988). Surf-zone dynamics. *Annual Review of Fluid Mechanics*, *20*, 257–293.

Beets, D. J., & van der Spek, A. J. F. (2000). The holocene evolution of the barrier and the back-barrier basins of belgium and the netherlands as a function of late weichselian morphology, relative sea-level rise and sediment supply. *Netherlands Journal of Geosciences*, *79*, 3–16.

Beets, D. J., van der Valk, L., & Stive, M. J. F. (1992). Holocene evolution of the coast of holland. *Marine Geology*, *103*, 423–443.

Bilge, A. H., Kirkil, G., Burak, S., & Incegul, M. (2016). Modeling of wind effects on stratified flows in open channels: A model for the istanbul strait (bosphorus). *Journal of Physics*, *738*.

Bosboom, J., & Stive, M. J. F. (2015). *Coastal dynamics 1 - lecture notes cie4305*. Delft Academic Press.

Chanson, H. (2004). *Environmental hydraulics of open channel flows*. Elsevier.

Cheng, R. T., Casulli, V., & Gartner, J. W. (1993). Tidal, residual, intertidal mudflat (trim) model and its applications to san fransisco bay, california. *Estuarine, Coastal and Shelf Science*, *36*, 235–280.

Colosimo, I., de Vet, P. L. M., van Maren, D. S., Reniers, A. J. H. M., Winterwerp, J. C., & van Prooijen, B. C. (2020). The impact of wind on flow and sediment transport over intertidal flats. *Journal of Marine Science and Engineering*, *8*, 1–26.

Compton, T. J., Holthuijsen, S., Koolhaas, A., Dekinga, A., ten Horn, J., Smith, J., … Piersma, T. (2013). Distinctly variable mudscapes: Distribution gradients of intertidal macrofauna across the dutch wadden sea. *Journal of Sea Research*, *82*, 103–116.

Dastgheib, A., Roelvink, J. A., & Wang, Z. B. (2008). Long-term process-based morphological modeling of the marsdiep tidal basin. *Marine Geology*, *256*, 90–100.

de Haas, T., Pierik, H. J., van der Spek, A. J. F., Cohen, K. M., van Maanen, B., & Kleinhans, M. G. (2018). Holocene evolution of tidal systems in the netherlands: Effects of rivers, coastal boundary conditions, eco-engineering species, inherited relief and human interference. *Earth-Science Reviews*, *177*, 139–163.

de Jonge, V. N., Essink, K., & Boddeke, R. (1993). The dutch wadden sea: a changed ecosystem. *Hydrobiologia*, *265*, 45–71.

Deltacommissie. (2008). Working together with water - a living land builds for its future.

Deltares. (2021). *Opendap deltares.* Retrieved from `https://opendap.deltares.nl/thredds/catalog.html`

Dronkers, J. (1986). Tidal asymmetry and estuarine morphology. *Netherlands Journal of Sea Research*, *20*, 117–131.

Duran-Matute, M., Gerkema, T., de Boer, G. J., Nauw, J. J., & Gräwe, U. (2014). Residual circulation and freshwater transport in the dutch wadden sea: a numerical modelling study. *Ocean Science*, *10*, 611–632.

Díaz-Carrasco, P., Vittori, G., Blondeaux, P., & Ortega-Sánchez, M. (2019). Non-cohesive and cohesive sediment transport due to tidal currents and sea waves: A case study. *Continental Shelf Research*, *183*, 87–102.

Ekman, V. W. (1905). On the influence of the earth's rotation on ocean-currents. *Arkiv för Matematik, Astronomi och Fysik*, *2*.

Elias, E. P. L. (2006). *Morphodynamics of texel inlet* (Unpublished doctoral dissertation).

Elias, E. P. L. (2019). Een actuele sedimentbalans van de waddenzee. *Deltares*.

Elias, E. P. L., & Bruens, A. (2012). Een quickscan van de morfologische ontwikkelingen van het eierlandse gat. *Deltares*.

Elias, E. P. L., & Pearson, S. (2020). Sedtrails - sediment transport visualization & lagrangian simulator, a novel method to visualize and analyse sediment transport pathways. *Deltares*.

Elias, E. P. L., Pearson, S. G., & van der Spek, A. (2020). Understanding the morphological processes at ameland inlet.

Elias, E. P. L., & van der Spek, A. J. F. (2006). Long-term morphodynamic evolution of texel inlet and its ebb-tidal delta (the netherlands). *Marine Geology*, *225*, 5–21.

Elias, E. P. L., van der Spek, A. J. F., Pearson, S. G., & Cleveringa, J. (2019). Understanding sediment bypassing processes through analysis of highfrequency observations of ameland inlet, the netherlands. *Marine Geology*, *415*.

Elias, E. P. L., van der Spek, A. J. F., Wang, Z. B., & de Rond, J. (2012). Morphodynamic development and sediment budget of the dutch wadden sea over the last century. *Netherlands Journal of Geosciences*, *91*, 293–310.

ESRI. (2020). *Geoprocessing tools.* Retrieved from `https://pro.arcgis.com/en/pro-app/latest/tool-reference/spatial-analyst/how-flow-accumulation-works.htm`

Fagherazzi, S., Palermo, C., Rulli, M. C., Carniello, L., & Defina, A. (2007). Wind waves in shallow microtidal basins and the dynamic equilibrium of tidal flats. *Journal of Geophysical Research*, *112*.

Fisher, J. J., & Simpson, E. J. (1982). Tidal deltas. *Beaches and Coastal Geology*.

Fitzgerald, D. M. (1984). Interactions between the ebb-tidal delta and landward shoreline: price inlet, south carolina. *Journal of Sedimentary Research*, *54*, 1303–1318.

Fitzgerald, D. M., Penland, S., & Nummedal, D. (1984). Control of barrier island shape by inlet sediment bypassing: East frisian islands, west germany. *Developments in Sedimentology*, *39*, 355–376.

Goldstein, M., & Gedney, R. T. (1973). Wind-driven currents in a shallow lake or sea. *Journal of Mechanics and Applied Mathematics*.

Green, M. O., & Coco, G. (2014). Review of wave□driven sediment resuspension and transport in estuaries. *Reviews of Geophysics*, *52*, 77–117.

Gross, E. S., MacWilliams, M. L., & Kimmerer, W. J. (2009). Three-dimensional modeling of tidal hydrodynamics in the san francisco estuary. *San Francisco Estuary and Watershed Science*, *7*.

Gräwe, U., Flöser, G., Gerkema, T., Duran-Matute, M., Badewien, T. H., Schulz, E., & Burchard, H. (2016). A numerical model for the entire wadden sea: Skill assessment and analysis of hydrodynamics. *Journal of Geophysical Research - Oceans*, *121*, 4435–5392.

Hamill, T. M., & Juras, J. (2005). Brier skill scores, rocs, and economic value diagrams can report false skill.

Hansen, J. E., Elias, E. P. L., List, J. H., Erikson, L. H., & Barnard, P. L. (2013). Tidally influenced alongshore circulation at an inlet-adjacent shoreline. *Continental Shelf Research*, *56*, 26–38.

Harrison, S. R., Bryan, K. R., & Mullarney, J. C. (2017). Observations of morphological change at an ebb-tidal delta. *Marine Geology*, *385*, 131–145.

Hayes, M. O. (1975). Morphology of sand accumulation in estuaries. *Estuarine Research*, *2*, 3–22.

Hoeksema, H. J., Mulder, H. P. J., Rommel, M. C., de Ronde, J. G., & de Vlas, J. (2004). Bodemdalingstudie waddenzee 2004 - vragen en onzekerheden opnieuw beschouwd. *Rapport RIKZ*.

Hofstede, J. L. A., Becherer, J., & Burchard, H. (2018). Are wadden sea tidal systems with a higher tidal range more resilient against sea level rise? *Journal of Coastal Conservation*, *22*, 71–78.

Jarrett, R. D., & Petsch Jr., H. E. (1985). *Computer program ncalc user's manual - verification of manning's roughness coefficient in channels*. U.S. Geological Survey.

Jeffreys, H., & Jeffreys, B. S. (1988). *Methods of mathematical physics, 3rd ed.* Cambridge University Press.

Kato, T. (2016). *Integration of distributed energy resources in power systems - implementation, operation and control*. Academic Press.

Khanarmuei, M., Suara, K., Sumihar, J., & Brown, R. J. (2020). Hydrodynamic modelling and model sensitivities to bed roughness and bathymetry offset in a micro-tidal estuary. *Journal of Hydroinformatics*, *22*, 1536–1553.

KNMI. (2017). *Daggegevens van het weer in nederland.* Retrieved from `https://www.knmi.nl/nederland-nu/klimatologie/daggegevens`

Kreitmair, M. J., Adcock, T. A. A., Borthwick, A. G. L., Draper, S., & van den Bremer, T. S. (2020). The effect of bed roughness uncertainty on tidal stream power estimates for the pentland firth. *Royal Society Open Science*, *7*.

Kruschwitz, J. D., List, D., Waller, L., Rubinov, M., & Walter, H. (2015). Graphvar: A user-friendly toolbox for comprehensive graph analyses of functional brain connectivity. *Journal of Neuroscience Methods*, *245*, 107–115.

Kvale, E. P. (2006). The origin of neap–spring tidal cycles. *Marine Geology*, *235*, 5–18.

Laan, S. (2019). Understanding coastal dynamics at an ebb-tidal delta in the wadden sea: A case study of schiermonnikoog nw with delft3d flexible mesh. *TU Delft Repository*.

Lanzoni, S., & Seminara, G. (1998). On tide propagation in convergent estuaries. *Journal of Geophysical Research*, *103*, 30,793–30,812.

Latteux, B. (1995). Techniques for long-term morphological simulation under tidal action. *Marine Geology*, *126*, 129–141.

Li, X., Leonardi, N., & Plater, A. J. (2019). Wave-driven sediment resuspension and salt marsh frontal erosion alter the export of sediments from macro-tidal estuaries. *Geomorphology*, *325*, 17–28.

Limerinos, J. T. (1970). Determination of the manning coefficient from measured bed roughness in natural channels. *GEOLOGICAL SURVEY WATER-SUPPLY PAPER*.

Lin, P., & Liu, P. L.-F. (1998). A numerical study of breaking waves in the surf zone. *Journal of Fluid Mechanics*, *369*, 239–264.

Longuet-Higgins, M. S. (1970). Longshore currents generated by obliquely incident sea waves, 1. *Journal of Geophysical Research*, *75*, 6778–6789.

Louters, T., & Gerritsen, F. (1994). *The riddle of the sands. a tidal system's answer to a rising sea level.* Rijkswaterstaat, National Institute for Coastal and Marine Management RIKZ.

Martyr-Koller, R. C., Kernkamp, H. W. J., van Dam, A., van der Wegen, M., Lucas, L. V., Knowles, N., … Fregoso, T. A. (2017). Application of an unstructured 3d finite volume numerical model to flows and salinity dynamics in the san francisco bay-delta. *Estuarine, Coastal and Shelf Science*, *192*, 86–107.

Mostertman, L. J. (1963). *Waves of long and short period*. Delft University of Technology.

Munk, W. H. (1949). The solitary wave theory and its application to surf problems. *Annals of the New York Academy of Sciences*, *51*, 376–424.

Murphy, A. H., & Epstein, E. S. (1989). Skill scores and correlation coefficients in model verification. *Monthly Weather Review*, *117*, 572–581.

NASA. (2005). *Nasa worldwind.* Retrieved from `https://worldwind.arc.nasa.gov/`

Nederhoff, K., Smits, B., & Wang, Z. B. (2017). Kpp kennisontwikkeling morfologie waddenzee. *Deltares*.

Nieuwhof, A., & Vos, P. C. (2018). New data from terp excavations on sea-level index points and salt marsh sedimentation rates in the eastern part of the dutch wadden sea. *Netherlands Journal of Geosciences*, *97*, 31–43.

Nolte, A., van Oeveren-Theeuwes, C., van der Werf, J., Tonnon, P. K., Grasmeijer, B., van der Spek, A., … Wang, Z. (2020). Technisch advies sedimentbehoefte kustfundament.

O'Brien, M. P. (1933). Review of the theory of turbulent flow and its relation to sediment-transportation. *Transactions, American Geophysical Union*, *14*, 487–491.

Oertel, G. F. (1975). Ebb-tidal deltas of georgia estuaries. *Estuarine Research*, *2*, 267–276.

Park, J.-R. (2009). Metadata quality in digital repositories: A survey of the current state of the art. *Cataloging & Classification Quarterly*, *47*.

Pearson, S. G. (2019). Spit connectivity.

Pearson, S. G., van Prooijen, B. C., Elias, E. P. L., Vitousek, S., & Wang, Z. B. (2020). Sediment connectivity: A framework for analyzing coastal sediment transport pathways. *Journal of Geophysical Research: Earth Surface*, *125*.

Price, G. R. (1972). Extension of covariance selection mathematics. *Annuals of Human Genetics*, *35*, 485.

Rijkswaterstaat. (2017). *Rijkswaterstaat waterinfo.* Retrieved from `https://waterinfo.rws.nl/#!/kaart/wind/`

Rijkswaterstaat. (2021). Kustgenese 2.0: kennis voor een veilige kust.

Rubinov, M., & Sporns, O. (2010). Complex network measures of brain connectivity: Uses and interpretations. *NeuroImage*, *52*, 1059–1069.

Savenije, H. H. G., Toffolon, M., Haas, J., & Veling, E. J. M. (2008). Analytical description of tidal dynamics in convergent estuaries. *Journal of Geophysical Research*, *113*.

Sha, L. P., & van den Berg, J. H. (1993). Variation in ebb-tidal delta geometry along the coast of the netherlands and the german bight. *Journal of Coastal Research*, *9*, 730–746.

Shields, A. (1936). *Anwendung der aehnlichkeitsmechanik und der turbulenzforschung auf die geschiebebewegung*. Preussischen Versuchsanstalt für Wasserbau.

Speer, P. E., & Aubrey, D. G. (1985). A study of non-linear tidal propagation in shallow inlet/estuarine systems part ii: Theory. *Estuarine, Coastal and Shelf Science*, *21*, 207–224.

Stevens, A. W., Elias, E. P. L., Pearson, S., Kaminsky, G. M., Ruggiero, P. R., Weiner, H. M., & Gelfenbaum, G. R. (2020). Observations of coastal change and numerical modeling of sediment-transport pathways at the mouth of the columbia river and its adjacent littoral cell. *U.S. Geological Survey*.

Stive, M. J. F. (1986). A model for cross-shore sediment transport. *Coastal Engineering*, 1550–1564.

Sutherland, J., Peet, A. H., & Soulsby, R. L. (2004). Evaluating the performance of morphological models. *Coastal Engineering*, *51*, 917–939.

Tonnon, P. K., & Nederhoff, K. (2016). Monitoring en evaluatie pilot zandmotor, eindevaluatie onderdeel morfologie (2016).

Townend, I., Wang, Z. B., Stive, M., & Zhou, Z. (2016). Development and extension of an aggregated scale model: Part 1 – background to asmita. *Chinese Ocean Engineering Society*, *30*.

van den Bremer, T. S., & Breivik, Ø. (2018). Stokes drift. *Philosophical Transactions of the Royal Society A*, *376*, 1–23.

van der Meer, J. W., Regeling, H. J., & de Waal, J. P. (2000). Wave transmission: spectral changes and its effects on run-up and overtopping.

Van der Spek, A. J. F. (2018). The development of the tidal basins in the dutch wadden sea until 2100: the impact of accelerated sea-level rise and subsidence on their sediment budget – a synthesis. *Netherlands Journal of Geosciences*, *97*, 71–78.

Van der Vegt, M., Schuttelaars, H. M., & de Swart, H. E. (2006). Modelling the equilibrium of tide-dominated ebb-tidal deltas. *Journal of Geophysical Research*, *111*.

Van Geer, P. (2007). *Long-term modelling of the western part of the dutch wadden sea*. WL | Delft Hydraulics.

van Houweninge, G., & de Graauw, A. (1982). The closure of tidal basins. *Coastal Engineering*, *6*, 331–360.

van Leeuwen, S. M., van der Vegt, M., & de Swart, H. E. (2003). Morphodynamics of ebb-tidal deltas: a model approach. *Estuarine, Coastal and Shelf Science*, *57*, 899-907.

van Rijn, L. C. (1993). *Principles of sediment transport in rivers, estuaries and coastal seas*. Aqua Publications.

Van Rijn, L. C. (1997). Sediment transport and budget of the central coastal zone of holland. *Coastal Engineering*, *32*, 61–90.

Vinther, N., Christiansen, C., Bartholdy, J., Sørensen, C., & Lund-Hansen, L. C. (2004). Sediment transport across a tidal divide in the danish wadden sea. *Danish Journal of Geography*, *104*, 71–86.

Vos, P. C. (2015). *Origin of the dutch coastal landscape*. Barkhuis.

Vroom, J. (2011). Tidal divides: A study on a simplified case and the dutch wadden sea. *Delft University of Technology*.

Wang, Z. B. (2018). Long term morphological development of the tidal inlet systems in the dutch wadden sea.

Wang, Z. B., Elias, E. P. L., van der Spek, A. J. F., & Lodder, Q. J. (2018). Sediment budget and morphological development of the dutch wadden sea: impact of accelerated sea-level rise and subsidence until 2100. *Netherlands Journal of Geosciences*, *97*, 183–214.

Wang, Z. B., Louters, T., & de Vriend, H. J. (1995). Morphodynamic modelling for a tidal inlet in the wadden sea. *Marine Geology*, *126*, 289–300.

Wang, Z. B., Vroom, J., van Prooijen, B. C., Labeur, R. J., & Stive, M. J. F. (2011). Development of tidal watersheds in the wadden sea. *River, Coastal and Estuarine Morphodynamics*.

Whitfield-Gabrieli, S., & Nieto-Castanon, A. (2012). Conn: A functional connectivity toolbox for correlated and anticorrelated brain networks. *Brain Connectivity*, *2*.

Winter, C., Chiou, M.-D., Riethmüller, R., & Ernstsen, V. B. (2006). The concept of “representative tides” in morphodynamic numerical modelling. *Geo-Marine Letters*, *26*, 125–132.

A

Calibration Roughness Field

This appendix deals with part of the calibration and validation process to determine the most suitable roughness field for the WadSea FM model. Much more runs were performed than are shown in the appendix, but the most important and decisive runs are discussed. The roughness fields themselves are not shown, but the results acquired with Matlab are. These figures present the modelled versus the observed M2 tidal amplitude and phase at each measurement station. The goal of the calibration and validation process was to determine the roughness field that best approached the tidal propagation between Den Helder and Harlingen, and that had the smallest percentage deviation overall.

The model that acted as the starting point had a Manning's value of 0.022 in the entire domain, with the exception of a polygon with a value of 0.028 in the Western Wadden Sea (Figure 3.1). To check the performance of both a roughness field with a uniform Manning's value of 0.022 (Figure A.1) and a roughness field with a uniform Manning's value of 0.028 (Figure A.2), these runs were the first step in the calibration process. In addition, the runs served the purpose of getting to know the model. The run with the uniform value of 0.022 performed best (7.56% deviation), thus this value formed the basis for the next runs. A depth-dependent roughness field was applied to the rest of the runs, with the largest values in the channels, and the smallest values in the littoral zones. First, a set of small range depth-dependent roughness fields was applied to the model. These performed overall the same as the uniform Manning's value of 0.022, but the configuration with values of 0.021, 0.020, 0.019, respectively, performed best (7.01% deviation). The results from the run are shown in Figure A.3. After that, a larger range of values was applied. The results from the best performing run (7.30% deviation) are shown in Figure A.4. This roughness field did not perform better than the one with the small range of values, but it indicated the beneficial influence of small values in the littoral zone. This lead to the roughness field that was chosen to be applied to the model, shown in Figure 3.4 with the results presented in Figure 3.2. The deviation with this configuration was 6.64%. Even smaller values than 0.010 in the littoral zone were also applied to the model, which resulted in an overall better performance (smallest deviation of 5.84%), but as these values are not physically substantiated, the results from these runs are not shown here. The refined grid for the roughness field configuration of Figure 3.4 performed slightly better than the coarse grid (6.56% deviation), but whether or not to choose the refined grid was already discussed in Chapter 3 and the further discussion is presented in Appendix B. Therefore, this configuration and its result are not shown here. In addition to applying three Manning's values to the entire domain, the performance of a linear varying roughness field and a roughness field with different values in the Western and Eastern Wadden Sea were assessed. The results from these runs are shown in Figures A.5 and A.6, respectively. The best run for the linear varying roughness field (Figure A.5) did not perform better than the previous chosen run (6.97% deviation). The runs with a difference in roughness between the Western and Eastern Wadden Sea however did perform much better, with the best overall performance at only 4.75% deviation (Figure A.6). However, the tidal propagation between Den Helder and Harlingen was modelled worse for these runs compared to the roughness field configuration shown in Figure 3.4. Distinguishing a difference in roughness between the Western and Eastern Wadden Sea stills shows potential, and even though it was not chosen for this research, further investigation in this method is recommended.

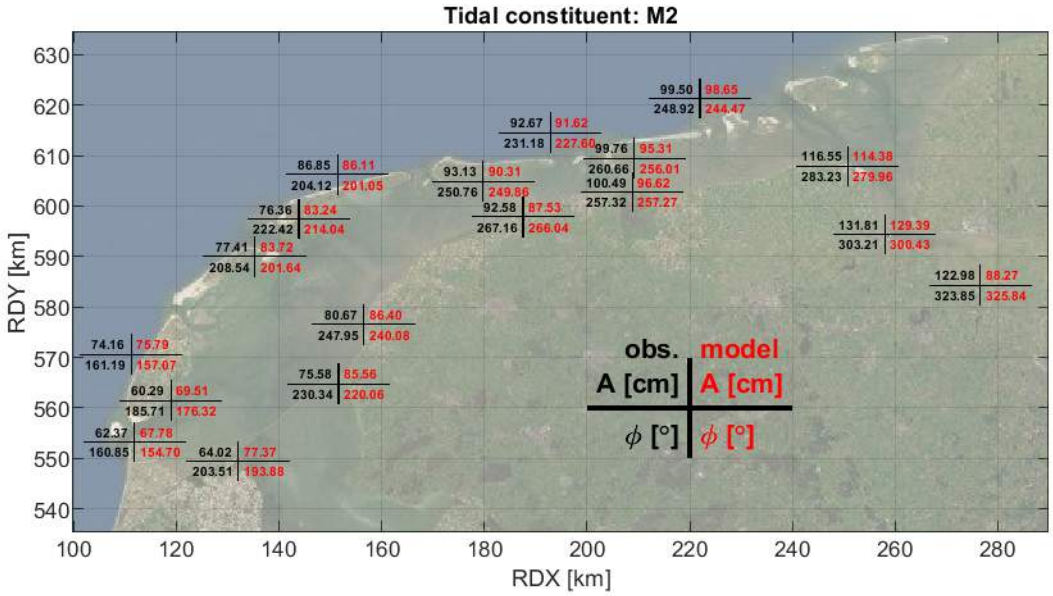

Figure A.1: Map of the Dutch Wadden Sea with both observed and modelled results for the M2 tidal amplitude and phase. The table on the bottom right of the figure indicates the meaning of the values at each measurement station. The applied roughness field has a uniform Manning's value of 0.022.

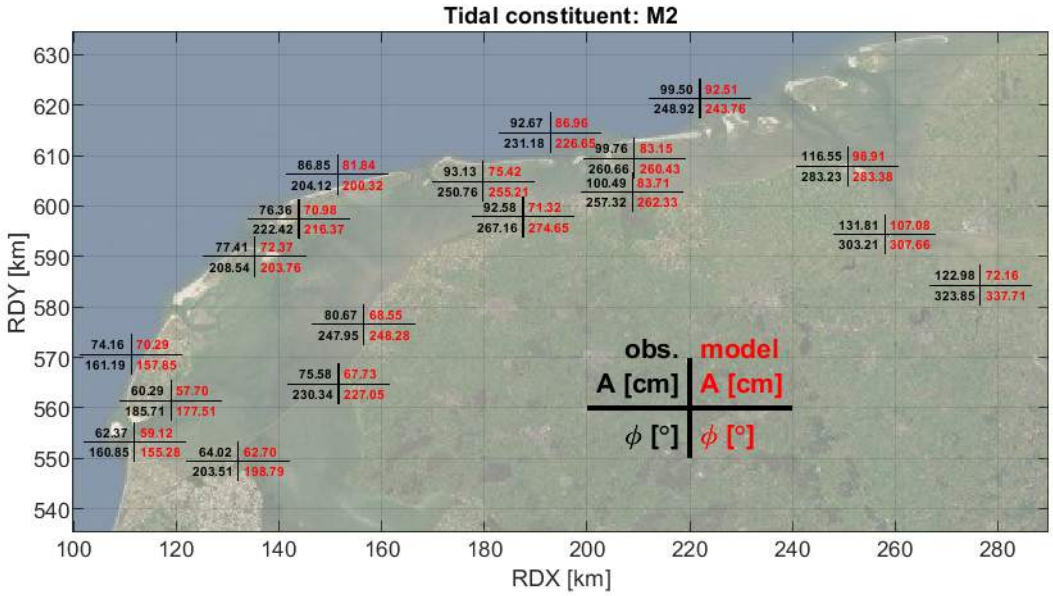

Figure A.2: Map of the Dutch Wadden Sea with both observed and modelled results for the M2 tidal amplitude and phase. The table on the bottom right of the figure indicates the meaning of the values at each measurement station. The applied roughness field has a uniform Manning's value of 0.028.

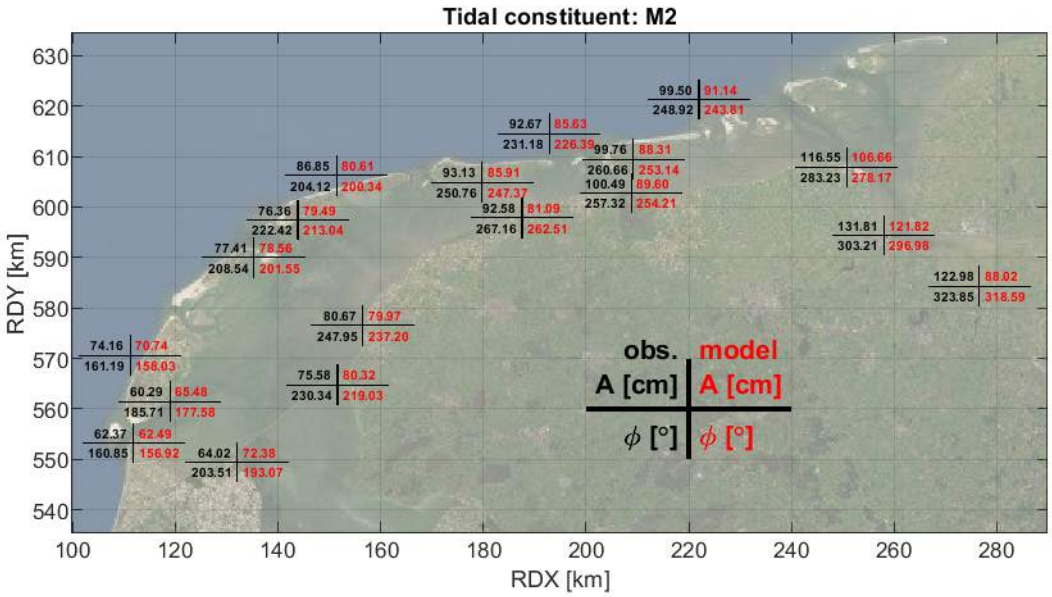

Figure A.3: Map of the Dutch Wadden Sea with both observed and modelled results for the M2 tidal amplitude and phase. The table on the bottom right of the figure indicates the meaning of the values at each measurement station. The applied roughness field has a Manning's value of 0.021 in the channel, a value of 0.020 in the sub-littoral zone and a value of 0.019 in the littoral zone.

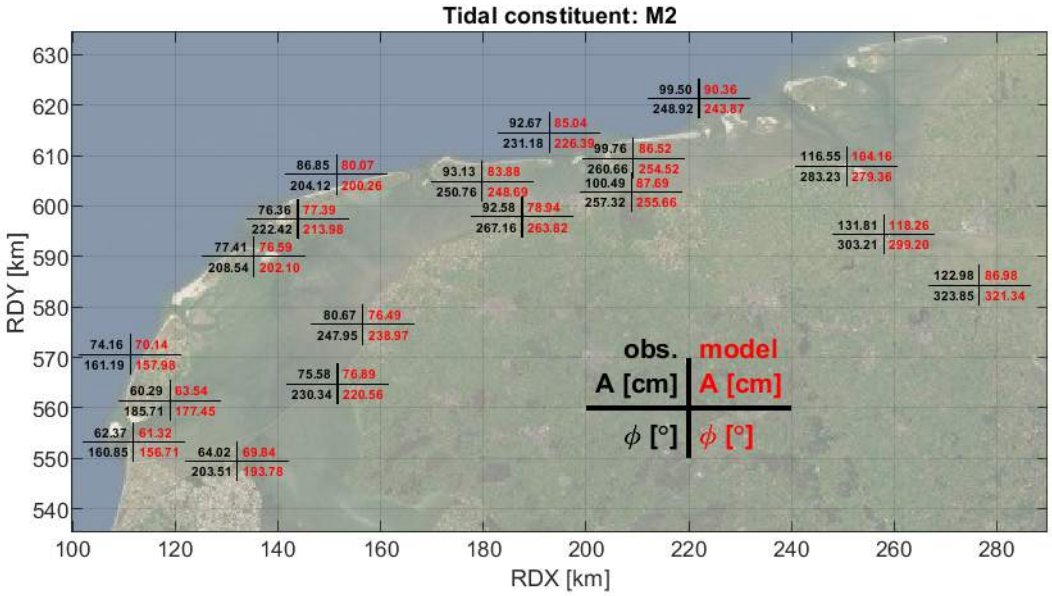

Figure A.4: Map of the Dutch Wadden Sea with both observed and modelled results for the M2 tidal amplitude and phase. The table on the bottom right of the figure indicates the meaning of the values at each measurement station. The applied roughness field has a Manning's value of 0.022 in the channel and the sub-littoral zone, and a value of 0.015 in the littoral zone.

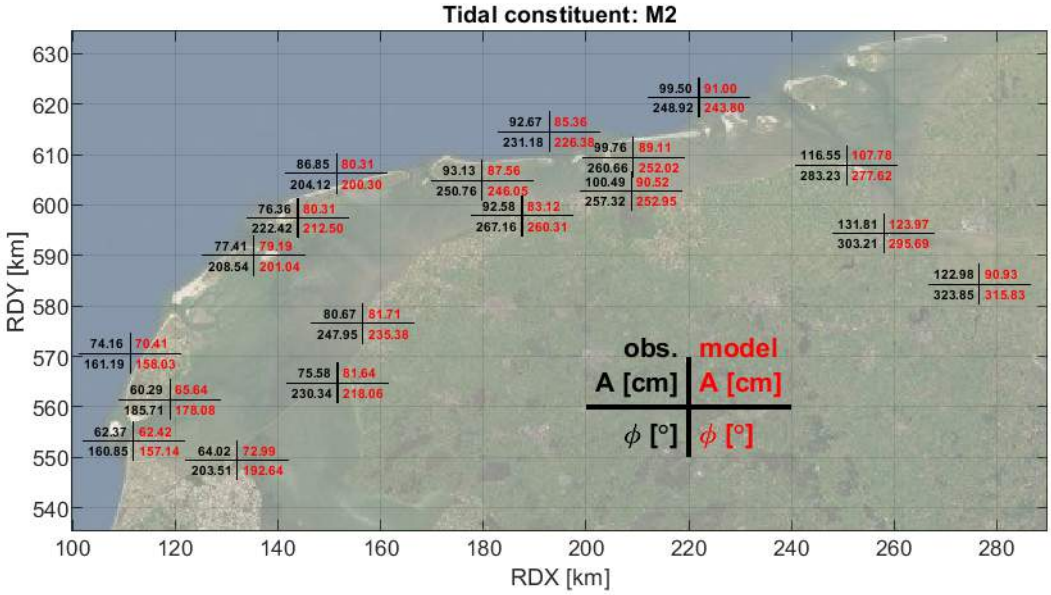

Figure A.5: Map of the Dutch Wadden Sea with both observed and modelled results for the M2 tidal amplitude and phase. The table on the bottom right of the figure indicates the meaning of the values at each measurement station. The applied roughness field has a Manning's value of that varies linearly between 0.022 in the channel and 0.016 in the littoral zone.

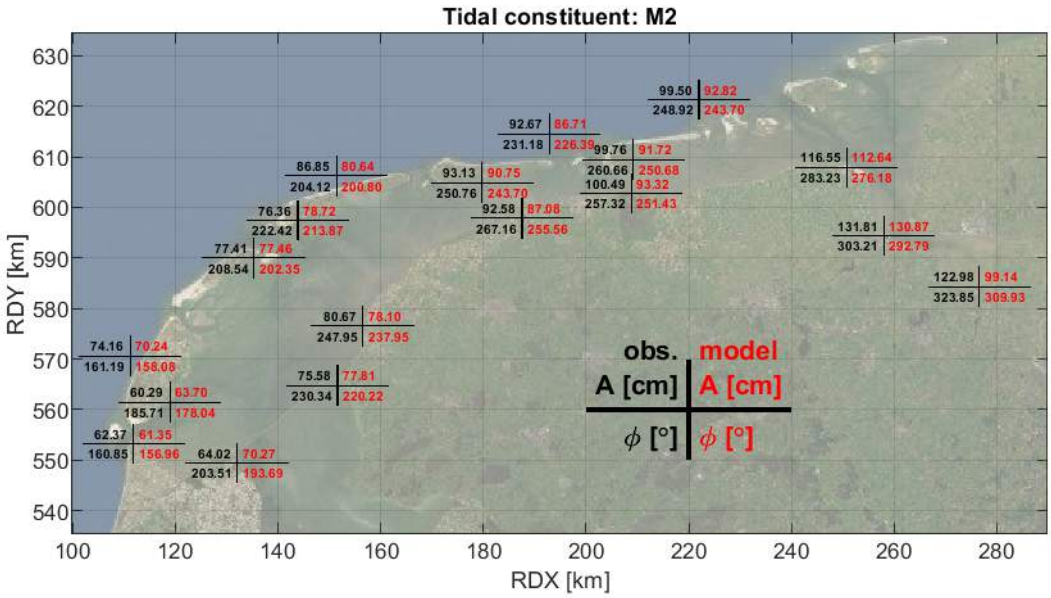

Figure A.6: Map of the Dutch Wadden Sea with both observed and modelled results for the M2 tidal amplitude and phase. The table on the bottom right of the figure indicates the meaning of the values at each measurement station. The applied roughness field has in the Western Wadden Sea a Manning's value of 0.022 in the channel, a value of 0.020 in the sub-littoral zone and a value of 0.015 in the littoral zone. In the Eastern Wadden Sea, the roughness field has a Manning's value of 0.019 in the channel, a value of 0.017 in the sub-littoral zone and a value of 0.010 in the littoral zone.

B

Probability Analysis

To further assess the accuracy of the chosen run, a probability analysis is performed on the model results. To determine which run would be used for further research, a deviation calculation was performed. This was an assessment of the percentage of total deviation from the measurements. The runs that performed best were the runs with very small values for the Manning's coefficient in the littoral zone, namely below 0.010. The values were an order smaller than the values at the sub-littoral zone and the channels, which is probably physically incorrect. The goal of this research was to come up with physically correct depth-dependent Manning's coefficient, thus the runs with very small values for the coefficient do not fit this profile. The chosen run still has a small Manning's coefficient, namely 0.010, which indicates a very smooth surface at the tidal flats. This values is however within the same order of magnitude as the other values, thus is considered good enough. It is still an empirical way of estimating the roughness field, but can be considered better than the previous roughness field applied.

To assess the performance of the run in one glance, a target diagram is constructed. The target diagram has proven to be very effective (Stevens et al., 2020; Martyr-Koller et al., 2017). For this, the variance (V) and the root mean square error (RMSE) of each run have to be determined. The bias and the mean of the results are not appropriate, as the bias will be negligible because the water levels are compared to the mean sea level, and the mean of the tidal amplitude will be approximately zero. The variance and the root mean square error take into account the inaccuracy of the run which can be visibly quantified, and are therefore more suitable for envisioning the accuracy of the run. The variance and the root mean square error are defined as follows (Kato, 2016):

$$V = \frac{1}{N}\sum_{i=1}^{N}\left(x_{f,i} - x_{0,i}\right)^2 \tag{B.1}$$

$$RMSE = \sqrt{\frac{1}{N}\sum_{i=1}^{N}\left(x_{f,i} - x_{0,i}\right)^2} \tag{B.2}$$

In addition to choosing the parameters for the probability analysis, the assessed data needs to be determined. In the Western Wadden Sea, the propagation of the tidal signal from Den Helder to Harlingen indicates the accuracy of the run the best. Additionally, the stations at Vlieland and Terschelling are relatively good stations for assessment of the tidal signal. However, as the performance of the run for the entire Wadden Sea is of interest, all measurement stations are included in the probability analysis. Additionally, the entire tidal signal is assessed, in comparison to the deviation analysis, which only included the M_2 constituent. The target diagram is shown in Figure B.1. The clear outlier is the Nieuw Statenzijl station. This is probably due to the fact that with the coarse grid, the observation point is not situated in a channel. The Harlingen measurement station performs badly compared to the other stations for the entire tidal signal, whereas it performed well for the M_2 constituent alone. The Den Helder station performs also for the entire signal the best overall.

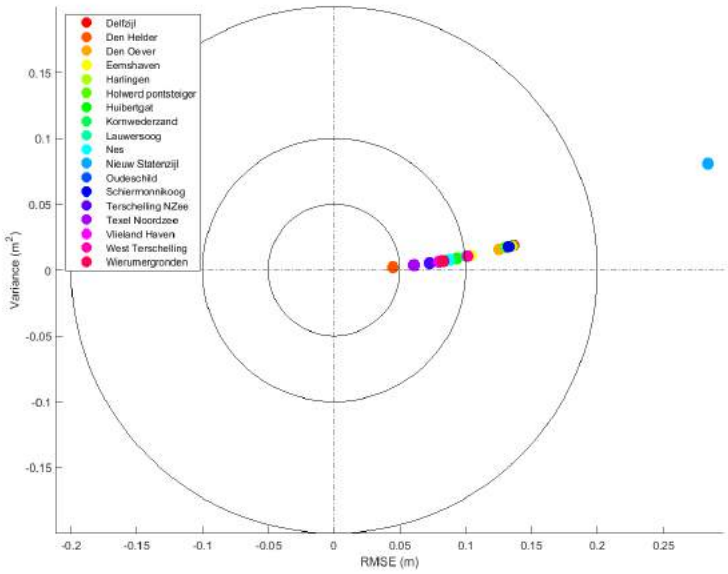

Figure B.1: Target diagram for run $'A09 - Coarse - 00212010'$. The diagram shows for each measurement station the variance and the root mean square error, with the variance on the y-axis and the root mean square error on the x-axis. Each colored represents a measurement station, which dot represent which station can be read from the legend.

Lastly, the earlier stated conclusion that the refined model does not perform better is indeed correct. The target diagram for the refined model is shown in Figure B.2. Here, it can be seen that the distribution of the errors is almost the same as for the coarse grid, thus the refined grid does not necessarily perform better than the coarse grid.

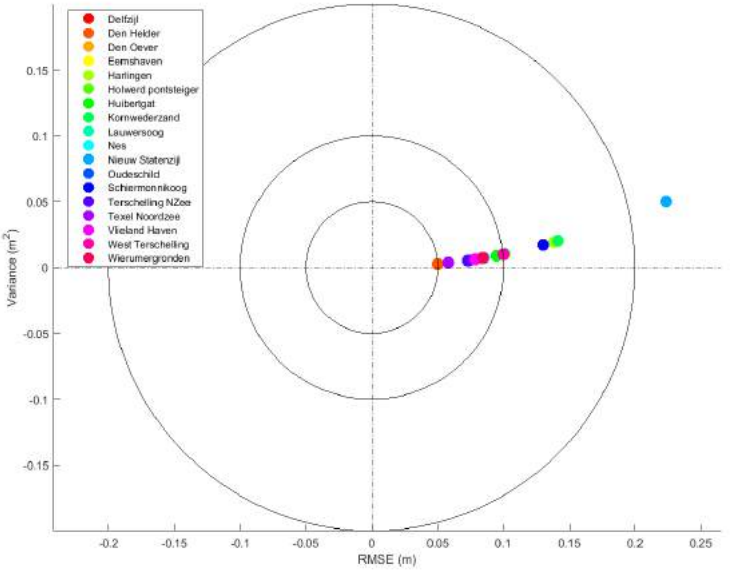

Figure B.2: Target diagram for run $'A09 - Refined - 00212010'$. The diagram shows for each measurement station the variance and the root mean square error, with the variance on the y-axis and the root mean square error on the x-axis. Each colored represents a measurement station, which dot represent which station can be read from the legend.

C

Brier Skill Score

In Chapter 4, the morphological tide was determined based on a visual evaluation of the difference in vectors between the annual mean sediment transport and the sediment transport due to the best performing tides. Here, the chosen representative tide at each tidal channel will be assessed with the Brier skill score. The Brier skill score (BSS) is a measure to indicate the performance of a model, where normally 1.0 is a perfect performance, 0.0 means that the performance has not improved, and a BSS lower than 0.0 indicates poorer performance (Hamill & Juras, 2005). It is most commonly used to assess weather model performance. The BSS is easily lowered by errors in models, and thus to know which errors contribute to this lowering a decomposition of the BSS can be performed, as was proposed by (Murphy & Epstein, 1989). In coastal engineering, for example the phase error, the amplitude error and the map mean error can be implemented (Sutherland et al., 2004). However, as the performance of the morphological tide is assessed on one specific, namely the difference in vector magnitude with the annual mean, the formula for the BSS at each grid point reduces to the following:

$$BSS_i = 1 - \frac{\langle (Y_i - X_i)^2 \rangle}{\langle (X_i)^2 \rangle} \tag{C.1}$$

Where Y_i is the vector magnitude of the morphological tide at grid point i and X_i is the vector magnitude of the yearly mean at grid point i. This implies that if the difference between the vector magnitude of the morphological tide and the yearly mean is very small, the BSS is almost equal to one. This is in accordance with the definition of the Brier skill score mentioned above. If the difference between the two increases, the skill score decreases. This can be observed in Figure C.1. As the tidal channels are the most important areas when considering sediment transport, the skill score maps were determined for the Texel Inlet, the Eierlandse Gat, the Vlie Inlet and the Ameland Inlet. These maps are all shown in Figure C.1. Each map has the limits of the skill score set between 1.0 and -1.0.

The morphological tide was determined based on a comparison between the mean annual sediment transport and the transport due to each tide at the Texel Inlet. The specific method for the determination of the morphological tide is described in Section 4.2.1. Looking at the Texel Inlet, both on the North Sea side (C.1a) and the Wadden Sea side (C.1b), the skill score is almost perfect in the middle of the channel. On the shallower parts of the channel, the skill scores are lower, but this can be explained by the fact that in the analysis for the determination of the morphological tide, the smaller vectors at the shallower parts were not as important. Here, no normalized vector is taken into account, which results in slightly lower skill scores than would be expected based on the earlier analysis. However, as the largest sediment transport vectors are most important for the eventual sediment transport patterns, it is mainly important that the skill scores in the middle of the channels are high. This is what is also seen in the Vlie Inlet, Figure C.1c and C.1d, and in the Eierlandse Gat, Figure C.1g. The channel that shows the lowest skill scores in the middle of the channel is the Ameland Inlet, see Figure C.1e and C.1f. This is not unexpected, as the Ameland Inlet is situated in the Eastern Wadden Sea and thus experiences different processes than the Texel Inlet. Still, the skill scores are around 0.0 or above in the channel,

which is acceptable in terms of deviations from the annual mean. Thus, based on the Brier skill score analysis, the determined morphological tide performs indeed well.

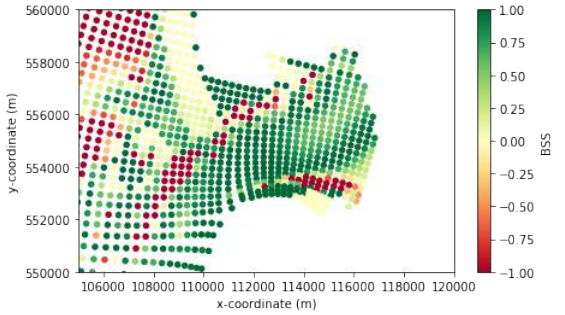

(a) Texelse Zeegat - North Sea side

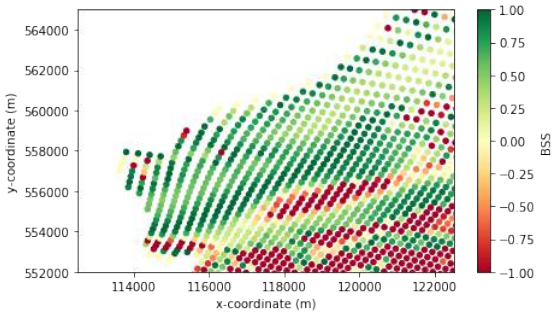

(b) Texelse Zeegat - Wadden Sea side

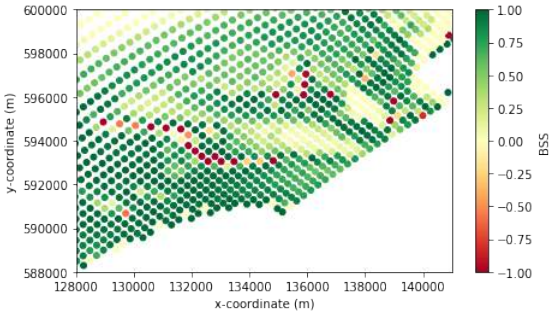

(c) Vliestroom - North Sea side

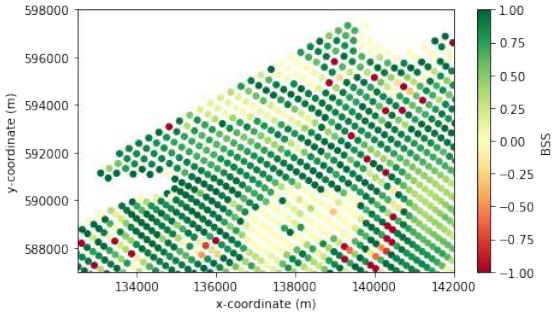

(d) Vliestroom - Wadden Sea side

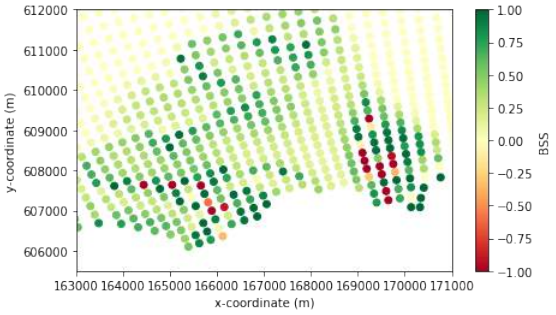

(e) Amelander Zeegat - North Sea side

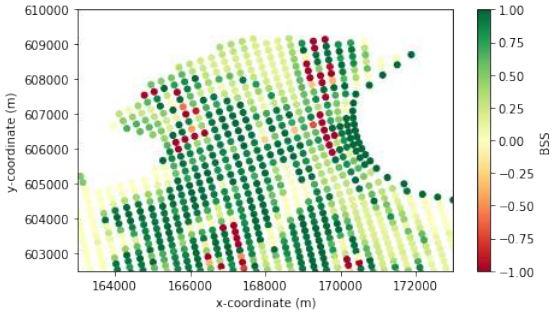

(f) Amelander Zeegat - Wadden Sea side

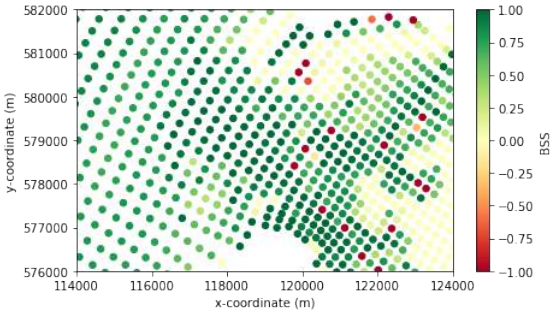

(g) Eierlandse Gat

Figure C.1: Brier skill scores at each grid point for the representative tidal channel areas. Each individual figure has its own specific varying value for the BSS, as the variation in vector magnitude varies strongly over the entire Wadden Sea. The individual descriptions give the location we are looking at.

D

Additional SedTRAILS Results

In addition to the representative and storm conditions, other wind and wave results were generated with SedTRAILS as well. Two other wind and wave directions with the representative wind speed were chosen, and an additional storm condition, better known as Storm Sebastian. The influence of other wind directions was discussed in Chapter 5, thus the additional are not further discussed in this appendix. The thirst three figures show the additional wind results, with their captions indicating the specific conditions. The second three figures show the additional wave results.

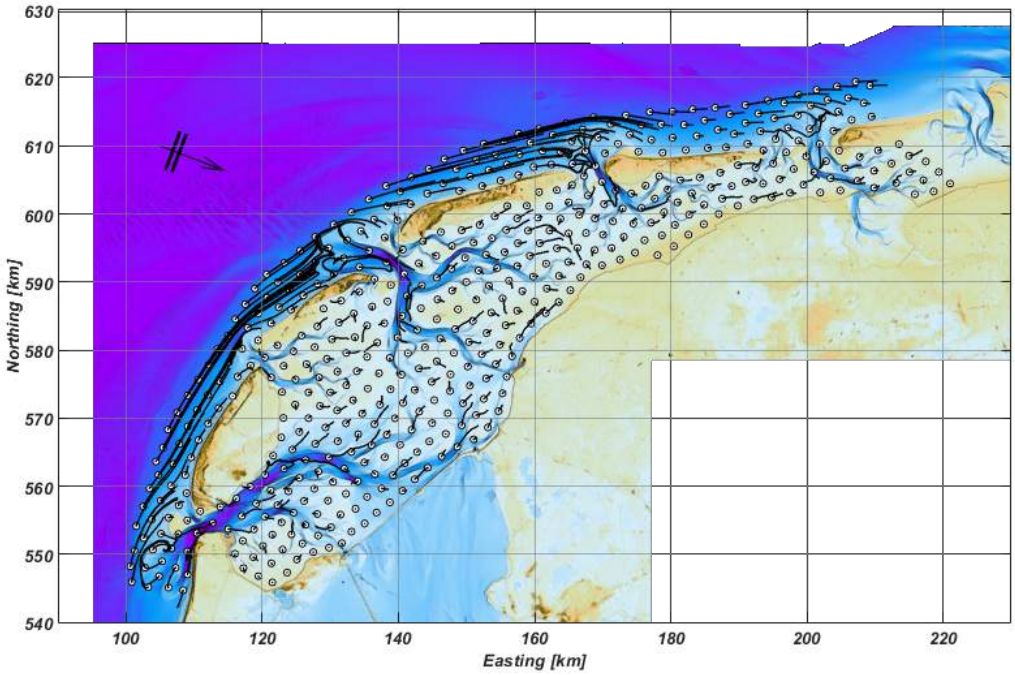

Figure D.1: Large-scale sediment transport pathways forced by the hydraulic tide and representative wind condition for the year 2017 applied to the northwest (U = 7.0 m/s, Dir = 291°N). The white circles indicate the starting position of the individual particles after placement in the system. The black lines indicate the pathways of the sediment particles. To obtain these particular pathways, an acceleration factor of 100 and a modelling period of 600 days were used.

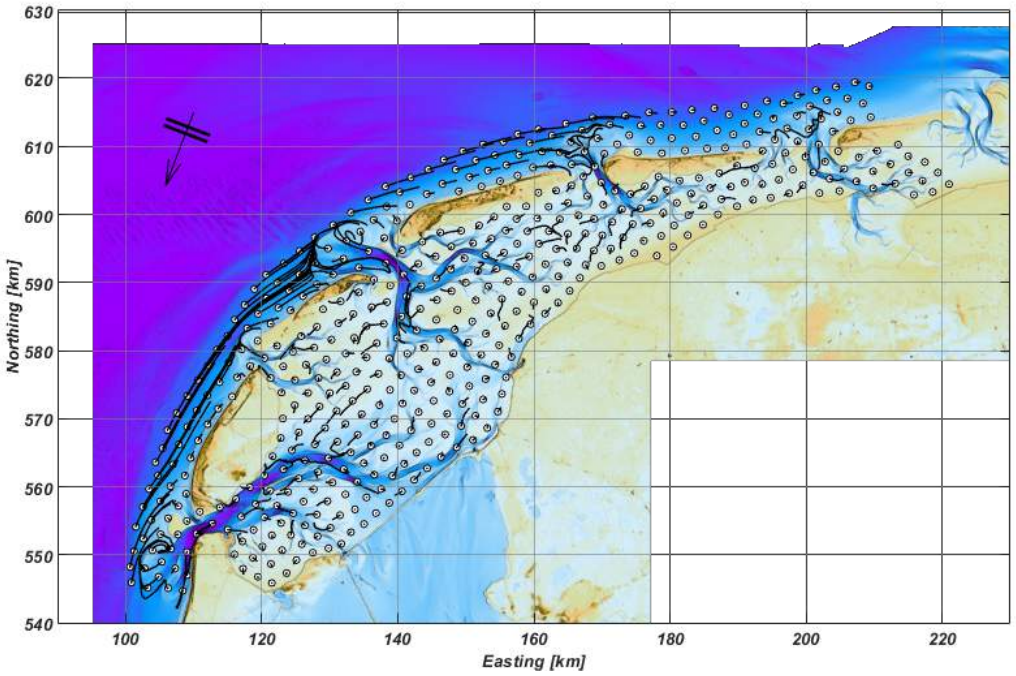

Figure D.2: Large-scale sediment transport pathways forced by the hydraulic tide and representative wind condition for the year 2017 applied to the northeast (U = 7.0 m/s, Dir = 21°N). The white circles indicate the starting position of the individual particles after placement in the system. The black lines indicate the pathways of the sediment particles. To obtain these particular pathways, an acceleration factor of 100 and a modelling period of 600 days were used.

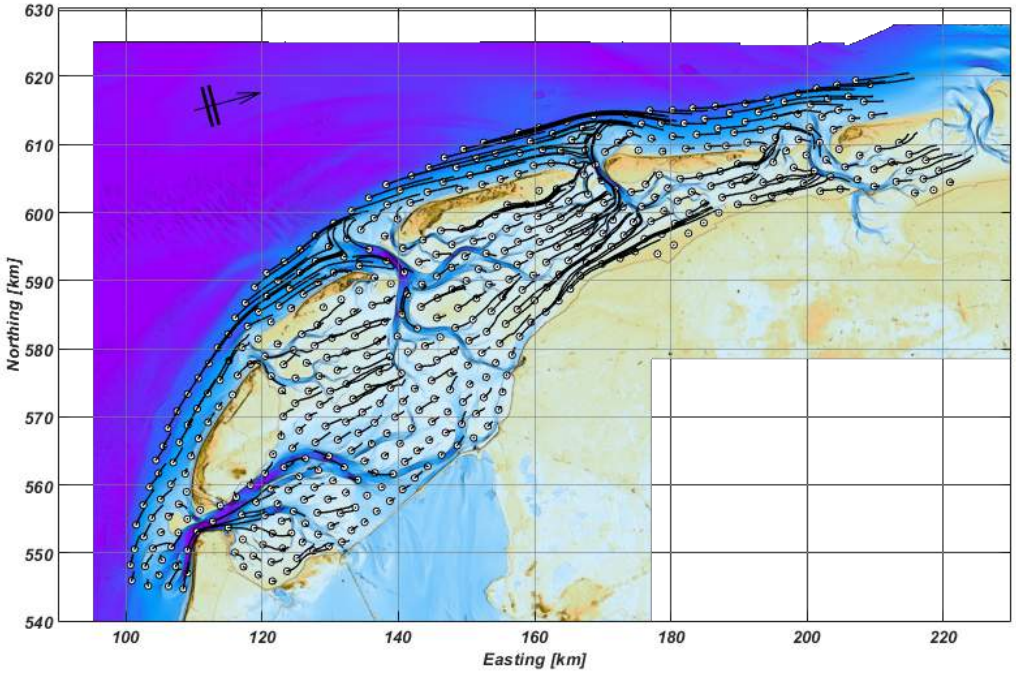

Figure D.3: Large-scale sediment transport pathways forced by the hydraulic tide and selected Storm Sebastian, which took place on the 13^{th} of September, 2017 (U = 18.0 m/s, Dir = 255°N). The white circles indicate the starting position of the individual particles after placement in the system. The black lines indicate the pathways of the sediment particles. To obtain these particular pathways, an acceleration factor of 10 and a modelling period of 200 days were used.

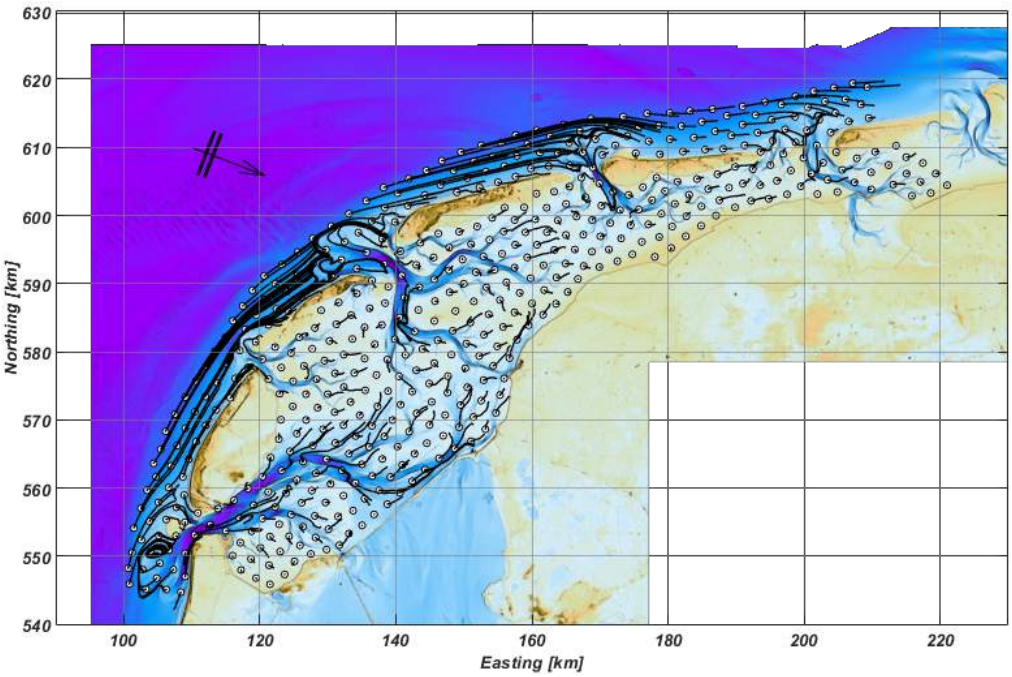

Figure D.4: Large-scale sediment transport pathways forced by the hydraulic tide, representative wind condition from the west-northwest (U = 7.0 m/s, Dir = 291°N) and the assumed representative wave condition (H_{m0} = 1.15 m, T = 4.50 s, Dir = 291°N). The white circles indicate the starting position of the individual particles after placement in the system. The black lines indicate the pathways of the sediment particles. To obtain these particular pathways, an acceleration factor of 100 and a modelling period of 600 days were used. The arrow indicates the wind and wave direction.

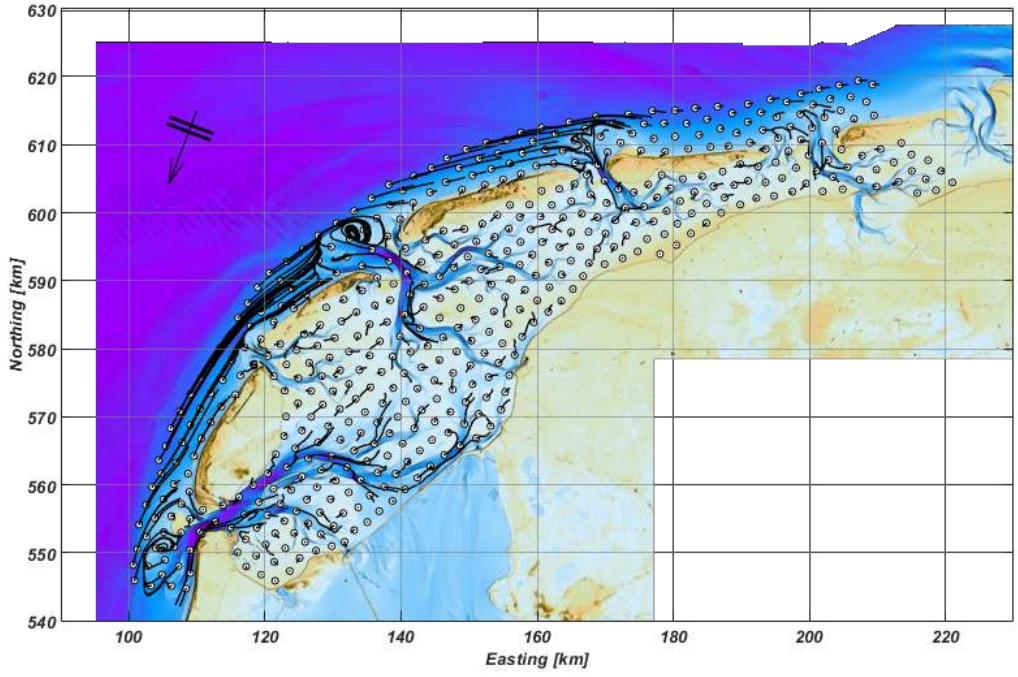

Figure D.5: Large-scale sediment transport pathways forced by the hydraulic tide, representative wind condition from the north-northeast (U = 7.0 m/s, Dir = 21°N) and the assumed representative wave condition (H_{m0} = 1.15 m, T = 4.50 s, Dir = 21°N). The white circles indicate the starting position of the individual particles after placement in the system. The black lines indicate the pathways of the sediment particles. To obtain these particular pathways, an acceleration factor of 100 and a modelling period of 600 days were used. The arrow indicates the wind and wave direction.

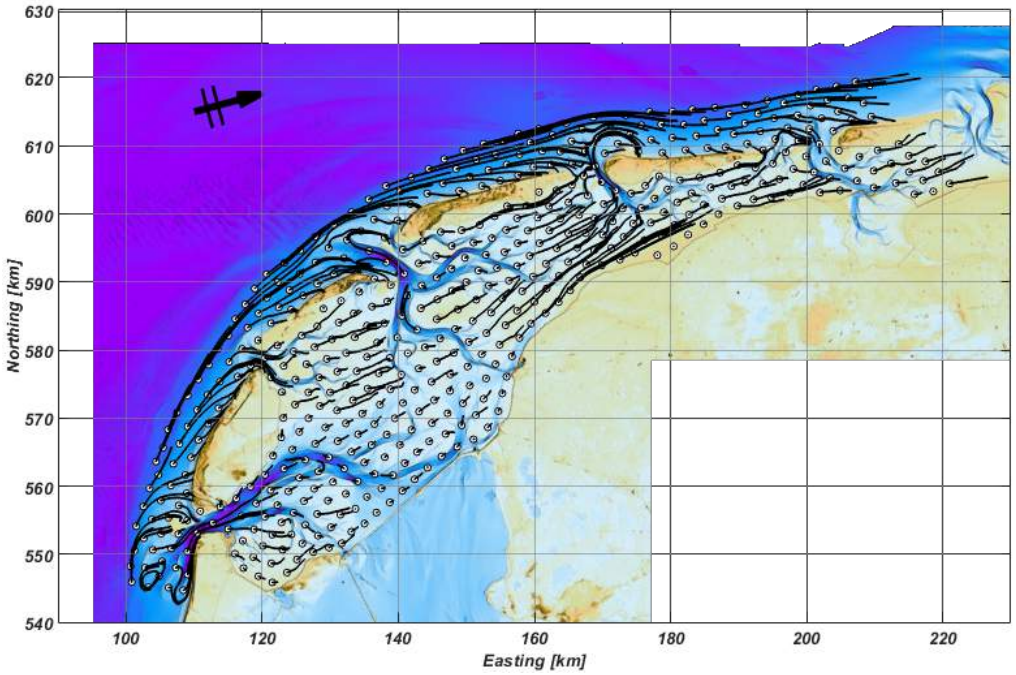

Figure D.6: Large-scale sediment transport pathways forced by the hydraulic tide and selected Storm Sebastian including waves, which took place on the 13^{th} of September, 2017 (U = 18.0 m/s, H_{m0} = 6.63 m, T = 8.24 s, Dir = 255°N). The white circles indicate the starting position of the individual particles after placement in the system. The black lines indicate the pathways of the sediment particles. To obtain these particular pathways, an acceleration factor of 10 and a modelling period of 200 days were used.

E

Additional Connectivity Diagrams

This appendix contains the additional unstructured network diagrams for both the wind runs (Figure E.1) and the wave runs (Figure E.2). The structured network diagrams are not included in the appendix, as the unstructured network diagrams overall show more detail in the connectivity patterns between the polygons. The numbers 1 to 10 represent the same polygons as all the network diagrams presented in Chapter 6. The sub-captions indicate the intended wind or wave run.

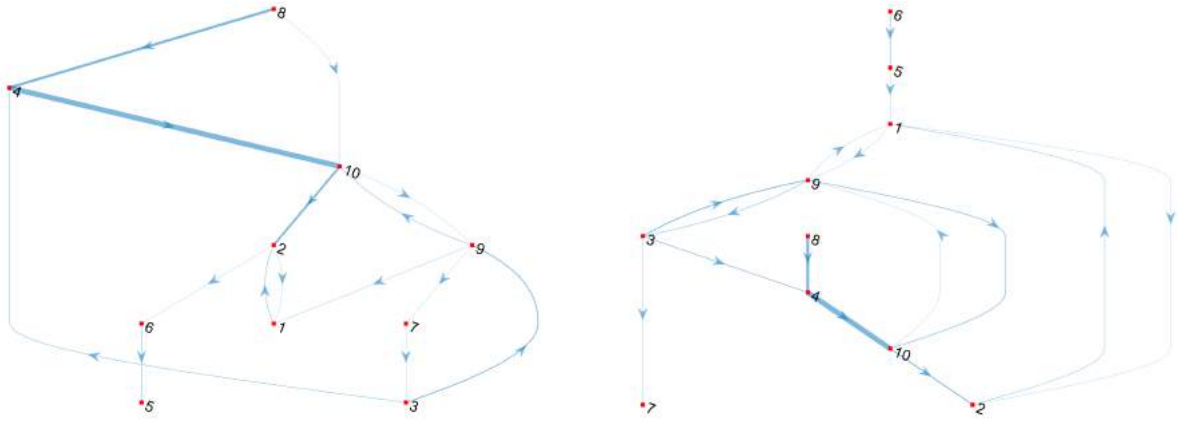

(a) Representative wind condition - 291°N

(b) Representative wind condition - 21°N

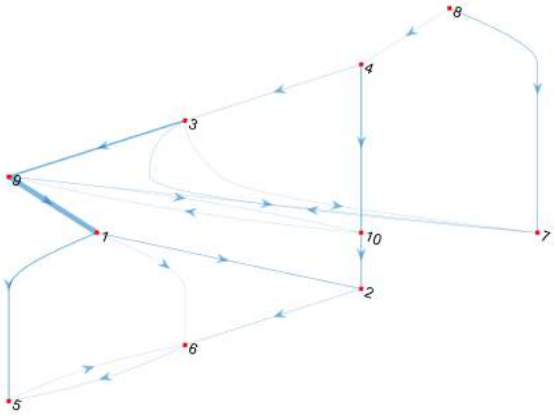

(c) Storm condition (U = 18.0 m/s) - 255°N

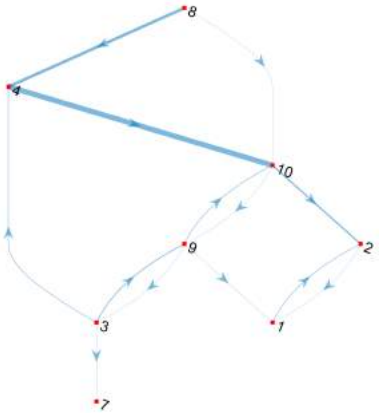

(d) Mild condition (U = 5.50 m/s) - 45°N

Figure E.1: Unstructured network diagrams for the additional wind runs. Thicker lines indicate a higher connectivity between polygons, the arrows present the direction of transport. For the specific polygon belonging to each number, see chapter 6. The sub-captions indicate the specific wind run.

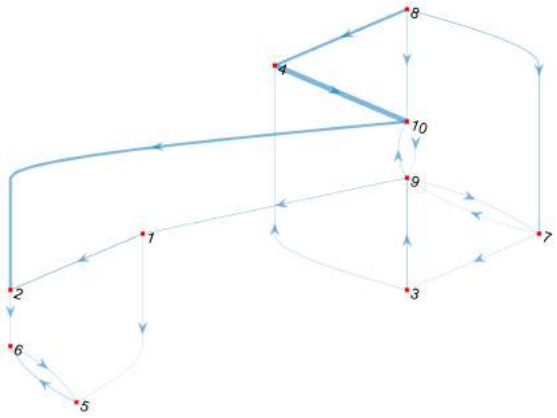

(a) Representative wave condition - 291°N

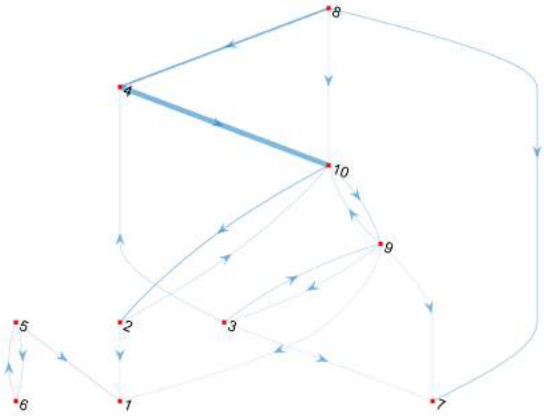

(b) Representative wave condition - 21°N

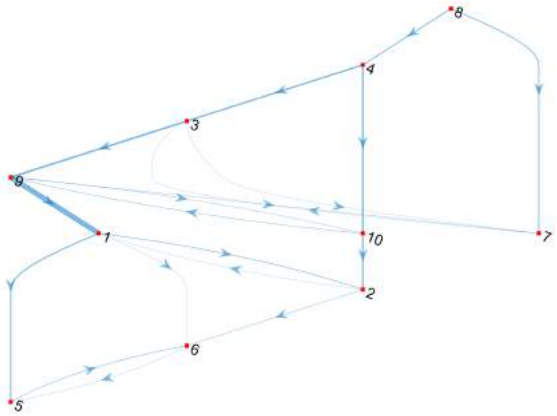

(c) Storm condition (U = 18.0 m/s) - 255°N

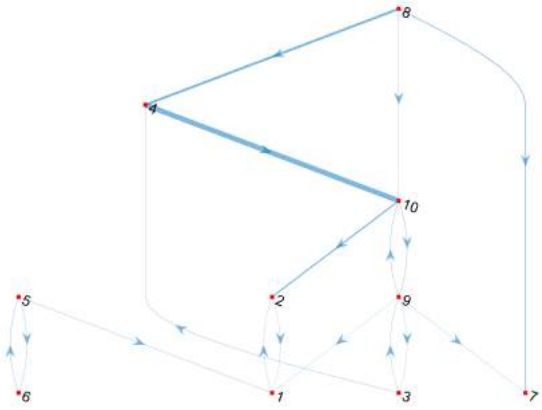

(d) Mild condition (U = 5.50 m/s) - 45°N

Figure E.2: Unstructured network diagrams for the additional wave runs. Thicker lines indicate a higher connectivity between polygons, the arrows present the direction of transport. For the specific polygon belonging to each number, see chapter 6. The sub-captions indicate the specific wave run.